HYDRODYNAMIC COEFFICIENTS OF COMPOUND CIRCULAR CYLINDERS IN HEAVE MOTION

by

MADAN VENUGOPAL

B.Tech(NA&SB), University of Cochin, 1980

A THESIS SUBMITTED IN PARTIAL FULFILMENT OF

THE REQUIREMENTS FOR THE DEGREE OF

MASTER OF APPLIED SCIENCE

in

FACULTY OF GRADUATE STUDIES

Department of Mechanical Engineering

We accept this thesis as conforming

to the required standard

THE UNIVERSITY OF BRITISH COLUMBIA

27th July, 1984

86

Department of Mechanical Engineering

THE UNIVERSITY OF BRITISH COLUMBIA
2075 Wesbrook Place
Vancouver, Canada
V6T 1W5

Date: 27th July, 1984

ABSTRACT

The added mass and damping coefficients of a compound circular cylinder in heave motion are computed theoretically using a semi analytical potential flow method. The method uses continuity of pressures and velocities between adjacent regions of the flow field. The heave exciting forces on the compound cylinder are calculated from the heave damping coefficient. The hydrodynamic coefficients and the heave exciting forces are compared to theoretical results obtained from a boundary element method.

The hydrodynamic coefficients of the compound circular cylinder are determined experimentally by forced harmonic oscillation of the cylinder model. The wave height at a point in the flow field was also measured during the experiment. The effects of variation of amplitude and frequency of oscillation and draft are also studied experimentally. The results are compared to the theoretical predictions.

The heave exciting forces on a compound cylinder model due to small amplitude, sinusoidal waves are measured experimentally in a towing tank. The results are compared to predictions by the theoretical method presented in this thesis and by a boundary element method. The heave exciting forces on single and double cylinder models are also determined experimentally. These results are compared to theoretical predictions by a boundary element method.

The comparisons between theory and experiment show the applicability of linear potential flow theory in the determination of the hydrodynamic coefficients of the compound cylinder model.

Table of Contents

LIST OF FIGURES

ACKNOWLEDGEMENTS

I am deeply indebted to Dr.S.M.Calisal for his patient guidance throughout the course of this research.I am also indebted to NSERC for the financial support for this project.

My sincere gratitude to Michael Desandoli for his assistance with the experiments and data analysis. Thanks are also due to Johnson Chan for the use of his boundary element program for computation of heave exciting forces on axisymmetric floating objects.

I would also like to thank Fraser Elhorn for redesigning the motion generator and John Hoar, and his technicians at the Machine Shop at the Mechanical Engineering Department for fabrication of the motion generator and the models. Special thanks are due to Bruce Hanson for doing an excellent job in reconstructing the motion generator.

I would like to thank Gerry Stensgaard for permission to use the towing tank at B.C.Research and George Roddan for his expert advice on the instrumentation. I would like to thank Marcel Lefrançois for his assistance with the instrumentation for data collection and Steve Thomson for assistance with the equipment handling.

Finally, I wish to thank Angela Runnals and Jon Nightingale for their assistance with the text processor TEXTFORM on which this thesis was prepared.

DEDICATION

This thesis is dedicated to my parents for their love and affection, and to my wife for her patient forebearance during the course of my studies.

1. INTRODUCTION

In the last few decades there has been an accelerated growth in the offshore industry. A wide variety of offshore structures have been designed and constructed, primarily for oil exploration, drilling, production and storage. The main features in the continuing growth of offshore structures are their size and the depth at which they are capable of operating.

Since there is considerable investment going into a large offshore structure and it is expected to have a fairly long design life (upto 100 years in some cases), considerable research has been and is being devoted to the problems associated with the design of these structures.

Of primary importance are the loads which the structure experiences and the motions it undergoes. The loading on the structure is primarily hydrodynamic, i.e. due to the action of the ocean waves on the structure. Even if the extreme sea states were known accurately, it would still be difficult to estimate exactly the nature of the loading on the structure.

To mathematically model the actual flow around a full scale offshore structure poses considerable difficulties and an exact picture of the problem is beyond the reach of the present state of the analytical techniques. Several simplifications have to be made in the mathematical modelling of the flow. These are discussed in relevance to the topic of this thesis in Chapter 2.

Most of the offshore structures in current use have component members of circular section. So, the study of flows around circular cylinders are of considerable importance and much research has been devoted to this topic.

To study the hydrodynamic loads and resulting motions of any structure floating in a fluid medium it is neccessary to determine two quantities (known as the hydrodynamic coefficients): the added mass and damping coefficients. In addition, it is also neccessary to know the exciting forces on the structure.

A body accelerating in a fluid medium experiences an additional force due to the acceleration of a part of the fluid also.This additional hydrodynamic force can be expressed as an added mass to the body's mass, being accelerated at the same rate. This fact was first recognized by Chevalier du Buat about 200 years ago. Since then several researchers including Bessel, Green, Plana, Stokes, Lamb, and even Sir Charles Darwin have worked on the problem /8/. Sir Charles Darwin showed that a cylinder moving through a fluid medium displaces fluid particles in the direction of its motion. Further, he showed that this permanently displaced mass of the fluid enclosed between the initial and final positions of the fluid particles is the added mass itself. Added mass can be expressed mathematically in various ways. One of the definitions is given later.

If we consider the Cartesian co-ordinate system shown in Fig. 1, translatory oscillations in the x, y, and z

directions are known as surge, sway and heave, respectively.Rotational motions about the same axes are known as roll, pitch and yaw, respectively. For each direction of motion there exist six added mass coefficients corresponding to the displacement of the fluid in the six degrees of freedom. Hence added mass may be expressed as a tensor a_{ij} where the first subscript refers to the direction of the body motion and the second to the direction of the hydrodynamic force. Of the 36 added mass coefficients, it can be shown that $a_{ij} = a_{ji}$ and hence there are only 21 independent coefficients. These may be further reduced for a body symmetric about one or more axes /5/.

When a body moves periodically in a fluid medium near the free surface, the hydrodynamic force develops frequency dependent components in-phase and out-of-phase with the acceleration. The component in-phase with the acceleration contributes to the added mass and the component in-phase with the velocity contributes to the damping coefficient.

Further, for a body with separated flow about it, the wake or cavity induces an added mass. This cavity induced mass varies with the instantaneous shape and volume of the cavity and its rate of change. The instantaneous value of the added mass depends on the time history of the motion.Also, for motion in a viscous fluid there exists some viscous damping too.

The added mass coefficients depend, in general, on the parameters characterizing the motion, time, a suitably

defined Reynold's number, etc. The determination of an expression for the the time dependent force on a body undergoing an arbitrary motion is a very complex problem.

This problem is simplified by considering simpler time dependent motions like harmonic oscillations. A further simplification is achieved by using the potential flow theory to describe the flow.

Several theoretical and experimental techniques have been devised to determine the hydrodynamic coefficients of a wide range of bodies.

The common approaches to solution of boundary value problems in potential flow theory are analytical methods like conformal mapping and numerical procedures like singularity techniques. In recent years the finite element methods have also been successfully used.

Conformal mapping can be used only for two dimensional problems. The singularity methods do not suffer from this limitation. They have been used extensively in hydrodynamic problems in recent years /1/.

Havelock(1955) determined the hydrodynamic coefficients of a sphere /12/. Kim (1974) studied the hydrodynamic coefficients for ellipsoidal bodies oscillating near the free surface /18/. Wang and Shen (1966) calculated the added mass and damping coefficients of a sphere in water of finite depth /21/.

Garrison (1975) used distributed singularities to calculate the hydrodynamic coefficients of vertical circular

cylinders in water of finite depth /15/. He formulated the general problem for arbitrary forms too. Bai and Yeung (1974) calculated added mass and damping coefficients for horizontal and vertical circular cylinders /14/. Bai (1976) calculated the hydrodynamic coefficients of axisymmetric ocean platforms /13/. Kritis (1979) used the hybrid integral method of Yeung (1975) /22/ to numerically calculate the hydrodynamic coefficients for a circular cylinder /19/.

While the singularity methods have several significant advantages and are extensively used in the design of offshore structures, they also have some disadvantages. There is considerable computation involved and the choice of the discretization of the body surface must be made carefully. Further, these methods sometimes give numerical problems at certain frequencies which are called "irregular frequencies" for the method. The finite element methods do not have this disadvantage, but they require the entire flow field to be discretized. This is considerably difficult unless it is handled by a computer.

Analytic methods can handle only a small number of well defined geometric shapes. Even for these, there is, sometimes considerable mathematical difficulty.

This thesis discusses the determination of the added mass and damping coefficients for a compound circular cylinder undergoing simple harmonic heave motion at the free surface in water of finite depth.The hydrodynamic coefficients are obtained using a theoretical method as well

as experiments. Experiments were also conducted to determine the heave exciting force due to harmonic waves incident on a rigid model. These results are also compared to theoretical predictions.

The theoretical method discussed here is applicable to a special class of axisymmetric bodies. It can be termed an analytic method as well as a macro-element technique, in the sense that the flow field is divided into a few elements. The value of the potential is explicitly known in the interior domain as a function of the vertical and radial coordinates.

The basis of the method is suggested by Garrett in his paper on wave loads on a circular dock /4/. This method has been applied to the case of a single circular cylinder by Sabuncu and Calisal with good results /1/. The method has also been applied by K.Kokkinowrachos et. al /3/ in the predicion of hydrodynamic coefficients of bodies of several arbitrary axisymmetric shapes.

The experimental results presented in this thesis correspond to the forced harmonic oscillation of a compound cylinder model in a towing tank. This gave the hydrodynamic coefficients of the cylinder model. A qualitative study of the vortex shedding during the cylinder motion was also made with the help of an underwater window at the towing tank. The heave exciting force due to small amplitude waves on three cylinder models of different shapes was determined at varying drafts for the models and different amplitudes of

the waves. These results were compared to a theoretical prediction using a boundary element technique applied by Chan /11/. The heave exciting forces for the compound circular cylinder model were also compared to predictions using the present theory.

2. THEORETICAL MODEL AND SOLUTION

Using dimensional analysis relating to the wave force on a fixed body, one can conveniently compare the relative importance of flow separation and diffraction effects /8/. A time invariant force on a fixed structure due to an incident wave can be expressed as,

$$F/\rho g H D^2 = f(d/L,\ H/L,\ D/L,\ Rn), \qquad \ldots(2.1)$$

where,

ρ = Density of water;

g = Acceleration due to gravity;

d = Depth of water;

L = Wavelength;

H = Wave height;

D = Representative diameter of body;

Rn = Reynolds number.

The body size to wavelength ratio, D/L is termed the diffraction parameter. As D/L becomes large, diffraction effects become important. When diffraction effects are important, flow separation is relatively unimportant and the problem can be studied by potential flow methods. Further, it is assumed that the wave steepness, H/L is small corresponding to linear wave theory /8/,/3/.

A linearised boundary value problem is thus formulated for the velocity potential in the flow field.

2.1 GENERAL FORMULATION OF THE BOUNDARY VALUE PROBLEM

Consider the compound circular cylinder shown in Fig.2 with a sinusoidal wave incident on it.

The fluid is assumed to be homogeneous, inviscid and incompressible. An earth fixed cylindrical coordinate system with origin on the seabed is defined as shown in Fig.2 with the z-axis coinciding with the vertical axis of the cylinder.

It is further assumed that the amplitude of the cylinder motion is small compared to the wavelength and that the amplitude of the incident wave is also small compared to the wavelength.

The velocity potential for the flow field in the presence of the cylinder can, in general, be expressed in the form:

$$\Phi(x,y,z,t) = \Phi_o(x,y,z,t) + \Phi_d(x,y,z,t) \qquad \ldots(2.2)$$

In the above Φ_o is the potential of the undisturbed waveform and Φ_d is the disturbance potential. As a consequence of linearisation, the potential Φ_d can be further expressed as,

$$\Phi_d(x,y,z,t) = \Phi_F(x,y,z,t) + \sum_{j=1}^{6} \dot{s}_{j_o} \, \phi_j \, (x,y,z,t) \qquad \ldots(2.3)$$

where, Φ_F is the potential due to a stationary body in the wavefield and ϕ_j are the potentials due to the motions of the body in the six component directions with unit velocity,

in undisturbed water. $\dot{s}_{j_o}$ is the magnitude of the velocity of the body motion in the jth direction. Hence,

$$\Phi(x,y,z,t) = \Phi_o(x,y,z,t) + \Phi_F(x,y,z,t) + \sum_{j=1}^{6} \dot{s}_{j_o} \phi_j (x,y,z,t) \qquad ...(2.4)$$

The potentials Φ, Φ_o, Φ_F , $\phi_{1..6}$ are harmonic, with the frequency of the incident wave and hence,

$$\Phi(x,y,z,t) = \phi(x,y,z)\, e^{-i\omega t} \qquad ...(2.5)$$

With the assumption that the cylinder motion is harmonic,

$$s_j = s_{j_o}\, e^{-i\omega t}$$

The problem can now be formulated in two parts. One due to the wave incident on a fixed structure (diffraction problem), and the second due to the motion of the body in undisturbed water. The assumption of linearisation enables us to consider the individual degrees of freedom independent of each other . The cross-coupling terms have to be considered if they are linear.

The potentials ϕ_j must satisfy the governing Laplace's equation,

$$\nabla^2 \phi_j (x,y,z) = 0 \qquad ...(2.6)$$

and the following boundary conditions. (i) Linearised free surface kinematic and dynamic boundary conditions.

$$\frac{\partial \phi_j}{\partial z} = \frac{\partial \eta}{\partial t} \quad \text{for } z=d \qquad \ldots(2.7)$$

$$\frac{\partial \phi_j}{\partial t} = -g\eta \text{ for } z=d \qquad \ldots(2.8)$$

The above can be written as,

$$\frac{\partial^2 \Phi_j}{\partial t^2} + g\frac{\partial \Phi_j}{\partial z} = 0$$

or,

$$-\omega^2 \phi_j + g\frac{\partial^2 \phi_j}{\partial z^2} = 0 \text{ for } z=d \qquad \ldots(2.9)$$

(ii) Ocean bottom boundary condition.

$$\frac{\partial \phi_j}{\partial z} = 0 \text{ for } z=0 \qquad \ldots(2.10)$$

(iii) Radiation condition.

$$\lim_{r\ \infty} \sqrt{r}\left(\frac{\partial \phi_j}{\partial r} - i(\omega^2/g)\ \phi_j \right) = 0 \qquad \ldots(2.11)$$

The following boundary conditions must also be satisfied on the body surface.

(iv) For a wave incident on a fixed structure, on the body surface S,

$$\frac{\partial \phi_o}{\partial n} = - \frac{\partial \phi_F}{\partial n} \qquad ...(2.12)$$

(v) For a floating body free to move in calm water,

$$\frac{\partial \Phi_j}{\partial n} = n_j \, e^{-i\omega t} \, |_S \qquad ...(2.13)$$

or,

$$\frac{\partial \phi_j}{\partial n} = n_j \, |_S$$

where, n_j is the component of the outward normal on the body surface S, in the jth direction as shown in Fig.1.

2.2 LOADS AND MOTIONS

The instantaeneous linearised pressure on the body is given by,

$$p_{inst} = -\rho \frac{\partial \Phi}{\partial t} \qquad ...(2.14)$$

Using (2.4), we can rewrite this as,

$$p_{inst} = i\omega\rho \, [\, \phi_o + \phi_F + \sum_{j=1}^{6} \dot{s}_{j_o} \, \phi_j \,] \, e^{-i\omega t}$$

It is expedient to divide the force into that due to the diffraction and that due to the motion.

The diffraction problem gives the exciting force due to the incident wave,

$$F_{E_k}(t) = -\iint_S p_{inst.}\, n_k\, dS$$

$$= -i\omega\rho\, e^{-i\omega t} \iint_S (\phi_o + \phi_F)\, n_k\, dS \qquad \ldots(2.15)$$

where, k=1,2,..6 .

The hydrodynamic forces due to the motion of the body in undisturbed water can be calculated using the potentials ϕ_j .

$$F_{H_k} = -i\omega\rho\, e^{-i\omega t} \iint_S \sum_{j=1}^{6} \dot{s}_{j_o}\, \phi_j\, n_k\, dS \qquad \ldots(2.16)$$

Now, we define the added masses, a_{kj} and damping coefficients, b_{kj} as in /3/.

$$-\rho \iint_S \phi_j\, n_k\, dS = a_{kj} + (i/\omega)\, b_{kj} \qquad \ldots(2.17)$$

where,

$$a_{kj} = -\rho\, \mathrm{Re}\, [\iint_S \phi_j\, n_k\, dS] \qquad \ldots(2.17a)$$

$$b_{kj} = -\rho\, \mathrm{Im}\, [\iint_S \phi_j\, n_k\, dS] \qquad \ldots(2.17b)$$

Now, we can write (2.16) in the form,

$$F_{H_k}(t) = \sum_{j=1}^{6} (a_{kj}\, \ddot{s}_j + b_{kj}\, \dot{s}_j) \qquad \ldots(2.18)$$

a_{kj} represent added mass in the case of translation and added mass moments of inertia in the case of rotational motions. b_{kj} are the damping coefficients. k indicates the

direction of the force and j indicates the direction of the motion.

Using the above we can, in general, write a system of six coupled differential equations for the motion of a floating body due to an incident wave as,

$$\sum_{j=1}^{6} (m_{kj} + a_{kj}) \ddot{s}_j + b_{kj} \dot{s}_j + c_{kj} s_j = F_{E_k} \qquad \ldots(2.19)$$

where, c_{kj} are the restoring force coefficients and m_{kj} are the masses or the mass moments of inertia of the body.

In the special case of a body restrained to undergo heave motion only, the above system reduces to an ordinary differential equation,

$$(m + a_{22}) \ddot{q} + b_{22} \dot{q} + c_{22} q = F_{E_2}(t) \qquad \ldots(2.20)$$

where q denotes heave motion.

2.3 HEAVE MOTION OF COMPOUND CYLINDER

Consider the compound cylinder with geometry as shown in Fig.2. The problem is to define the potential during the heave motion of the cylinder. The flow field is subdivided as follows.

2.3.1 DEFINITION OF FLOW FIELD

The subdivision is shown in Fig.3. Though only a section is shown because of the axial symmetry, the elements are actually cylindrical.

Region 1 is defined as the volume within the surface $r=a_1$, $0 \le z \le d_1$.

Region 2 is defined as the volume within the surfaces $r=a_1$, $0 \le z \le d_2$ and $r=a_2$, $0 \le z \le d_2$.

Region 3 is defined as the volume within the surfaces $r=a_3$, $d_3 \le z \le d$ and $r=a_2$, $d_3 \le z \le d$.

The exterior region is defined as the volume exterior to the surface $r=a_2$, $0 \le z \le d$.

Using Garrett's method potentials are defined in the four regions as Φ_1, Φ_2, Φ_3, Φ_E , respectively.

2.3.2 GOVERNING EQUATIONS AND BOUNDARY CONDITIONS

The velocity potentials Φ must satisfy Laplace's equation from the irrotational assumption made earlier /9/.

$$\nabla^2 \phi = \frac{\partial^2 \phi}{\partial r^2} + (1/r) \frac{\partial \phi}{\partial r} + (1/r^2) \frac{\partial^2 \phi}{\partial \theta^2} + \frac{\partial^2 \phi}{\partial z^2} = 0 \qquad ...(2.6)$$

The equation is defined in cylindrical coordinates defined as in Fig.2. ϕ can be written as,

$$\phi(r,\theta,z) = R(r)\ T(\theta)\ Z(z) \qquad ...(2.21)$$

if the variables are assumed to be independent of each other. Using separation of variables, (2.6) can be written

as three ordinary linear differential equations as,

$$\frac{d^2T}{d\theta^2} + A^2T = 0 \qquad ...(2.22)$$

$$\frac{d^2Z}{dz^2} - B^2Z = 0 \qquad ...(2.23)$$

$$\frac{d^2R}{dr^2} + (1/r)\frac{dR}{dr} + (B^2-A^2/r^2)R = 0 \qquad ...(2.24)$$

Since the flow is axisymmetric the axial function has to be an even function. Hence,

$$T(\theta) = \cos(m\theta) \qquad ...(2.25)$$

We can write the potential Φ as

$$\Phi(r,\theta,z,t) = \phi(r,z)\, e^{-i\omega t} \qquad ...(2.26)$$

The coefficient m is taken as zero on the assumption that the most significant contribution comes from the first term of the cosine series for θ.

2.3.3 DEFINITION OF POTENTIALS

The potentials Φ_1, Φ_2, Φ_3, Φ_E are defined such that they satisfy the governing equations and boundary conditions as below.

2.3.3.1 Region 1

The potential $\Phi_1 = \phi_1 V_H d\, e^{-i\omega t}$ has to satisfy the following boundary conditions. V_H is the velocity in the heave direction.

$$\frac{\partial\phi_1}{\partial z} = 1 \text{ at } z=d_1 \qquad ...(2.27)$$

$$\frac{\partial\phi_1}{\partial z} = 0 \text{ at } z=0 \qquad ...(2.28)$$

The potential Φ_1 satisfies the governing equation (2.22) and (2.23) and the boundary conditions (2.27) and (2.28). The potential ϕ_1 comprises of the particular solution,

$$\phi_{1p} = [(z^2-r^2/2)/2dd_1] \qquad \ldots(2.29a)$$

and the homogeneous solution,

$$\phi_{1h} = A_0/2 + \sum_{n=1}^{\infty} A_n \, (I_0(n\pi r/d_1)/I_0(n\pi \, a_1/d_1))\cos(n\pi z/d_1)] \qquad \ldots(2.29b)$$

Hence,

$$\Phi_1 = V_H \, d \, e^{-i\omega t} \, [(z^2-r^2/2)/2dd_1 + A_0/2 + \sum_{n=1}^{\infty} A_n \, (I_0(n\pi r/d_1)/I_0(n\pi a_1/d_1)) \cos(n\pi z/d_1)] \qquad \ldots(2.29)$$

The coefficients A_0 and A_n are unknown and will be fixed later in the solution. I_0 is the modified Bessel function of the first kind.

2.3.3.2 Region 2

The potential $\Phi_2 = \phi_2 \, V_H \, d \, e^{-i\omega t}$ has to satisfy the following boundary conditions.

$$\frac{\partial \phi_2}{\partial z} = 1 \text{ at } z=d_2 \qquad \ldots(2.30)$$

$$\frac{\partial \phi_2}{\partial z} = 0 \text{ at } z=0 \qquad \ldots(2.31)$$

The potential Φ_2 satisfies the governing equation (2.22) and (2.23) and the boundary conditions (2.30) and (2.31). The potential ϕ_2 comprises of the particular solution

$$\phi_{2p} = (z^2-r^2/2)/2dd_2 \qquad \ldots(2.32a)$$

$$\phi_{2h} = B_0 + \sum_{n=1}^{\infty} \{B_n V_n (r) + C_n W_n (r)\} \cos(n\pi z/d_2) \quad \ldots(2.32b)$$

and adding the above,

$$\Phi_2 = V_H d e^{-i\omega t} [(z^2 - r^2/2)/2dd_1 + B_0 + \sum_{n=1}^{\infty} \{B_n V_n (r) + C_n W_n (r)\} \cos(n\pi z/d_2)] \quad \ldots(2.32)$$

where

$$V_n (r) = \frac{I_0(n\pi r/d_2) + (I_1(n\pi a_1/d_2) / K_1(n\pi a_1/d_2)) K_0(n\pi r/d_2)}{I_0(n\pi a_2/d_2) + (I_1(n\pi a_1/d_2) / K_1(n\pi a_1/d_2)) K_0(n\pi a_2/d_2)} \quad \ldots(2.33)$$

$$W_n (r) = \frac{I_0(n\pi r/d_2) + (I_0(n\pi a_2/d_2) / K_0(n\pi a_2/d_2)) K_0(n\pi r/d_2)}{I_1(n\pi a_1/d_2) + (I_0(n\pi a_2/d_2) / K_0(n\pi a_2/d_2)) K_1(n\pi a_1/d_2)} \quad \ldots(2.34)$$

B_0 and B_n are unknown coefficients which are determined by the radial boundary conditions.

Φ_2 as defined in (2.32) satisfies (2.22), (2.23), (2.30) and (2.31).

2.3.3.3 Region 3

The potential in this region $\Phi_3 = \phi_3 V_H d e^{-i\omega t}$ satisfies the governing equation and the boundary conditions

$$\frac{\partial \phi_3}{\partial z} = 1 \text{ at } z=d_3 \qquad \ldots(2.35)$$

and

$$-\omega^2 \phi_3 + g \frac{\partial \phi_3}{\partial z} = 0 \text{ at } z=d \qquad \ldots(2.36)$$

The velocity potential in this region is defined by a particular solution,

$$\phi_{3p} = (z/d+g/(\omega^2 d)-1) \qquad \ldots(2.37a)$$

and a homogeneous solution,

$$\phi_{3h} = D_0 X_0 \bar{Y}_0 + \sum_{n=1}^{\infty} D_n X_n \bar{Y}_n \qquad \ldots(2.37b)$$

Combining the above,

$$\Phi_3 = V_H d e^{-i\omega t} [(z/d+g/(\omega^2 d)-1) + D_0 X_0 \bar{Y}_0 + \sum_{n=1}^{\infty} D_n X_n \bar{Y}_n] \qquad \ldots(2.37)$$

where,

$$X_0 = \frac{J_0(m_0 r) - (J_1(m_0 a_3) / H_1(m_0 a_3)) H_0(m_0 r)}{J_0(m_0 a_2) - (J_1(m_0 a_3) / H_1(m_0 a_3)) H_0(m_0 a_2)} \qquad \ldots(2.38)$$

$$X_n = \frac{I_0(m_n\ r) + (\ I_1(m_n\ a_3)\ /\ K_1(m_n\ a_3)\ )\ K_0(m_n\ r)}{I_0(m_n\ a_2) - (\ I_1(m_n\ a_3)\ /\ K_1(m_n\ a_3)\ )\ K_0(m_n\ a_2)} \qquad ...(2.39)$$

In this formulation,

$$\tilde{Y}_0 = M_0^{-1/2} \cosh[m_0(z-d_3)] \qquad ...(2.40)$$

$$M_0 = [1+\sinh\{2m_0(d-d_3)\}/2m_0(d-d_3)]/2 \qquad ...(2.40a)$$

$$\tilde{Y}_n = M_n^{-1/2} \cos[m_n\ (z-d_3)] \qquad ...(2.41)$$

$$M_n = [1+\sin\{2m_0(d-d_3)\}/2m_0(d-d_3)]/2 \qquad ...(2.41a)$$

where m_0 and m_n are the roots of,

$$\omega^2 - g\ m_0 \tanh[m_0(d-d_3)] = 0 \qquad ...(2.42)$$

$$\omega^2 + g\ m_n\ \tan[m_n\ (d-d_3)] = 0 \qquad ...(2.42a)$$

respectively.

2.3.3.4 Exterior region

The potential in the exterior region $\Phi_E = \phi_E V_H d e^{-i\omega t}$ has to satisfy the governing equation (2.6) and the following boundary conditions,

$$\frac{\partial \Phi_E}{\partial z} = 0 \text{ at } z=0 \qquad \ldots(2.43)$$

$$-\omega^2 \phi_E + g \frac{\partial \phi_E}{\partial z} = 0 \text{ at } z=d \qquad \ldots(2.44)$$

The potential Φ_E describing the free wave and the waves reflected off the rigid cylinder is given by,

$$\Phi_E = V_H d e^{-i\omega t}[-E_0(H_0(k_0 r)/H_1(k_0 a_2))Z_0(z)$$

$$- \sum_{n=1}^{\infty} E_n (K_0(k_n r)/K_1(k_n a_2)) Z_n(z)] \qquad \ldots(2.45)$$

where,

$$Z_0 = N_0^{-1/2} \cosh[k_0 z] \qquad \ldots(2.46a)$$

$$N_0 = [1+\sinh\{2k_0 d\}/2k_0 d]/2 \qquad \ldots(2.46b)$$

$$Z_n = N_n^{-1/2} \cos[k_n z] \qquad \ldots(2.47a)$$

$$N_n = [1+\sin\{2k_o d\}/2k_o d]/2 \qquad \ldots(2.47b)$$

E_o and E_n are unknown coefficients determined as described later and k_o and k_n are the roots of

$$\omega^2 - gk_o \tanh[k_o d] = 0$$

$$\omega^2 + gk_n \tan[k_n d] = 0$$

respectively.

Φ_E as defined in (2.43) satisfies (2.22), (2.23), (2.43) and (2.44).

In the above, I is the modified Bessel function of the first kind, K is the modified Bessel function of the second kind, J is the Bessel function of the first kind and H is the Hankel function of the first kind.

2.4 SOLUTION FOR UNKNOWN COEFFICIENTS FOR POTENTIALS

The unknown coefficients of the series for the potentials A_n , B_n , C_n , D_n and E_n are determined by matching the pressures and velocities between adjacent regions.

The procedure is detailed in Appendix 1. The matching of the pressures and velocities between adjacent regions

results in five systems of linear simultaeneous equations. The number of equations in each system is equal to the number of terms taken for the series and is also equal to the number of unknown coefficients.

The system of equations is solved using a Gaussian elimination routine CDSOLN which permits the use of double precision complex variables. The routine is available on the Michigan Terminal System at the University of British Columbia and is efficient. Typically, for 20 terms in the series, the procedure involves solving a 100 X 100 matrix and the Amdahl 470 V/8 computer accomplishes this in 2.6 seconds.

2.5 CALCULATION OF THE ADDED MASS AND DAMPING COEFFICIENTS

The added mass and damping coefficients of the compound cylinder in heave motion are related to the potential as follows from (2.15).

$$a_{22} /\rho V + i b_{22} /\rho V \omega = 1/V \iint_S \phi(r, \theta, z)\, n_2 \, dS \qquad ...(2.49)$$

ρ = Density of the medium.

V = Volume of the cylinder

ω = Frequency of the motion.

a_{22} = Added mass in heave motion.

b_{22} = Damping coefficient in heave motion.

n_2 = Unit normal in the z direction.

S denotes integral over the surface of the cylinder. The added mass and damping coefficient are non-dimensionalized as shown.

The potential ϕ is defined as different potentials in different regions. Hence the integral in (2.49) can be written as,

$$\iint_S \phi(r, \theta, z)\, n_z\, dS = \int_0^{2\pi} \left[\int_0^{a_1} \phi_1 + \int_{a_1}^{a_2} \phi_2 + \int_{a_3}^{a_2} \phi_3(-1) \right] r\, dr\, d\theta \qquad \ldots(2.50)$$

Using the axial symmetry of the potential functions (50) can be written as,

$$\iint_S \phi(r, \theta, z)\, n_z\, dS = 2\pi \left[\int_0^{a_1} \phi_1 + \int_{a_1}^{a_2} \phi_2 + \int_{a_3}^{a_2} \phi_3(-1) \right] r\, dr\, d\theta \qquad \ldots(2.51)$$

Evaluating the three integrals in (2.51) independently we can rewrite (2.49) as below,

$$a_{22} / \rho V + i b_{22} / \rho V \omega = (2\pi/V)\, [IN_1 + IN_2 + IN_3] \qquad \ldots(2.52)$$

where IN_1, IN_2, IN_3 are as evaluated in Appendix 1.

2.6 CALCULATION OF HEAVE EXCITING FORCE

The amplitude of the heave exciting force can be calculated from the damping coefficient b_{22} using a relationship given by Newman /8/ as follows.

$$F_{22} = (\rho g H^2 b_{22} \omega / 2k^2) \; [1 + 2kd/\sinh(2kd)]\}^{-1/2} \qquad ...(2.53)$$

The heave exciting force computed as above is compared to the experimental results and a prediction by a boundary element program, later. In (2.53),

F_{22}	= Heave exciting force
b_{22}	= Heave damping coefficient
ρ	= density of medium
g	= acceleration due to gravity
H	= incident wave height
ω	= wave circular frequency
d	= water depth
k	= Wave number

2.7 CALCULATION OF WAVE AMPLITUDE

The wave elevation at any point on the free surface can be computed from the potential for the flow field using the following equation from linear theory /9/.

$$\eta = -(1/g) \frac{\partial \Phi}{\partial t} \qquad ...(2.54)$$

where, η is the wave elevation and g is the acceleration due to gravity. Φ is the potential function for the region in the flow field where the wave elvation is desired.

2.8 COMPUTER PROGRAM

A computer program, CYLINDER was written to set up and solve the system of equations to determine the unknown coefficients for the potentials as described earlier in this chapter. The program also computes the potentials and their normal derivatives at any point in the flow field. Finally, the program computes the added mass and damping coefficients for the compound circular cylinder in heave motion.

The program requires as input the dimensions a_1, a_2, a_3, d_1, d_2 and d_3 of the compound circular cylinder as shown in Fig. 2. It also requires the frequency of the motion, the depth of water, d and the number of terms to be taken in the series for the potential.

The program takes 2.8 seconds to compute the added mass and damping coefficient for the compound cylinder at one frequency.

3. EXPERIMENTAL WORK

Experiments were conducted in the towing tank at the Ocean Engineering Centre (O.E.C.) at B.C.Research, Vancouver to verify the theoretical results.

3.1 PURPOSE OF EXPERIMENTS

Two different sets of experiments were conducted. The first set of experiments were performed to evaluate the hydrodynamic coefficients in heave motion of a compound circular cylinder model. The experiments were conducted to verify the theoretical predictions of the hydrodynamic coefficients. The compound cylinder model was tested at four different drafts to estimate the effect of the depth of Region 3 (fig. 3) on the added mass and damping coefficient. Wave heights at a fixed distance from the cylinder centreline were measured to compare them with the theoretically predicted wave heights using Eqn. 2.54.

The second set of experiments were conducted to evaluate the heave exciting force on three models - a compound cylinder, a double cylinder and a single cylinder. Dimensions of the three cylinders are shown on Figs. 4, 5, and 6. Descriptions of the models are given in Appendix 2. The exciting forces on the compound cylinder model were used to compare with the values theoretically computed from the heave damping coefficient calculated using the matching technique. This provides a method for verifying the heave damping coefficient computed using the matching technique,

as well as a verification of the relationship between the heave damping coefficient and the heave exciting force (Eqn. 2.53). The experiments with the single and double cylinder models were used to verify a prediction using the boundary element method.

The experimental facilities used are described in Appendix 2. Besides the experiments mentioned above, a qualitative observation of the vortex shedding during the compound cylinder motion was also made.

3.2 DETERMINATION OF HYDRODYNAMIC COEFFICIENTS

Forced harmonic oscillations of the compound cylinder model were used to determine its hydrodynamic coefficients in heave motion.

Fig.7 shows a photograph of the towing tank. Its dimensions and other particulars are given in Appendix 2. Fig. 8 shows a photograph of the motion generator used along with the associated pump and control gear. A brief description is given in Appendix 2. The cylinder model was mounted as shown , ballasted suitably so that it was nearly neutrally buoyant. Fig.9 shows the equipment on board the O.E.C. towing carriage which was used for the data collection. These are also described in Appendix 2.

The motion generator gives a small amplitude sinusoidal motion to the cylinder model at a fixed frequency. The amplitude of oscillation can be varied. The force on the cylinder is measured continuously with the help of

dynamometers. Two types of dynamometers were used. One is a 3-component measuring device which is capable of reading a vertical force, a horizontal force and moment simultaneously. Interaction effects of the three quantities are minimized by a suitable circuit design. The second type of dynamometer used were Universal Shear Beams manufactured by HBM Inc. of Framingham, MA. These were capable of measuring only vertical forces. Two of these used in conjunction. Moments and horizontal forces were excluded by design. The dynamometers are described in Appendix 2.

The cylinder motion was measured by a sonar displacement measurement device positioned over the cylinder model.

Tests were performed at two different amplitudes of motion of 10 mm. and 15 mm. to check the dependence of the force measurements and hence the added mass and damping coefficient on the amplitude of motion.

Thus, continuous simultaneous records of the vertical forces on the cylinder and the displacement of the cylinder were obtained. The signals were suitably amplified using amplifiers on the O.E.C. towing carriage and stored on the O.E.C. MINC-11 computer. The data collection software is described in Appendix 2. The data was multiplexed and stored on disk.

3.2.1 DATA ANALYSIS

The data was demultiplexed and a spectral analysis was performed on the force and displacement records, using Fast Fourier Transforms. This was done to eliminate noise and extraneous measurements other than at the driving frequency.

The spectral analysis yielded the force and displacement amplitudes and phases at the driven frequency. The phases were corrected for the phase shifts induced by the amplifiers. Knowing these the forces in phase with the acceleration, F_A and in phase with the velocity, F_V were computed. Then,

$$F_A = (m+a_{22})\ddot{x} = -(m+a_{22})\omega^2 x_0 \, e^{-i\omega t} \qquad ...(3.1)$$

and,

$$F_V = b_{22}\,\dot{x} = -i\omega(b_{22}\,x_0)\,e^{-i\omega t} \qquad ...(3.2)$$

where,

x_0 = Amplitude of the displacement.

m = mass of cylinder

ω = Driven frequency

a_{22} = Added mass coefficient

b_{22} = Damping coefficient

From the above a_{22} and b_{22} for the driven frequency are calculated as,

$$a_{22} = -(F_A/\omega^2 x_0) - m$$

$$b_{22} = F_V/\omega x_0$$

Experiments were performed at about ten frequencies for each draft. The experiments were repeated for different drafts. The results are plotted in non-dimensional form as

described later. The software used for the data collection and analysis are described in Appendix 2.

3.3 DETERMINATION OF HEAVE EXCITING FORCE

For these experiments the cylinder was held stationary at a specified draft. Small amplitude sinusoidal waves were generated using the paddle type wavemaker at the O.E.C. Fig.10 shows a photograph of the wavemaker. A brief description of its operation and components is given in Appendix 2.

A resistance wave probe was used to measure the wave height. A description is given in Appendix 2. The vertical exciting force on the model was recorded using the 3-component dynamometer. The MINC-11 computer and the O.E.C. towing carriage were used for data collection as before.

A spectral analysis on the wave record using Fast Fourier Transforms gave the wave amplitude and phase at a particular frequency. The same analysis on the force record gave the force amplitude and phase. The wave phase was adjusted for the position for the wave probe. Thus, the vertical exciting force due to a wave at a specified amplitude and frequency was determined. The experiments were repeated for different frequencies for each draft for three cylinder models. The configurations were as shown in Figs. 4,5, and 6.

The non-dimensional exciting force per foot of wave height was plotted versus frequency. The results are

compared with a theoretical prediction by a boundary element method by Chan /11/ . The results are discussed later. The software used is described in Appendix 2.

3.4 FLOW VISUALIZATION

Flow visualization tests were conducted to observe qualitatively the vortex shedding process on a single cylinder model and a compound cylinder model.

Dye was injected through points on the cylinder's surface by means of capillary tubing. The cylinder was oscillated and the vortex shedding was observed through an illuminated underwater window at the towing tank. A record was made on video tape. Fig. 11 shows a photograph illustrating the vortex shedding.

4. RESULTS AND DISCUSSION

The added mass and damping coefficient computed numerically using the matching technique are compared to the results from a boundary element method by Chan /11/ .

The heave added mass and damping coefficient are determined experimentally for the compound cylinder model for four drafts of 35.5", 39.5", 43.5", 47.5". These correspond to a step size, D' of 6", 10", 14" and 18" respectively. D' is as defined in Fig.2. The heave added mass and damping coefficient are determined for two different amplitudes of oscillation of 10mm and 15mm for the 35.5" draft. This is done to check the effect of the amplitude of oscillation on the hydrodynamic coefficients. For each draft the tests are conducted for over 10 frequencies in the range 0.2 to 2.5 Hz. Wave amplitude at a distance of 33" from the centreline of the oscillating cylinder is measured during the tests. Measurement of all quantities were done for at least 10 frequencies at each draft. The hydrodynamic coefficients determined experimentally and the wave height measured during the experiments are compared to theoretical predictions using the matching technique.

Flow visualisation tests were conducted during the oscillation of the compound cylinder model. They were conducted to observe the vortex shedding process.

Heave exciting forces due to small amplitude sinusoidal waves on a single cylinder, a double cylinder and a compound

cylinder were measured. The single cylinder was tested at two drafts of 7" and 10.5". The double cylinder was tested at two drafts of 23.5" and 27.5". The compound cylinder was tested at four drafts of 35.5", 38.375", 42.625" and 49.5". The configurations for the three cylinder models were as shown in Figs. 6,5 and 4 respectively. For each draft, tests were performed for at least two different amplitudes to check the dependence of the exciting forces on the amplitudes of the waves. For each draft, at each amplitude setting, the tests were performed for at least seven wave frequencies over the range of 0.25 to 2.5 Hz.

The experimental results for the compound cylinder are compared to theoretical predictions by the matching technique and a boundary element method. The experimental results for the single and double cylinder are compared only to the theoretical predictions by the boundary element method.

The theoretical method using the matching technique is as described in Chapter 2 and Appendix 1. The experimental technique, equipment and software are described in Chapter 3 and Appendix 2.

4.1 PRESENTATION OF DATA

The data is presented in the form of non-dimensional plots. Exceptions are the plots of wave height and heave exciting forces.

The heave added mass is plotted as $a_{22}/\rho V$ versus $\omega^2 a/g$. a_{22} is the heave added mass, ρ is the density of fresh water, and V is the volume of buoyancy for the cylinder at the respective draft. ω is the circular frequency of oscillation of the cylinder in radians/second, a is the maximum radius of the cylinder and g is the acceleration due to gravity. The heave damping coefficient is non-dimensionalised as $b_{22}/\rho V\omega$, where, b_{22} is the heave damping coefficient. The damping coefficient is plotted against the same non-dimensional frequency as the added mass. The wave amplitude in inches is plotted against the same non-dimensional frequency.

The heave exciting force, F is plotted as $F/\rho VgA$ versus $\omega^2 a/g$. Here ω is the wave circular frequency and A is the wave amplitude in feet. All other quantities are as above .

4.2 DISCUSSION OF THEORETICAL RESULTS

The computer program CYLINDER computes the added mass and damping coefficient in heave motion for the compound circular cylinder using the matching technique. For all results reported here, 20 terms were taken for each of the Fourier series for the potentials. The program was run for 5, 10, 15, 20, and 30 terms for the series and it was seen that satisfactory convergence of the hydrodynamic coefficients were acheived with 20 terms. The program takes 2.8 seconds of CPU time on the Amdahl 470 V/8 computer to calculate the hydrodynamic coefficients for the compound

cylinder at one frequency of oscillation when 20 terms are taken for the series.

The matching technique satisfies the continuity of pressure and velocity between adjacent regions in which potentials are defined (Chapter 2). But, this continuity is satisfied as an integral over the depth and not at every point on the common boundary between adjacent regions. Hence, when pressures and velocities are computed using the solved potentials, they are not continuous radially at points along the boundary between adjacent regions defined in Chapter 2. This discontinuity is more apparent in the radial derivatives of the potentials, than in the potentials themselves. Since the potentials are not affected significantly by this fact, the hydrodynamic coefficients which are computed using the potentials are not affected.

The computer program CYLINDER was run for the compound cylinder configuration shown in Fig. 4 at different drafts. Numerical difficulties were observed with step sizes, D', less than 6". These are due to the difficulty solving the dispersion relation for waves generated by a very shallow step size, D'.

The comparison of the results using the matching technique with predictions by the boundary element method show very good agreement. Fig.13 shows added mass values for the compound cylinder at a draft of 42.625" (D'=13.125"). The matching technique overpredicts the added mass in comparison to the boundary element method by approximately

4% at the higher frequencies. The agreement improves as the frequency decreases. Fig.14 shows a comparison of the damping coefficients computed by the matching technique and the boundary element methods. Here, the matching technique underpredicts the damping coefficient in comparison to the boundary element method. But, the difference is within 1% for most frequencies.

4.3 DISCUSSION OF EXPERIMENTAL RESULTS

4.3.1 HYDRODYNAMIC COEFFICIENTS

The experiments to determine the hydrodynamic coefficients in heave motion for the compound cylinder were first conducted in the Summer of 1983. However, the motion generator used for the experiments did not perform satisfactorily. The hydraulic pump and motor used for running the motion generator could not handle the load adequately. The scotch-yoke mechanism used in the motion generator induced considerable extraneous loads on the dynamometers due to vibrations. Further, it failed to produce a smooth sinusoidal motion.

For the above reasons the motion generator was redesigned and reconstructed and the tests repeated in June, 1984. The redesigned motion generator gave a smooth sinusoidal motion over a frequency range of 0.2 to 2.5 Hz. It was also capable of handling the imposed loads well. Fig.12 shows a time record of the motion and Fig.12a shows

an amplitude spectrum of the time record. It can be seen that the spectrum does not show any prominent peaks except at the driving frequency. Descriptions of the motion generator are given in Appendix 2.

Two 500 lb load cells were added to the system to verify the force measurement by the 80lb force block. They corroborated the readings of the 80 lb. force block which was used primarily for the data analysis. Details of the mounting of the 500 lb. force blocks are visible in Fig.8a.

Fig.15 shows a plot of the heave added mass of the compound cylinder model at a draft of 35.5" (D'=6"). The theoretical prediction is by the matching technique. The experimental plots show results for two amplitudes of oscillation of 0.39" and 0.5". The experimental results show an apparent increase of added mass with frequency. Reliable experimental results could not be obtained at frequencies below 1 Hz, because the magnitude of the forces measured were too small and the sensitivity of the dynamometers was not sufficient enough to measure values less than 0.5% of the full scale range accurately . The deviation in the added mass results with change in amplitude setting is not sufficient enough within the limits of the experimental accuracy to warrant any conclusions regarding non-linearity. The experiments at the remaining three drafts were conducted at the 0.5" amplitude setting, so that the forces would be large enough to measure at the lower frequencies. The theoretical curve shows a well defined peak at a frequency

of about 0.75 Hz. The added mass coefficient then drops sharply till a frequency of about 1.5 Hz and remains fairly constant till about 2.5 Hz, the upper end of the frequency range. The best agreement between the theoretical and experimental results is at frequencies close to 1.25 Hz. In general the experimental values are higher than the theoretical results.

Fig.16 shows a plot of the heave damping coefficient for the compound cylinder model at a draft of 35.5". The experimental results are compared to the theoretical prediction by the matching technique. The experimental results follow the same trend as the theoretical curve, but the experimental values are considerably higher than the theoretical values. Though the peak value appears at the same frequency for both experiment and theory, the magnitude of the damping coefficient as shown by experiment is higher by about 80% when compared to the theoretical result.

Fig.17 shows plots of the wave amplitude measured at a distance of 33" from the oscillating cylinder during the experiments. The theoretical curve is a prediction by the matching technique. The theoretical prediction is considerably higher than the experimentally measured values. They differ by about 50%. The difference may possibly be due to the interference from the tank walls.

Figs. 18,21 and 24 are plots of the added mass for the compound cylinder at drafts of 39.5", 43.5" and 47.5", respectively. The amplitude of oscillation is 0.5" in all

cases. The comparison between experiment and theory is much the same as for the 35.5" draft. However, the absolute value of the non-dimensional added mass decreases with increasing draft, according to the theoretical prediction. The experimental results, however, show the same range of variation for all the drafts.

Figs. 19, 22 and 25 are plots of the heave damping coefficient for cylinder drafts of 39.5", 43.5" and 47.5" respectively. The trends in the comparison between the theory and experiment are similar to those for the 35.5" draft. The value of the non-dimensional damping coefficient decreases with increasing draft. This is shown by both theory and experiment. This can be explained by the increase in step size, D' with increasing draft. This leads to a decreasing wavemaking action and hence a smaller damping coefficient at the deeper drafts.

Figs. 20, 23 and 26 are plots of the wave amplitude measured at a distance of 33" from the compound cylinder centreline for drafts of 39.5", 43.5" and 47.5". These plots show the same trend as Fig.17 for the 35.5" draft. The theoretical prediction is higher than the experimentally measured wave amplitudes. But, the experimental values show the same trend as the theoretical curve. The theoretical maximum wave amplitudes steadily decrease from about 0.3" at the 35.5" draft to about 0.1" at the maximum draft of 47.5". This can be attributed to the decreasing wavemaking action with increasing draft as mentioned in the previous

paragraph. The experimental results also show the same trend, decreasing from a maximum wave amplitude of about 0.15" at a 35.5" draft to a maximum of about 0.04" at the maximum draft of 47.5".

The added masses and damping coefficients determined experimentally do not show very close agreement with the theoretical results. This can be due to two reasons. The theory does not take into account the viscosity of the fluid medium, which exists in actual fact. The viscosity induces vortex shedding during the cylinder motion. This was observed during the flow visualisation tests conducted on the compound cylinder model (Chapter 3 and Fig.11). Vortex shedding takes place at the corners of the cylinder during the cylinder motion. This introduces viscous damping in addition to the potential damping due to the wavemaking action. This may explain why the experimentally determined damping coefficient is considerably higher than the theoretically predicted value. The extent of the viscous damping can be determined by modelling the vortex shedding at the corners theoretically.

The second cause for the difference between experimental and theoretical values may be due to the effect of the walls of the towing tank on the flow field during the cylinder motion. The walls are at a distance of 62" from the cylinder centreline on one side and 82" on the other side. The effect of the presence of the walls can only be isolated by performing the same tests in a very large basin and

comparing the results.

A further cause for the difference between the experimental and theoretical results may be inaccuracies in the measurement of the force, displacement and the phase shifts of the amplifiers. Care was taken in the calibration process to eliminate these as much as possible. However, a very small change of phase introduced electronically in the data collection process may affect the force in phase with the acceleration more than the force in phase with the velocity, since the former is proportional to the cosine of the phase and the latter is proportional to the sine of the phase. Thus, if a small error is introduced in the phase this will affect the added mass more than the damping coefficient and the error will increase as the forces measured increase. This may explain the reason for the increase in the added mass with frequency.

4.3.2 FLOW VISUALISATION TESTS

These tests were conducted in June,1983. A description of the tests is given in Chapter 3. They show the presence of vortex shedding at the corners of the compound circular cylinder. They suggest that the effects of viscosity may be important. The tests were recorded on video tape and photographs were also taken during the tests. Fig.11 shows one such photograph.

4.3.3 HEAVE EXCITING FORCES

Heave exciting forces due to small amplitude sinusoidal waves were measured on three different cylinder models. These experiments were performed in July, 1983 at the towing tank at B.C.Research. The purpose of these experiments was to verify the relationship between the heave damping coefficient and the heave exciting force for the compound cylinder model. These experiments were also intended to be a further verification of the heave damping coefficient for the compound cylinder model theoretically calculated using the matching technique. The experimental results for the other cylinder models were intended as a verification of the heave exciting forces computed by a boundary element method. The boundary element method applied by Chan /11/ used linear diffraction theory and hence can be considered a more direct computation of the exciting force. The experimental procedure is described in Chapter 3 and a description of the equipment is given in Appendix 2.

Fig.27 is a plot of the heave exciting force on single cylinder model at a draft of 7". The range of wave frequency is from 0 to 2.5 Hz. The experimental results are compared to a theoretical prediction by a boundary element method. The experimental measurements were made for waves of three different amplitude settings of 0.12", 0.2" and 0.4". The amplitudes are approximate since the wave amplitudes cannot be duplicated exactly. The waveform obtained was also slightly irregular. The causes for this are discussed in

Appendix 2. The results show quite good agreement with the theoretical prediction by the boundary element method. The experimentally measured peak exciting forces are at about 0.5 Hz and are higher than the theoretically predicted peak value which occurs at the same frequency. The experiments results show a scatter of about 15% at a frequency of 1.25 Hz. These can be due to the inaccuracies in the measurement of the forces and the wave heights caused by the irregularity of the generated waveform.

Fig.28 is a plot of the phase difference between the exciting force and the wave. The experimentally measured values show considerable scatter and deviation from the theoretical prediction by the boundary element method. This scatter may again be due to inaccuracies in the measurement of the waves because of their irregularity.

Fig.29 shows the heave exciting force results for the single cylinder model at a draft of 10.5". The scatter in the experimental results is less than for the 7" draft. The experimental results show quite good agreement with the theoretical prediction by the boundary element method. Fig.30 shows a plot of the phase difference between the heave exciting force and the wave for the 10.5" draft. The phase values do not show good agreement with the theoretical prediction.

Figs. 31 and 33 show the plots of heave exciting forces for the double cylinder model (Fig.5) at drafts of 23.5" and 27.5" respectively. Here, the agreement with theoretical

prediction by the boundary element method is not very good. There is considerable scatter in the data. In general, the experimental results are higher than the theoretical prediction. Figs. 32 and 34 show plots of the phase difference between the exciting force and the wave. The experimental values show considerable scatter and do not show good agreement with the theory.

Fig.35 is a plot of the heave exciting force for the compound cylinder model (Fig.4) at a draft of 35.5". Experimental results are compared with theoretical predictions by the matching technique and the boundary element method. Both theoretical methods overpredict the exciting force at frequencies above 1.25 Hz. The boundary element method gives a lower value of the exciting force except at the lower frequencies. Both theoretical methods show good agreement. The agreement is best at the lowest and highest frequencies. At frequencies lower than 0.75 Hz, the experimentally measured exciting forces are higher than the theoretical prediction. Fig.36 shows a plot of the force-wave phase difference for the compound cylinder at a draft of 35.5". The phase plot shows considerable scatter in the experimental values and the agreement between theory and experiment is not good.

Fig.37 shows heave exciting force for the compound cylinder at a draft of 38.375". Here the theoretical results by the boundary element method underpredicts the exciting force in comparison to the matching technique at most

frequencies. The boundary element method results show good agreement with the results from the matching technique. In general, the experimental results show good agreement with the theoretical predictions. The scatter in the experimental data is low except at around 0.25 Hz. Fig.38 shows the force-wave phase difference for the compound cylinder at 35.5" draft. The experimental results show scatter and do not agree well with the theoretical prediction.

Fig.39 shows the heave exciting force for the compound cylinder at a draft of 42.625". Here, the prediction by the boundary element method is close to that by the matching technique at all frequencies. The agreement is best at the highest and lowest frequencies. The experimental results are mostly lower than the theoretical predictions. They show good agreement with the theory at two frequencies. Fig.40 shows the force-wave phase difference for the same draft. Again, the agreement with theory is not good.

Fig.41 shows the heave exciting force for the compound cylinder at a draft of 49.5". The theoretical prediction by the boundary element method is close to that by the matching technique. The agreement is best at the higher frequencies. In general, the experimental results show good agreement with the theoretical predictions. However, there are a few scattered points which show considerably higher exciting forces than the theory. Fig.42 shows a plot of the force-wave phase difference. Again, the experimental values show scatter and do not agree well with theory.

In general, the exciting force measurements show good agreement with theoretical predictions. The exciting forces computed from the damping coefficients calculated by the matching technique are close to the values computed directly by the boundary element method. Hence, it can be inferred that the relationship suggested by Newman is good. It can be inferred that the theoretical results computed using linear diffraction theory can be corroborated by experimental results. Though there is some scatter in the experimental forces measured from different amplitude waves, there is enough evidence to suggest validity of the linear theory for waves of these amplitudes. The measurement of phases is not sufficiently reliable to enable any definite conclusions regarding their trends.

CONCLUSIONS

1.

The theoretical method presented here, using the continuity of pressure and velocity between regions of the flow field and a Fourier series representation for the potentials, provides a good method for determining the hydrodynamic coefficients in heave motion for the compound circular cylinder theoretically. The comparison with the boundary element shows good agreement. The input data required for the present method is minimal. The method is capable of computing the pressures and velocities at any point in the flow field, and hence the wave height at any point on the free surface also.

2.

The computer program CYLINDER, used to compute the added mass and damping coefficient for the compound circular cylinder in heave motion is efficient. It takes 2.8 seconds of CPU time on the Amdahl V-8/470 computer to compute the hydrodynamic coefficients for one frequency of oscillation.

3.

The theoretical method being a potential flow method is unable to account for the viscosity of the fluid medium and hence the vortex shedding during the oscillation fo the cylinder. The method also gives numerical problems when the step size, D' is made very small. Further, in the computation of radial velocities in the flow field, exact continuity of velocity is not acheived at every point on the

common boundary between two adjacent regions in the flow field.

4.

The experimental results for the added mass show larger values than the theoretical prediction by the matching technique. The experimental results also show an increase with frequency. This can be due to an error in measurement of the phase shift. Experimental values could not be determined at frequencies lower than 1 Hz, due to lack of sufficient sensitivity in the force recording equipment.

5.

The experimental heave damping coefficient values show the same trends as the theoretical values, but are considerably higher than the theoretical values. This can partly be due to viscous effects during the cylinder motion and partly due to the effects of the walls of the towing tank on the flow field.

6.

The flow visualisation tests show the vortex shedding occuring at the corners of the cylinder. This suggests the presence of viscous damping, which is not accounted for theoretically.

7.

The added masses and damping coefficients obtained using different amplitudes of oscillation do not show significant deviation.

8.

The wave amplitudes measured during oscillation of the compound cylinder model do not show good agreement with the theoretical prediction by the matching technique. During the tests interference with waves reflected off the side walls of the towing tank was observed. This may be one of the reasons for the large difference between theoretical and experimental results. Further, the actual magnitude of the wave heights measured is small. Hence, the sensitivity of the wave probe may have some effect on the recorded data.

9.

The heave damping coefficients and the wave heights for the compound cylinder model decrease significantly as the draft increases due to decreasing wavemaking action. Both theoretical and experimental results show this trend.

10.

The heave exciting forces measured experimentally for the compound cylinder model show good agreement with theoretical predictions by the matching technique and the boundary element method. This suggests that linear diffraction theory provides results which can be corroborated by experiment. The agreement with the results from the matching technique show the validity of the relationship between the heave damping coefficient and the heave exciting force.

11.

The heave exciting forces measured on the single cylinder model show very good agreement with theoretical predictions by the boundary element method. The agreement between theory

and experiment is not very good for the tests on the double cylinder model.

12.

The phases measured during the heave exciting force tests on all three cylinder models do not show good agreement with theoretical results. They also show considerable scatter. No reliable inference can be made from these results. The scatter can be attributed to inaccuracy in measurement of the wave elevation due to irregularity of the waveform generated.

13.

Though the heave exciting forces measured for the different amplitude settings show some scatter there is enough evidence to justify the assumption of linearity for small amplitude waves.

14.

The tests show that the effects of viscosity of the fluid medium are more important for the measurement of forces on the oscillating cylinder than for the measurement of exciting forces due to small amplitude waves.

15.

Fig. 43 shows hydrodynamic coefficients for a single cylinder measured by McCormick /1/, /20/. These tests were conducted in a towing tank at the U.S. Naval Academy. The frequency of oscillation is 3 radians/sec. The experimental results show very much higher values than the theoretical results. These results are comparable to present comparison

between theory and experiment for the compound cylinder model. ANU/MH in Fig.43 is the added mass non-dimensionalized by mass of the cylinder of height equal to the depth of water.

RECOMMENDATIONS

The experimental results for the heave added mass and damping coefficients do not show very good agreement with the theoretical predictions by the matching technique. The heave exciting forces computed theoretically from the damping coefficient show better agreement with the experimental results. The flow visualisation tests show the presence of vortex shedding during the cylinder oscillation. These suggest that the effects of viscosity may be relatively important. Also, the effects of the interference due to the presence of the side walls of the towing tank are not assessed at present. To estimate the effects of the above it would be desirable to do the following.

1.

Theoretically model the vortex shedding using ring vortices at the corners of the cylinder.

2.

Theoretically model the effects of the tank walls by a potential flow method such as the method of images.

3.

Repeat the same tests for the oscillating cylinder in an open basin where the restraining efects of the tank walls would not be felt.

NOMENCLATURE FOR PLOTS

HEAVE EXCITING FORCE PLOTS

F	=Heave exciting force
RO	=Density of medium
V	=Buoyancy in cu. ft. of cylinder model
g	=Acceleration due to gravity
AMP	=Wave amplitude in ft.
W	=Wave frequency
A	=Maximum radius of cylinder model

HYDRODYNAMIC COEFFICIENTS AND WAVE AMPLITUDE PLOTS

a22	=Heave added mass
RHO	=Density of fresh water
V	=Buoyancy in cu. ft. of cylinder model
g	=Acceleration due to gravity
b22	=Heave damping coefficient
W	=Cylinder oscillation frequency
A	=Maximum radius of cylinder model

LIST OF SYMBOLS

ρ = Density of water.

ω = Circular frequency of cylinder or wave motion.

k_0, k_n = Wave number.

m_0, m_n = Wave number.

Φ, ϕ = Velocity potential

J_0, J_1 = Bessel function of the first kind.

I_0, I_1 = Modified Bessel function of the first kind

K_0, K_1 = Modified Bessel function of the second kind

H_0, H_1 = Hankel function of the first kind.

d = Depth of water a_1, a_2, a_3

= Cylinder radii.

d_1, d_2, d_3

= Depth from cylinder.

g = Acceleration due to gravity

NOTE This list of symbols is not complete. The various symbols are defined at the points in the text where they are used.

BIBLIOGRAPHY

1. SABUNCU,T. and CALISAL, S.M., "Hydrodynamic coefficients for vertical circular cylinders at finite depth," Ocean Engineering vol.8, 1981.

2. KOKKINOWRACHOS,K. et al. "Belastungen und bewegungen groβvolumiger seebauwerke durch wellen," Nr.2905/ Fachgruppe Maschinenbau / Verfahrenstechnik Forschungsbericht des Landes Nordrhein-Westfalen, 1980

3. KOKKINOWRACHOS,K., HOEFELD,J., "Theoretische und experimentelle untersuchungen des bewegungsverhaltens von Halbtauchern," Nr.2915/ Fachgruppe Umwelt / Verkehr Forschungsbericht des Landes Nordrhein-Westfalen, 1980

4. GARRETT,C.J.R., "Wave forces on a circular dock," Journal of Fluid Mechanics, vol.46, part 1, 1971

5. WEHAUSEN, J.V., "The motion of floating bodies," Annual Review of Fluid Mechanics, vol.3, 1971.

6. KRITIS, Ir. B., "Heaving motion of axisymmetric bodies," Journal of Ship Research, vol.5, No.3, 1979.

7. RAMBERG, S.E., and NIEDZWECKI, J.M., Ocean Engineering vol.9, No.1,1982

8. ISAACSON, M., and SARPKAYA,T., "Mechanics of Wave Forces on Structures," Van Nostrand Publications, 1980

9. NEWMAN, J.N., "Marine Hydrodynamics," The MIT Press, 1980.

10. MacCAMY, R.C., FUCHS,R.A., "Wave Forces on Piles : A Diffraction Theory," Tech. Memorandum No.69 Beach Erosion Board 1954

11. CHAN, J.L.K.," Hydrodynamic coefficients for axisymmetric bodies,"M.A.Sc. Thesis, University of British Columbia, 1984

12. HAVELOCK, T.H., "Collected papers," ONR/ACE-103, U.S. Government Printing Office, Washington D.C., 1963

13. BAI, J., "The added mass and damping coefficients of and the exciting forces on four axisymmetric ocean platforms," Naval Ship Research and Development Center, Report No. SPD-670-01, 1974

14. BAI, K.J. and YEUNG, R.W., "Numerical solutions to free-surface flow problems," Tenth Symposium Naval Hydrodynamics, Cambridge, Mass. 1974

15. GARRISON, C.J., "Hydrodynamics of large objects in the sea, Part II. Motion of free-floating bodies," J. Hydronautics 9 (2), 1975

16. ISSHIKI, H. and HWANG, J.H., "An axi-symmetric dock in waves," Seoul National University, Korea, College of Engineering, Dept. of Naval Architecture, Report No. 73-1, 1973

17. NEWMAN, J.N., "The interaction of stationary vessels with regular waves," Eleventh Symposium Naval Hydrodynamics, London, 1976

18. KIM, W.J., "On the harmonic oscillations of a rigid body on a free surface," J. Fluid Mech. 21, 1974

19. ABRAMOWITZ, M. and STEGUN, I.A., "Handbook of mathematical functions," National Bureau of Standards, Washington, D.C. 1964

20.McCORMICK, M.E., COFFEY, J.P. and RICHARDSON, J.B., "An experimental study of wave power conversion by a heaving vertical circular cylinder in restricted waters," U.S. Naval Academy, Engineering Report EW 10-80 1980

21. WANG and SHEN, "The hydrodynamic forces and pressure distributions for an oscillating sphere in a fluid of finite depth,"M.I.T. Department of Naval Architecture and Marine Engineering, Doctoral Thesis 1966

22. YEUNG, R.W., "A hybrid integral-equation method for time harmonic free surface flow,"1st Int. Conf. Numer. Ship Hydrodynamics, Gaithersburg, Maryland 1975

5. APPENDIX 1 - EVALUATION OF POTENTIAL FUNCTIONS

The coefficients of the potential functions described in chapter 2 are obtained by solving a system of linear simultaeneous equations.

Five systems of equations are written and solved to give the coefficients of the five series needed to describe the potentials for the flow model. These are obtained by equating the pressures (potentials) and velocities (normal derivatives of potentials) along the boundaries of the regions defined in chapter 2.

For example, let Φ_A and Φ_B be the potentials in two adjoining regions given by,

$$\Phi_A = V_H \, d \, e^{-i\omega t} \, \phi_A$$

and

$$\Phi_B = V_H \, d \, e^{-i\omega t} \, \phi_B$$

Along a common boundary for continuity of pressure,

$$p_A = -\rho \, \Phi_{A,t} = i\omega\rho \, V_H \, d \, e^{-i\omega t} \, \phi_A =$$

$$p_B = -\rho \, \Phi_{B,t} = i\omega\rho \, V_H \, d \, e^{-i\omega t} \, \phi_B$$

Or,

$$\phi_A = \phi_B \qquad \ldots(I.1)$$

And for continuity of radial velocity

$$\Phi_{A,r} = V_H \, d \, e^{-i\omega t} \, \phi_{A,r} =$$

$$\Phi_{B,r} = V_H \, d \, e^{-i\omega t} \, \phi_{B,r}$$

where the suffix 'r' denotes derivative with respect to

r.Or,

$$\phi_{A,r} = \phi_{B,r} \qquad \ldots(I.2)$$

However,the above denotes continuity of pressure and velocity at a point along a common boundary. Actually,in order to separate the coefficients of the series, the orthonormal properties of the potential functions are made use of. This is done by equating the integral of the function over the depth as shown below.

Using a continuity of pressure and integrating as below,

$$_{d_l}\int^{d_u} \phi_A \; Z(z)dz = {}_{d_l}\int^{d_u} \phi_B \; Z(z)dz$$

one obtains a set of equations.

Here, $Z(z)$ is an orthonormal function for $d_l \leq z \leq d_u$. By substituting the normal derivative of the potential for the potential we have a similar relation for continuity of velocity.

Because the problem is formulated in this manner, the solution does not satisfy continuity of pressure and velocity at all points along the boundary exactly. But, the integral of the velocity and pressure along the depth for one region will be equal to the respective integral in the adjoining region. An alternative formulation would be to equate the pressures and velocities in adjoining regions at a number of points along the boundary. The exact number of points would be equal to the number of unknown coefficients

in the series for the potential. However,the method of solution used here involves no discretization of the boundary of adjoining regions. Also, it enables one to use the orthonormal properties of the potential functions.

5.1 POTENTIALS

The potentials in the various regions are as given below.

5.1.1 REGION 1

$$\Phi_1 = V_H\, d\, e^{-i\omega t}\, [(z^2-r^2/2)/2dd_1 + A_0/2 + \sum_{n=1}^{\infty} A_n\, (I_0(n\pi r/d_1)/I_0\,(n\pi\, a_1/d_1))\cos(n\pi z/d_1)] \quad \ldots(I.3)$$

5.1.2 REGION 2

$$\Phi_2 = V_H\, d\, e^{-i\omega t}\, [(z^2-r^2/2)/2dd_2 + B_0 + \sum_{n=1}^{\infty} \{B_n\, V_n\,(r) + C_n\, W_n\,(r)\}\cos(n\pi z/d_2)] \quad \ldots(I.4)$$

where,

$V_n\,(r) =$

$$\frac{I_0(n\pi r/d_2) + (\, I_1(n\pi a_1/d_2)\ /\ K_1(n\pi a_1/d_2)\ )\ K_0(n\pi r/d_2)}{I_0(n\pi a_2/d_2) + (\, I_1(n\pi a_1/d_2)\ /\ K_1(n\pi a_1/d_2)\ )\ K_0(n\pi a_2/d_2)}$$

$W_n\,(r) =$

$$\frac{I_0(n\pi r/d_2) + (\, I_0(n\pi a_2/d_2)\ /\ K_0(n\pi a_2/d_2)\ )\ K_0(n\pi r/d_2)}{I_1(n\pi a_1/d_2) + (\, I_0(n\pi a_2/d_2)\ /\ K_0(n\pi a_2/d_2)\ )\ K_1(n\pi a_1/d_2)}$$

It is easily seen that V_n (r) and W_n (r) have the following properties.

At $r=a_1$ $V_n'(a_1) = 0$, $W_n'(a_1) = n\pi/d_2$

where the primes indicate derivative with respect to r.

At $r=a_2$, $W_n(a_2) = 0$

$V_n(a_2) = 1$

5.1.3 REGION 3

The velocity potential in this region is defined as:

$$\Phi_3 = V_H\, d\, e^{-i\omega t}\, [(z/d+g/(\omega^2 d)-1) + D_0 X_0 \bar{Y}_0 + \sum_{n=1}^{\infty} D_n X_n \bar{Y}_n] \qquad \ldots(I.5)$$

where

$$X_0 = \frac{J_0(m_0 r) - (J_1(m_0 a_3) / H_1(m_0 a_3)) H_0(m_0 r)}{J_0(m_0 a_2) - (J_1(m_0 a_3) / H_1(m_0 a_3)) H_0(m_0 a_2)}$$

$$X_n = \frac{I_0(m_n r) + (I_1(m_n a_3) / K_1(m_n a_3)) K_0(m_n r)}{I_0(m_n a_2) - (I_1(m_n a_3) / K_1(m_n a_3)) K_0(m_n a_2)}$$

In this formulation,

$$\bar{Y}_0 = M_0^{-1/2} \cosh[m_0(z-d_3)]$$

$$M_0 = [1+\sinh\{2m_0(d-d_3)\}/2m_0(d-d_3)]/2$$

$$Y_n = M_n^{-1/2} \cos[m_n (z-d_3)]$$

$$M_n = [1+\sin\{2m_0(d-d_3)\}/2m_0(d-d_3)]/2$$

where m_0 and m_n are the roots of

$$\omega^2-gm_0\tanh[m_0(d-d_3)] = 0$$

$$\omega^2+gm_n \tan[m_n (d-d_3)] = 0$$

respectively.

It is easily seen that X_0 and X_n have the following properties.

At $r=a_3$ $\quad X_0'(a_3) = 0,\ X_n'(a_3) = 0,$

and at $r=a_2$ $\quad X_0(a_2) = 1,\ X_n(a_2) = 1$.

The primes denote derivative with respect to r.

5.1.4 <u>EXTERIOR REGION</u>

The free wave and standing waves are defined with the potential Φ_E as:

$$\Phi_E = V_H\, d\, e^{-i\omega t} [-E_0(H_0(k_0r)/H_1(k_0a_2))Z_0(z)$$

$$- \sum_{n=1}^{\infty} E_n (K_0(k_n r)/K_1(k_n a_2)) Z_n(z)] \qquad \ldots(I.6)$$

where,

$$Z_o = N_o^{-1/2} \cosh[k_o z]$$

$$N_o = [1+\sinh\{2k_o d\}/2k_o d]/2$$

$$Z_n = N_n^{-1/2} \cos[k_n z]$$

$$N_n = [1+\sin\{2k_o d\}/2k_o d]/2$$

where k_o and k_n are the roots of

$$\omega^2 - gk_o \tanh[k_o d] = 0$$

$$\omega^2 + gk_n \tan[k_n d] = 0$$

respectively.

5.2 GENERATION OF SYSTEMS OF EQUATIONS FOR SOLUTION

The five systems of equations neccessary to solve for the coefficients of the five series for the potentials are obtained by matching the pressures and velocities at common boundaries between the regions defined .

5.2.1 CONTINUITY OF PRESSURE BETWEEN REGIONS 1 AND 2

Expressing the velocity potential Φ as $\Phi = V_H d\, e^{-i\omega t}\, \phi$, for continuity of pressure between regions 1 and 2, we can express

Pressure, $p = -\rho\Phi_{1,t} = -\rho\Phi_{2,t}$
using linearised Bernoulli's equation.

As proved in equation (I.1) we can write $\phi_1 = \phi_2$, for continuity of pressure at points on the interface $r=a_1$, $0 \le z \le d_1$. Integrating the above equation between the limits 0 and d_1 after multiplying by the orthogonal function $2\cos(k\pi z/d_1)/d_1$ we have,

$$(2/d_1)\int_0^{d_1} \phi_1 \cos(k\pi z/d_1)dz = (2/d_1)\int_0^{d_1} \phi_2 \cos(k\pi z/d_1)dz$$

Using the orthonormal properties of the cosine function we can rewrite the above equation as ,

$$A_k - \sum_{n=0}^{\infty} \alpha_{kn} B_n \sum_{n=1}^{\infty} \beta_{kn} C_n = a_k \qquad \ldots(I.7)$$

where,

$$\alpha_{00} = 1 \ , \ \alpha_{k0} = 0$$

$$\alpha_{0n} = 2d_2[V_n(a_1)]\sin(n\pi d_1/d_2)/\pi d_1 n \qquad n=1,2,3,..$$

$$\beta_{0n} = 2d_2[W_n(a_1)]\sin(n\pi d_1/d_2)/\pi d_1 n \qquad n=1,2,3,..$$

$$\alpha_{kn} = 2d_1d_2n[V_n(a_1)]\sin(n\pi d_1/d_2)(-1)^k/\pi(d_1{}^2n^2-d_2{}^2k^2)$$

$$\beta_{kn} = 2d_1d_2n[W_n(a_1)]\sin(n\pi d_1/d_2)(-1)^k/\pi(d_1{}^2n^2-d_2{}^2k^2)$$

$$a_0 = -d_1(1-(d_1/d_2)[1/3 - (a_1/d_1)^2]/d$$

$$a_k = -2d_1(1-d_1/d_2)(-1)^k /d\ (k\pi)^2$$

(I.7) gives the first system of equations.

5.2.2 CONTINUITY OF VELOCITY BETWEEN REGIONS 1 AND 2

For continuity of velocities between regions 1 and 2 along the boundary $r=a$, $0 \le z \le d_1$, we have, following equation (I.2)

$$\phi_{1,r} = \phi_{2,r}$$

Multiplying by $\cos(k\pi z/d_2)$ and integrating as follows,

$$\int_0^{d_1} \phi_{1,r} \cos(k\pi z/d_2)dz = \int_0^{d_2} \phi_{2,r} \cos(k\pi z/d_2)dz \text{ at } r=a_1$$

we have the second system of equations. The second integral is from 0 to d_2. Hence the normal velocity on the surface $r=a_1$, $d_1 \le z \le d_2$ is implicitly set to zero.

Using the orthonormal properties of $\cos(k\pi z/d_2)$ we arrive at the second system of equations as

$$C_k - \sum_{n=0}^{\infty} \gamma_{kn} = b_k \qquad \text{...(I.8)}$$

where

$$C_0 = 0$$

$\gamma_{00} = 0$; $\gamma_{0n} = 0$ for n=1,2,..

$\gamma_{k0} = 0$ for k=1,2,..

$$\gamma_{kn} = 2d_1d_2\ n(-1)^n \sin(k\pi d_1/d_2)\ I_1(n\pi a_1/d_1)/\pi\ I_0(n\pi a_1/d_1)$$
$$[d_1{}^2k^2 - d_2{}^2n^2] \quad \text{for } k=n=1,2,..$$

$b_0 = 0$

$b_k = -a_1d_2 \sin(n\pi d_1/d_2)/d_1d\ (n\pi)^2$

5.2.3 <u>CONTINUITY OF PRESSURE BETWEEN REGION 2 AND THE EXTERIOR REGION</u>

Using a procedure similar to the one used for equation (I.7) we equate the pressure on the interface $r=a_2$, $0 \le z \le d_2$ between region 2 and the exterior region. Multiplying by the function $\cos(k\pi z/d_2)$ and integrating from 0 to d_2 one obtains:

$$(2/d_2)\int_0^{d_2} \phi_2 \cos(k\pi z/d_2)dz = (2/d_2)\int_0^{d_2} \phi_E \cos(k\pi z/d_2)dz$$
for $r=a_2$

Using the orthonormal properties of the cosine function we can rewrite the above equation in the form,

$$B_k - \sum_{n=1}^{\infty} \epsilon_{kn} E_n = c_k \qquad \ldots(I.9)$$

(I.9) is the third system of equations, where,

$$\epsilon_{k0} = -(H_0(k_0 a_2)/H_1(k_0 a_2))G_{k0} \text{ for } k=0,1,2,.. \; ; \; n=0$$

$$\epsilon_{kn} = -(K_0 (k_n a_2)/H_1(k_n a_2))G_{kn} \text{ for } k=0,1,2,.. \; ; \; n=1,2,..$$

$$G_{00} = (2/d_2) \int_0^{d_2} Z_0 \, dz$$

$$= 2N_0^{-1/2} \sinh(k_0 d_2)/k_0 d_2$$

$$G_{k0} = (2/d_2) \int_0^{d_2} Z_0 \cos(k\pi z/d_2) \, dz$$

$$= 2N_0^{-1/2} \sinh(k_0 d_2) k_0 d_2 (-1)^k / [(k_0 d_2)^2 + (k\pi)^2]$$

$$G_{0n} = (2/d_2) \int_0^{d_2} Z_n \, dz$$

$$= 2N_n^{-1/2} \sin(k_n d_2)/k_n d_2$$

$$G_{kn} = (2/d_2) \int_0^{d_2} Z_n \cos(k\pi z/d_2) \, dz$$

$$= 2N_n^{-1/2} \sin(k_n d_2) k_n d_2 (-1)^n / [(k_n d_2)^2 - (k\pi)^2]$$

$$c_0 = -(d_2/d)[1/3 - (a_2/d_2)^2/2]$$

$$c_k = -2d_2(-1)^k/d(k\pi)^2$$

5.2.4 CONTINUITY OF PRESSURE BETWEEN REGION 3 AND THE EXTERIOR REGION

We have the fourth system of equations by equating the pressures on the boundary $r=a_2$, $d_3 \le z \le d$, between region 3 and the exterior region. Following eqn. (I.1) we have,

$$\phi_3 = \phi_E$$

Multiplying by the function $\Upsilon(z-d_3)$ and integrating between d_3 and d , we have,

$$(1/(d-d_3)) \int_{d_3}^{d} \phi_3 \, \Upsilon(z-d_3)dz$$

$$= (1/(d-d_3)) \int_{d_3}^{d} \phi_E \, \Upsilon(z-d_3)dz$$

Using the orthonormal properties of the function $\Upsilon(z-d_3)$ we can rewrite the above equation to give the fourth system of equations as,

$$D_k - \delta_{kn} E_n = d_k \qquad \text{...(I.10)}$$

where,

$\delta_{k0} = -(H_0(k_0 a_2)/H_1(k_0\ a_2))L_{k0}$ for k=0,1,2,.. ; n=0

$\delta_{kn} = -(K_0\ (k_n\ a_2)/K_1(k_n\ a_2))L_{kn}$ for k=0,1,2,.. ; n=1,2,..

L_{kn} is a special function defined as below.

$$L_{00} = (1/(d-d_3)) \int_{d_3}^{d} Z_0(z)\mathfrak{Y}_0\ (z-d_3)dz$$

$$= -(M_0\ N_0\ )^{-1/2}\ k_0 \sinh(k_0 d_3)/[(d-d_3)\ (k_0{}^2 - m_0{}^2)]$$

$$L_{k0} = (1/(d-d_3)) \int_{d_3}^{d} Z_0(z)\mathfrak{Y}_k\ (z-d_3)dz$$

$$= -(M_k\ N_0\ )^{-1/2}\ k_0 \sinh(k_0 d_3)/[(d-d_3)\ (k_0{}^2 + m_k{}^2)]$$

$$L_{0n} = (1/(d-d_3)) \int_{d_3}^{d} Z_n\ (z)\mathfrak{Y}_0\ (z-d_3)dz$$

$$= -(M_0\ N_n\ )^{-1/2}\ k_n\ \sin(k_n\ d_3)/[(d-d_3)\ (k_n{}^2 + m_0{}^2)]$$

$$L_{kn} = (1/(d-d_3)) \int_{d_3}^{d} Z_n\ (z)\mathfrak{Y}_k\ (z-d_3)dz$$

$$= -(M_k\ N_n\ )^{-1/2}\ k_n\ \sin(k_n\ d_3)/[(d-d_3)\ (k_n{}^2 - m_k{}^2)]$$

$$d_0 = -M_0{}^{-1/2}/\ d(d-d_3)(m_0)^2$$

$$d_k = -M_k{}^{-1/2}/\ d(d-d_3)(m_k\ )^2$$

5.2.5 CONTINUITY OF VELOCITIES BETWEEN REGIONS 2, 3 AND THE EXTERIOR REGION

We have the fifth and final system of equations by equating the radial velocities from regions 2 and 3 to the radial velocity from the exterior region on the boundary $r=a_2$, $0 \le z \le d_2$, $d_3 \le z \le d$. The normal velocity on the surface $r=a_2$, $d_2 \le z \le d_3$ is implicitly assigned to be zero. Using equation (2) we have,

$$\phi_{2,r} = \phi_{E,r} \text{ , for } r=a_2 \; 0 \le z \le d_2 \qquad \text{...(I.11a)}$$

$$\phi_{3,r} = \phi_{E,r} \text{ , for } r=a_2 \; d_3 \le z \le d \qquad \text{...(I.11b)}$$

Adding (I.11a) and (I.11b) and multiplying throughout by the function Z_k (z) and integrating between the limits as shown we have the fifth system of equations.

$$(1/dk_k) \int_0^{d_2} \phi_{2,r} Z_k(z)dz + (1/dk_k) \int_{d_3}^{d} \phi_{3,r} Z_k(z)dz$$

$$= (1/dk_k) \int_0^{d} \phi_{E,r} Z_k(z)dz$$

Integrating using the orthonormal properties of the function Z_k (z), and rewriting we have the fifth system of equations as (I.11).

$$-\kappa_{kn} B_n - \theta_{kn} C_n - \psi_{kn} D_n + E_k = e_k \qquad \ldots(I.11)$$

The terms in (I.11) are defined as below.

$\kappa_{kn} = (n\pi/2dk_k)V_n'(a_2)\ G_{kn}$ for $k=0,1,2,..;\ n=1,2,..;$

$\theta_{kn} = (n\pi/2dk_k)W_n'(a_2)\ G_{kn}$ for $k=0,1,2,..;\ n=1,2,..;$

$\psi_{kn} = [(d-d_3)m_n/dk_k)\ X_n'(a_2)\ F_{kn}$

$e_0 = -a_2 N_0^{-1/2} \sinh(k_0 d_2)/2(k_0 d)^2 d_2$

$e_k = -a_2 N_k^{-1/2} \sin(k_k d_2)/2(k_k d)^2 d_2$

$V_n'(a_2) =$

$$\frac{I_1(n\pi a_2/d_2) - (I_1(n\pi a_1/d_2)\ /\ I_1(n\pi a_1/d_2))\ K_1(n\pi a_2/d_2)}{I_0(n\pi a_2/d_2) + (I_1(n\pi a_1/d_2)\ /\ K_1(n\pi a_1/d_2))\ K_0(n\pi a_2/d_2)}$$

$W_n'(a_2) =$

$$\frac{I_1(n\pi a_2/d_2) + (I_0(n\pi a_2/d_2)\ /\ I_0(n\pi a_2/d_2))\ K_1(n\pi a_2/d_2)}{I_1(n\pi a_1/d_2) + (I_0(n\pi a_2/d_2)\ /\ K_0(n\pi a_2/d_2))\ K_1(n\pi a_1/d_2)}$$

$$X_0'(a_2) = \frac{J_1(m_0 a_2) + (J_1(m_0 a_3)\ /\ H_1(m_0 a_3))\ H_1(m_0 a_2)}{J_0(m_0 a_2) + (J_1(m_0 a_3)\ /\ H_1(m_0 a_3))\ H_0(m_0 a_2)}$$

$$X_n'(a_2) = \frac{I_1(m_n a_2) + (I_1(m_n a_3) / K_1(m_n a_3)) K_1(m_n a_2)}{I_0(m_n a_2) + (I_1(m_n a_3) / K_1(m_n a_3)) K_0(m_n a_2)}$$

$$F_{00} = [1/(d-d_3)]_{d_3} \int^{d} \mathfrak{Y}_0 (z-d_3) Z_0 (z) dz$$

$$= (M_0 N_0)^{-1/2} k_0 \sinh(k_0 d_3)/[(d-d_3)(k_0^2 - m_0^2)]$$

$$F_{k0} = [1/(d-d_3)]_{d_3} \int^{d} \mathfrak{Y}_0 (z-d_3) Z_k (z) dz$$

$$= (M_0 N_k)^{-1/2} k_k \sin(k_k d_3)/[(d-d_3)(k_k^2 + m_0^2)]$$

$$F_{0n} = [1/(d-d_3)]_{d_3} \int^{d} \mathfrak{Y}_n (z-d_3) Z_0 (z) dz$$

$$= (M_n N_0)^{-1/2} k_0 \sinh(k_0 d_3)/[(d-d_3)(k_0^2 + m_n^2)]$$

$$F_{kn} = [1/(d-d_3)]_{d_3} \int^{d} \mathfrak{Y}_n (z-d_3) Z_k (z) dz$$

$$= (M_n N_k)^{-1/2} k_k \sin(k_k d_3)/[(d-d_3)(k_k^2 - m_n^2)]$$

$$G_{0n} = (2/d_2) \int_0^{d_2} Z_0(z) \cos(n\pi z/d_2) dz$$

$$= 2N_0^{-1/2} \sinh(k_0 d_2) k_0 d_2 (-1)^n / [(k_0 d_2)^2 + (n\pi)^2]$$

$$G_{kn} = (2/d_2) \int_0^{d_2} Z_k(z) \cos(n\pi z/d_2)\, dz$$

$$= 2N_k^{-1/2} \sin(k_k d_2) k_k d_2 (-1)^k / [(k_k d_2)^2 - (n\pi)^2]$$

5.2.6 SOLUTION FOR COEFFICIENTS OF SERIES

Equations (I.7) to (I.11) form the five systems of linear equations which are solved simultaneously to obtain the coefficients A_n , B_n , C_n , D_n and E_n of the series for the potential functions.

The above system of equations are equivalent to

$$[M]|x| = |v| \qquad \text{...(I.12)}$$

where [M] is a complex square matrix of order (5m-1), |x| is a complex vector comprising of the unknown coefficients of the series and |v| is a complex vector comprising of the right hand side of the system of equations (I.7) to (I.11).

The system of equations (I.12) is solved by a complex, double precision routine CDSOLN available on the UBC Michigan Terminal System. The routine solves the system by Gaussian elimination. CPU time required for solving a system of 100 equations, corresponding to 20 terms for each series for the potentials, is typically 2.6 seconds on the Amdahl 470 V/8 computer. Details of the formulation of the system

of equations (I.12) are given in the write-up on the computer program.

5.3 INTEGRALS FOR EVALUATION OF HYDRDOYNAMIC COEFFICIENTS

The integrals IN_1, IN_2 and IN_3 in equation (2.51) of chapter 2 are as given below.

$$IN_1 = \int_0^{a_1} \phi_1 \, r \, dr \text{ at } z=d_1$$

$$= [a_1^2 d_1/4d - a_1^4/16dd_1 + A_0 a_1^2/4$$

$$+ \sum_{n=1}^{\infty} A_n (-1)^n (a_1 d_1/n\pi) \, I_1(n\pi a_1/d_1)/I_0(n\pi a_1/d_1)] \qquad \ldots(I.13)$$

$$IN_2 = \int_{a_1}^{a_2} \phi_2 \, r \, dr \text{ at } z=d_2$$

$$= [(a_2^2 - a_1^2)d_2/4d - (a_2^4 - a_1^4)/16dd_2$$

$$+ B_0^2(a_2^2 - a_1^2)/4$$

$$+ \sum_{n=1}^{\infty} B_n (-1)^n (d_2/n\pi) \, \tilde{V}_n (a_2)$$

$$+ \sum_{n=1}^{\infty} C_n (-1)^n (d_2/n\pi) \, \tilde{W}_n (a_2)] \qquad \ldots(I.14)$$

where,

$\tilde{V}_n\ (a_2) =$

$$a_2 \frac{I_1(n\pi a_2/d_2) - (I_1(n\pi a_1/d_2) / I_1(n\pi a_1/d_2)) K_1(n\pi a_2/d_2)}{I_0(n\pi a_2/d_2) + (I_1(n\pi a_1/d_2) / K_1(n\pi a_1/d_2)) K_0(n\pi a_2/d_2)}$$

$\tilde{W}_n\ (a_2) =$

$$a_2 \frac{I_1(n\pi a_2/d_2) + (I_0(n\pi a_2/d_2) / I_0(n\pi a_2/d_2)) K_1(n\pi a_2/d_2)}{I_1(n\pi a_1/d_2) + (I_0(n\pi a_2/d_2) / K_0(n\pi a_2/d_2)) K_1(n\pi a_1/d_2)}$$

$- a_1$

$$IN_3 = \int_{a_3}^{a_2} \phi_3\ r\ dr \text{ at } z=d_3$$

$$= [d_3/d + g/\omega^2 d - 1]\ (a_2^2 - a_3^2)$$

$$+(D_0\ M_0^{-1/2}\ a_2/m_0)$$

$$\frac{J_1(m_0 a_2) + (J_1(m_0 a_3) / H_1(m_0 a_3)) H_1(m_0 a_2)}{J_0(m_0 a_2) + (J_1(m_0 a_3) / H_1(m_0 a_3)) H_0(m_0 a_2)}$$

$$+ (\sum_{n=1}^{\infty} D_n\ M_n^{-1/2}\ a_2/m_n)$$

$$\frac{I_1(m_n\ a_2) + (I_1(m_n\ a_3) / K_1(m_n\ a_3)) K_1(m_n\ a_2)}{I_0(m_n\ a_2) + (I_1(m_n\ a_3) / K_1(m_n\ a_3)) K_0(m_n\ a_2)} \quad \ldots(I.15)$$

6. APPENDIX 2 - EXPERIMENTAL SET-UP

6.1 EXPERIMENTAL FACILITIES

The facilities of the Ocean Engineering Centre at B.C. Research, Vancouver, were utilised for the experiments. The facilities used are described below.

6.1.1 THE TOWING TANK

This is a 220'x12'x10' tank primarily used for ship model resistance tests. It is equipped with a towing carriage fitted with data collection equipment, which traverses the length of the tank on rails. A photograph of the tank is shown in Fig.7. The tank is equipped with a hinged paddle type wavemaker at one end and a wave damping beach at the opposite end. The tank is also equipped with underwater windows for flow visualization experiments and an overhead lifting hook fixed at a position halfway along the length of the tank but capable of moving transversely. The latter was used for equipment handling during the tests.

6.1.2 WAVEMAKER

The wavemaker consists basically of three units.

6.1.2.1 The Wave Signal Generator

This device generates a time varying voltage signal to represent the wave. The device has the capability to generate quasi-random waves or regular repeated waveforms. The operation of this device is complicated. Instead, a

sinusoidal wave generator was used. This enables easy variation of amplitudes and frequencies for sinusoidal waveforms and is much simpler to operate.

6.1.2.2 Wave Synthesizer

The wave synthesizer serves the dual purpose of boosting the input signal and correcting for any irregularities in the motion. The input signal is boosted to voltage and current levels appropriate to the hydraulic actuator. A displacement transducer on the wave paddle provides the synthesizer with the actual position of the paddle at any instant. The wave synthesizer sends a corrected signal to the hydraulic actuator after comparing the actual position of the paddle to the desired paddle location.

6.1.2.3 Wave Paddle

A photograph of the wave paddle is shown in Fig.10. This is an aluminium paddle which spans the width of the towing tank. The paddle is hinged approximately four feet below the water surface. The paddle is oscillated by a hydraulic piston controlled by the hydraulic actuator which in turn is controlled by the wave synthesizer.

Any irregularities in the waves generated and propagating along the tank may be due to one or more of the following reasons.

The wave paddle has a natural, undriven oscillation. The amplitude of this oscillation varies with time and and

becomes more pronounced as the actuator heats up. The oscillation is approximately 0.4" at a frequency of 2.3Hz. Except for experiments near this frequency, the effects can be isolated by spectral analysis. This oscillation decreased considerably on installation of a new hydraulic actuator valve. So, only a few experiments were affected by this oscillation. The above oscillation causes an irregular waveform.

At certain frequencies, beats were observed in the waveform. This can be directly attributed to the presence of a large seakeeping basin adjacent to the towing tank. The two are separated only by an aluminium half-wall. Beats are generated in the waveforms at certain frequencies, normally higher than 1Hz. The frequency of the interfering waveforms differs by about 1Hz. from the driven frequency. The beats in the waveforms may possibly have been generated by a cross-flow between the tanks.

Other iregularities in the waveform may be induced by reflections from the tank walls or disturbances due to air currents or gusts disturbing the water surface.

6.2 MOTION GENERATOR

The motion generator is a hydraulically driven scotch yoke mechanism. Fig. 8 shows a photograph of the unit. The unit was redesigned since it did not provide a smooth sinusoidal oscillation in its original form.

At present it consists of a horizontal fixed frame 12'x4' made up of two I-beams. A vertical frame is mounted on this frame and holds the moving frame which provides the vertical harmonic oscillation. The moving frame is connected to the scotch yoke mechanism which drives it. The moving frame is also connected to the cylinder model through a connecting block.

The scotch yoke itself is driven by a radial piston hydraulic motor having a displacement of 12.7 cu. in./ revolution. The motor is capable of an output torque of 500 ft.-lbs. A closed loop variable displacement hydrostatic transmission circuit is used to ensure tight control of angular velocity over the speed range of 3 to 150 rpm. Owing to limitations in the available electrical power supply the hydraulic motor can only deliver rated torque upto a frequency of 0.83 Hz, with torque capacity diminishing to 167 ft.-lbs at a frequency of 2.5 Hz.

The hydraulic power unit consists of a variable displacement axial piston pump having a maximum displacement of 2.5 cu. in./ revolution, driven by a 1750 rpm 5 H.P. electric motor. The pump displacement is limited by external mechanical stops to a maximum of 1.25 cu. in./ revolution to prevent overloading of the motor. A cross-port releif valve set at 3000 psi is used to prevent excessive circuit pressures and to limit motor torque to 500 ft-lbs.

The scotch yoke mechanism and the hydraulic system were redesigned by Fraser Elhorn, a graduate of the Mechanical

Engineering Department at UBC. The moving frame was constructed at the Machine Shop at the Mechanical Engineering Department. The hydraulic motor and power unit were supplied by Fleck Hydraulics Inc., Vancouver B.C.

6.3 DATA COLLECTION SYSTEM

The O.E.C. data collection system was used. This consisted of a MINC-11 computer and amplifiers and amplifiers and signal conditioners mounted on the towing carriage.

6.3.1 AMPLIFIERS AND SIGNAL CONDITIONERS

The towing carriage carries ten signal conditioners. Internal registers can be set to high,low or band-pass. Externally, dials allow amplification of the input voltage signal by a factor of 10. A few of the amplifiers are differential amplifiers and permit amplifications upto 1000. For these experiments, low pass filtering was chosen with varying amplification. The amplifiers induce a phase shift in the signal which was analyzed and corrected for.

6.3.2 MINC-11 COMPUTER

The hardware for the system comprises of the following.

6.3.2.1 Main Console

This incorporates analog and digital input ports with clocking capabilities. A maximum of 16 analog ports can be used. Each port will accept as input ±5.12 volts with a resolution of 2.5mV. Voltages in excess of the limits are

removed by the MINC-11. Analog voltages are converted to integer values for internal use, the voltage range being translated from 0 to 4096. Time difference between the sampling of two channels is of the order of microseconds and so was not of concern for these experiments.

6.3.2.2 Dual Floppy Disk Drive System

System and often used programs are stored on one disk and data and development programs are stored on the other.

6.3.2.3 VT105 Video Terminal

The terminal has graphic display capabilities. It can display upto a maximum of two single valued functions. This enabled visual observation of the recorded signal and comparison of two different channels.

6.3.2.4 Line Printer

A high speed variable character size line printer is used to obtain hard copies of data and program listings.

6.3.2.5 Tektronix Screen Dump Printer

This printer generates a duplicate of the video screen contents on heat sensitive paper. This is useful for obtaining plots of the recorded data.

Software used for the experiments were partly existing on the system and partly written or modified. These are described later.

6.4 MODELS

Three types of models were used for the experiments. Their dimensions and shapes are as shown in Figs. 4, 5, and 6.The models were constructed by the machine shop at the Department of Mechanical Engineering.

The single cylinder model was made of PVC tubing 15" O.D. The ends were sealed with aluminium plating. The cylinder was connected to the block on the motion generator by means of four threaded rods fixed on the bottom plate. These rods also served as a mounting for lead weights used to ballast the cylinder to achieve neutral buoyancy. The draft T, was varied during the experiments.

The double cylinder model was similar in construction except for the fact that the top plate was replaced by an aluminium unit comprising of an 8.625" O.D. aluminium cylinder mounted on a plate. The dimensions of the model are shown in Fig. 5.

The compound cylinder model had, in addition, another unit mounted on the bottom, similar to the aluminium unit mounted on the top for the double cylinder. The dimensions are as shown in Fig. 6.

6.5 EQUIPMENT USED

Electronic equipment used in association with the data collection system are described below.

6.5.1 STRAIN INDICATORS

Strain indicators were use in association with the wire resistance wave probe and the dynamometers used to measure forces. These were model P-350A strain indicators, manufactured by Vishay Instruments Inc. The output ports of the indicator excites the connected bridge circuits with a 1.5 volts R.M.S., 1000Hz square wave. The output is a maximum of ± 250 mV DC. This is too low to be used in association with the MINC-11, and hence had to be amplified.

The specifications are as follows.

Accuracy : ±0.5% of reading or 5$\mu\epsilon$ (whichever is greater.)

Sensitivity

: 0.2 to 20$\mu\epsilon$/mV

Output : Linear range ±250 mV DC

Noise & Ripple

: 3$\mu\epsilon$, 1mV.

6.5.2 SONAR LEVEL MONITOR

This is a solid state device used for measurement of displacement. The device was manufactured by Wesmar Marine Electronics Inc.,Seattle,USA. The device measures the time required for a sonar pulse to travel to and from an object. Various range settings are available with a manual multiplier dial which gives a continuous control of the sensitivity. The specifications are as follows.

Output ripple : <0.1% of fullscale

Output Drift stability

: Better than 0.25% of full scale/hour after warm-up.

Resolution : Better than 0.5% of measured range.

Linearity : Better than 0.5% of full scale.

Operating temperature

: 45° to 140°F

Beam emitted : 3° in span.

Pulse repetition rate

: 160 Hz at 7" to 30" range.

6.5.3 WAVE PROBE

This is a simple device used to measure the water surface elevation and hence the wave profile. The device basically consists of two separated wires in the water, which act as the fourth arm of a Wheatston bridge. The changing water level provides a recordable change in circuit resistance. A Vishay indicator is used to input a 1.5 Volts R.M.S. 1000 Hz square wave.

6.5.4 FORCE RECORDING EQUIPMENT

These consisted primarily of an 80 lb. dynamometer and two 500 lb. Universal Shear beams used to measure vertical forces.

6.5.4.1 80 lb. Dynamometer

The dynamometer is capable of measuring a vertical force, a horizontal force and a moment. 80 lbs. is the maximum range for the vertical force. The effects of any one

of the forces on the others are excluded by a suitably designed circuit. The measuring devices are foil bonded strain gauges Type CEA-06- 125-OT-350. A full Wheatstone bridge arrangement is used for each parameter the bridge circuits were excited by voltages from Vishay strain indicators. The dynamometer was designed and constructed by the Ocean Engineering Centre at B.C.Research. All the bridges have self compensating gauges to provide self temperature correction. This dynamometer was used for the wave force tests on static cylinders.

6.5.4.2 Universal Shear Beam

Two Universal Shear Beams (USB) were used to measure the vertical forces on the oscillating cylinder model. The USBs were manufactured by Hottinger Baldwin Measurements Inc. of Framingham, MA. The specifications as supplied by the manufacturer are as follows.

Rated Capacity	: 500lbs
Rated Output	: 1.9925 mV/V
Non-linearity	: -0.02% of rated ouptut.
Hysteresis	: 0.01% of rated output.
Non repeatability	: 0.01% of rated output
Excitation voltage	: 18V DC or AC RMS max.
Side Load rejection	: 500:1
Max. Load, Safe	: 150%

The USBs were mounted below the two vertical shafts of the moving frame on the motion generator as shown in Fig. 8a. They were pin-jointed to exclude moments and measure only

vertical forces.

6.5.5 CALIBRATION

The sonar level recorder and the wave probe were calibrated before each set of experiments by moving them known distances and recording the output voltages. A calibration program existing on the O.E.C. data collection system was used to obtain the slope and intercept of the calibration data.

The 80 lb. dynamometer and the USBs were calibrated statically in compression on the Universal Testing Machine at the Mechanical Engineering Department, and also dynamically using the motion generator. They were also calibrated in tension by suspending known weights from them when the dynamometers were mounted on the motion generator.

6.6 SOFTWARE USED

Two different sets were used for the experiments. One set was used for data collection on the O.E.C. MINC-11 system. The other set was used for data analysis on the PDP-11 system at the Department of Mechanical Engineering at UBC, which was similar to the MINC-11. Part of the software neccessary was already existing at the O.E.C. Some of it had to be adapted for these experiments. However, some of the software was developed specifically for these experiments.

6.6.1 DATA COLLECTION SOFTWARE

The data collection software was used on the MINC-11 system at the O.E.C.. The data files were stored on disk and transferred to the PDP-11 at the Mechanical Engineering Department at UBC.

6.6.1.1 ADCAL

This is a calibration program that is run before data collection. This program reads input voltage on a specified channel which can be indexed to any desired value. By varying the range of measurements for a device with the corresponding input of such variations a series of calibration points is established. At least five points are required. The program then establishes the best fit straight line through these points by least squares minimization. The slope, intercept, variance and delta of the data line is output. This information is also stored in a matrix on a user specified file. The file contains calibration data for several channels.

If calibration cannnot be carried out before the experiments a dummy calibration file has to be created to run the demultiplexing program.

6.6.1.2 ADMAIN

This is the principal program for data collection. The program collects data on several channels, upto a maximum of 16 simultaneously. The sampled data is stored in a multiplexed group for memory minimization. The program also

allows real time viewing of any channel prior to sampling. This is useful as a check to ensure that recording is occuring.

6.6.1.3 ADMUX

This program is used to separate each channel's unique signal and store the data points as numeric values on user specified files. The program demultiplexes the stored data. This program is available on the MINC-11 system.

6.6.1.4 GRAPH

This program displays upto two graphs on the video terminal. The program has the ability to display either an x-y graph or real time plot of a channel. It can also shade from various portions of the graph field to the data points. Further, the program can calculate and display a cubic moving spline fit to the data. Comments, title and axes labels can be input. The program can also display various portions of a curve. ie, scaling can be changed to magnify some portion of a curve.

6.6.2 DATA ANALYSIS SOFTWARE

The data analysis software was used on the PDP-11 at the Mechanical Engineering Department. They were mostly written for the specific purpose of these experiments.

6.6.2.1 DEMUX

This program demultiplexes one or more signals of the collected data, converts the digitized voltage levels to

user values and stores the time record on a user specified file. If the calibration was not done before the experiments, but later, these calibration values can be input before the demultiplexing.

6.6.2.2 AMP

This program takes as input a time record of some measured data and calculates the Fourier spectrum of the record using the Fast Fourier Transform algorithm (FFT). The program outputs the frequency vs amplitude and the frequency vs phase (in radians) to two separate data files. The phase depends on the starting time of the experiment. It can be used to judge the the relative phases of two simultaneously sampled channels.

6.6.2.3 PHAMP

This program removes phase shifts caused by the O.E.C. signal conditioners. The amplifiers were calibrated prior to the experiments to determine their phase shifts. In general, all amplifiers were set up as low pass filters to remove high frequency noise and interference. The program takes as input a phase file and the slope and intercept of the phase shift caused by the amplifier used. The output file contains the corrected phase values.

6.6.2.4 DELAY

This program adjusts the phase of the wave probe record to account for the distance between the centreline of the cylinder and the wave probe. It takes as input the phase

record of the wave and the distance from the wave probe to the cylinder centreline. The output is the adjusted phase of the wave.

6.6.2.5 SPECADD

This program adds or subtracts spectra. For the purpose of these experiments it was used to remove a reference phase from one or more phase spectra. Thus the phase of one record can be expressed relative to another.

6.6.2.6 ZERO

This is a program used to zero the spectrum of some record. Here, it was used to zero the reference phase spectrum.

6.6.2.7 TABLE

This program scans an amplitude spectrum for local maxima. A cut off amplitude value can be input and the user can selectively chose the frequency/amplitude point to output.This way driving frequency harmonics can be ignored. The harmonics are a result of a finite time record sampled at definite intervals. The program outputs the amplitude and phase of the record for the chosen frequency. The 90° and 180° components of the vector can also be output if required.

6.6.2.8 FINAL

This program calculates the added mass and damping coefficents from the 90° and 180° components of the vertical

force. The cylinder mass, the cross sectional area of the cylinder, and the buoyancy are input for non-dimensionalisation.

6.6.2.9 STAT

This program performs the same function as FINAL, but for the calculation of the non-dimensional exciting force from the vertical exciting force and the wave amplitude records.

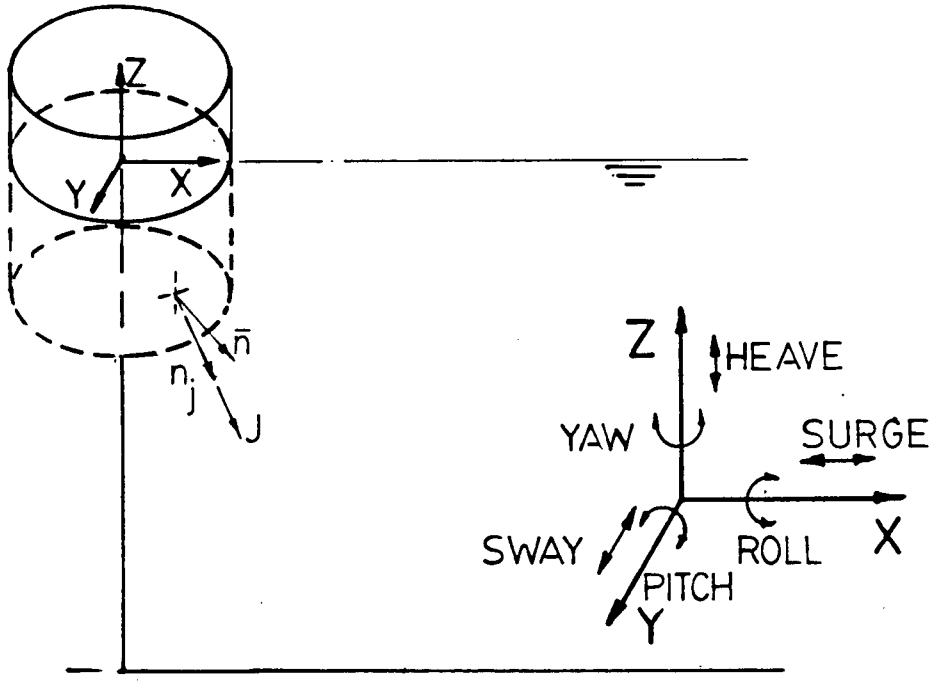

Fig.1 Definition of motions

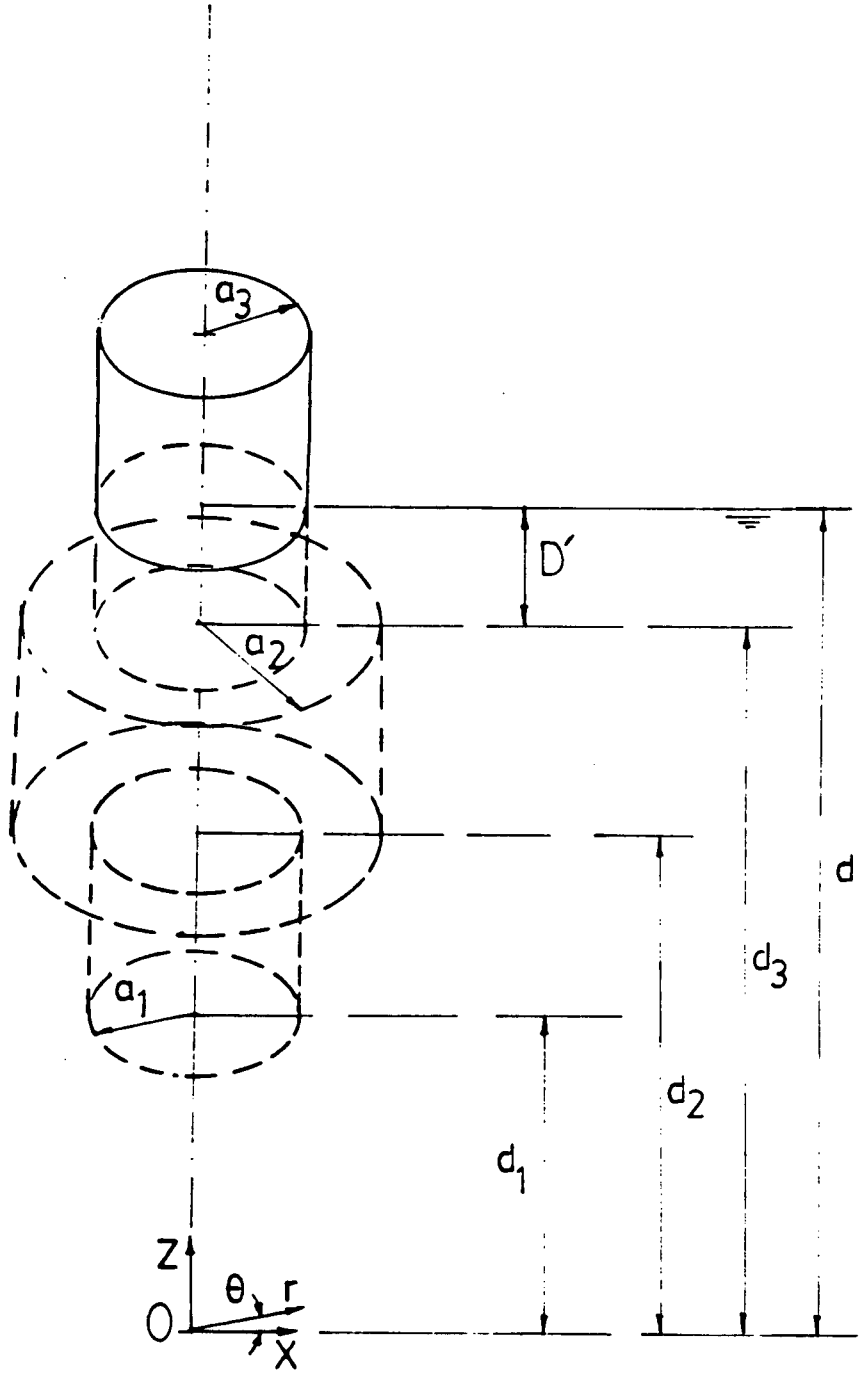

Fig.2 Compound cylinder geometry

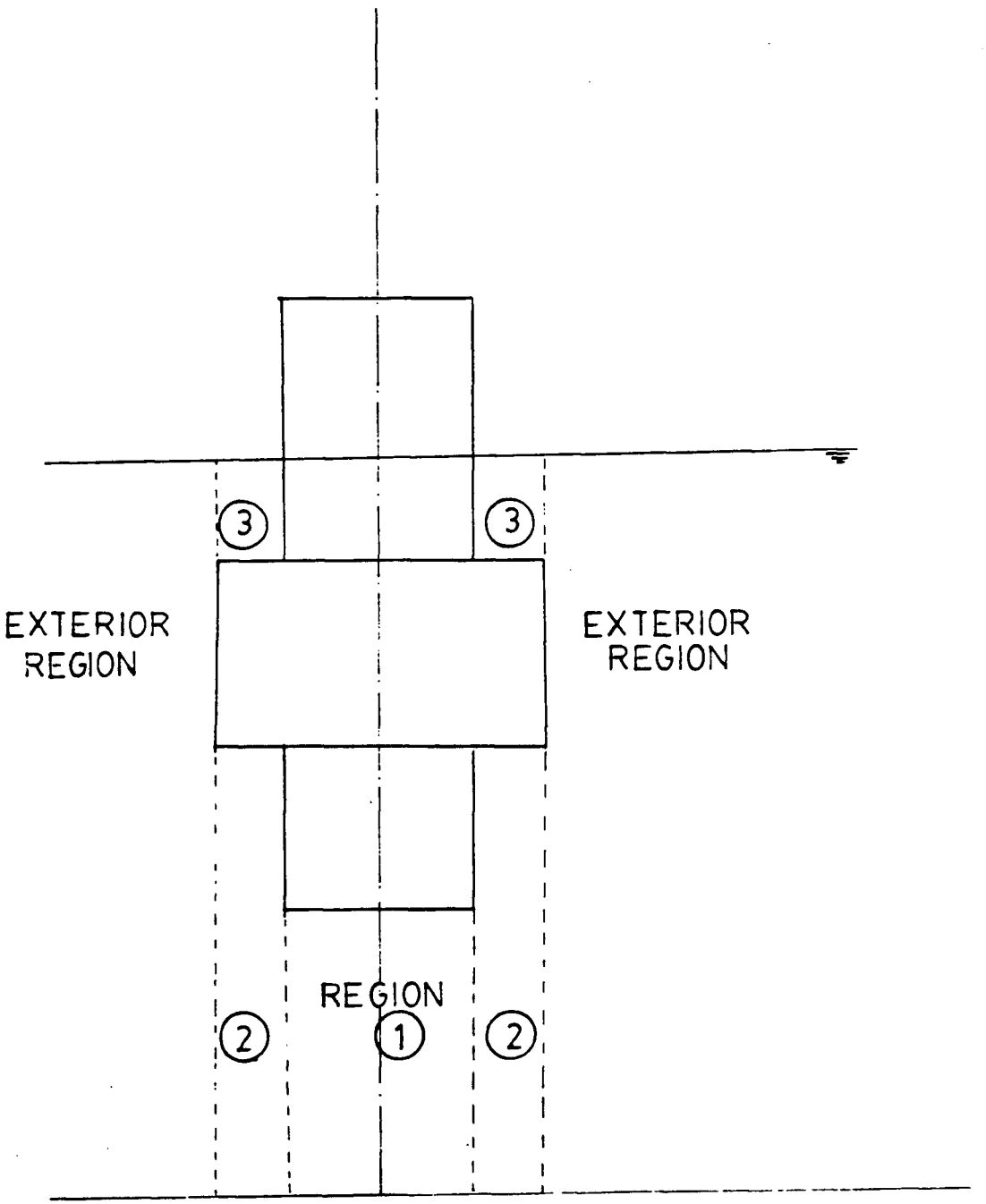

Fig.3 Subdivision of flow field

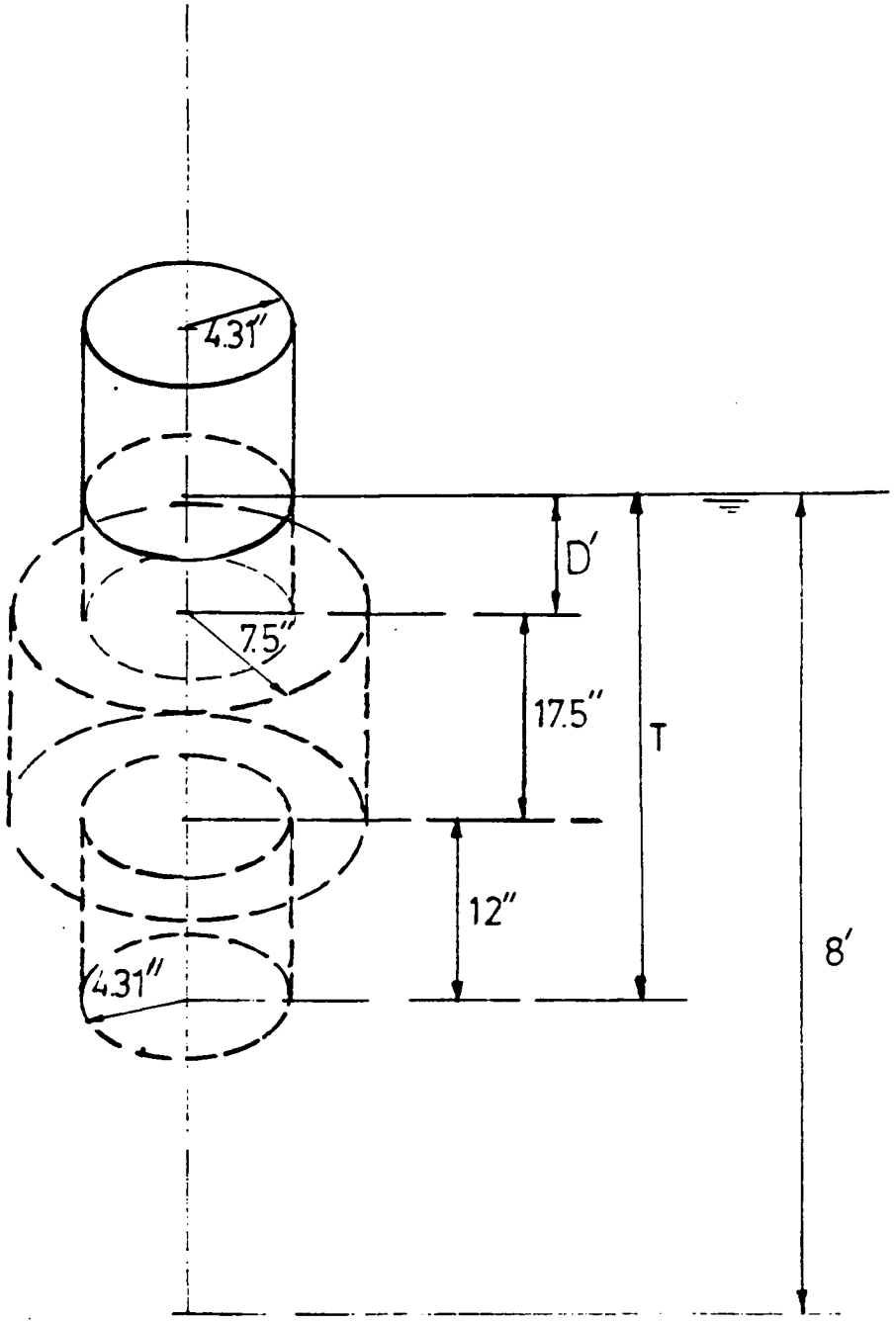

Fig.4 Compound cylinder model

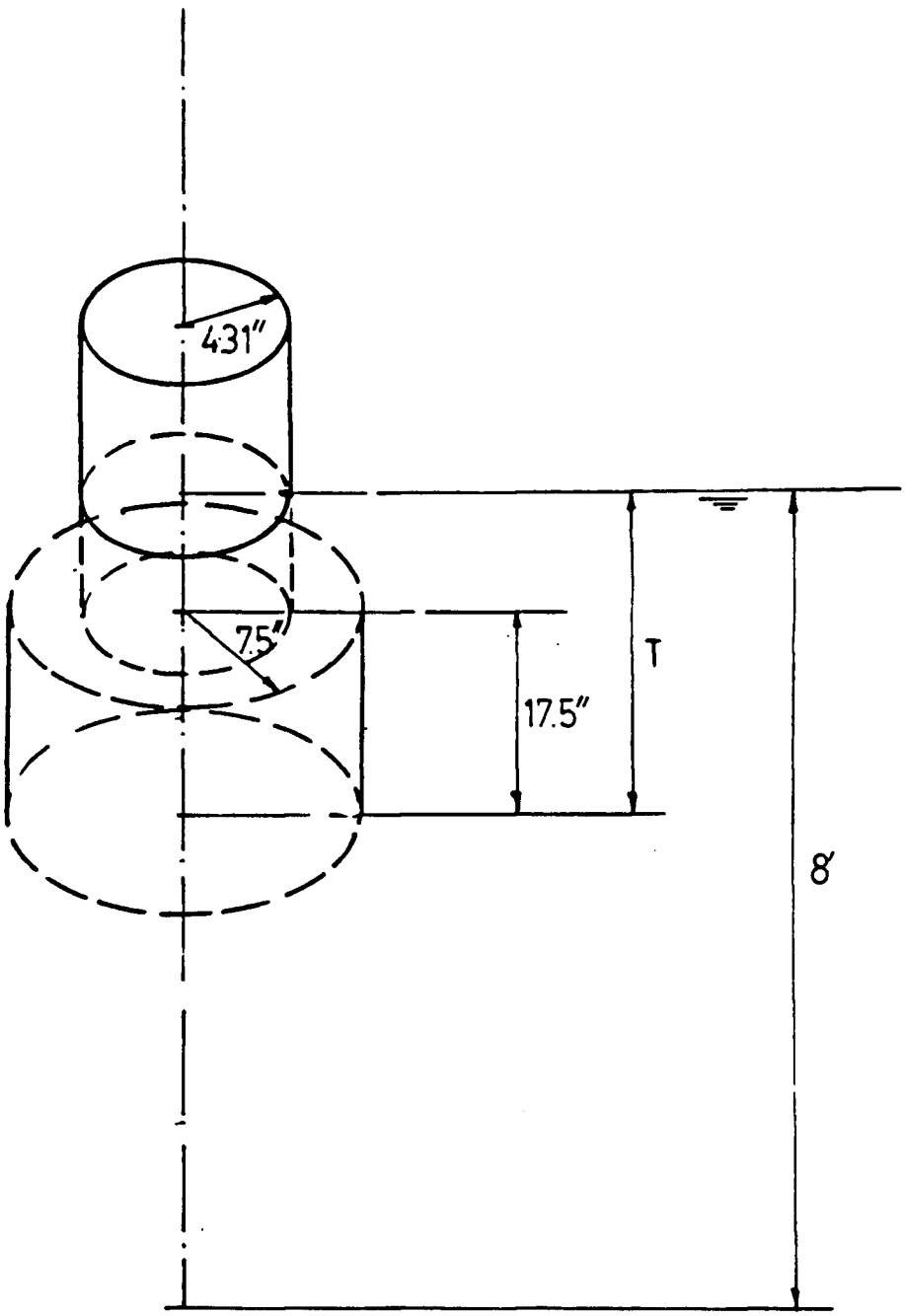

Fig.5 Double cylinder model

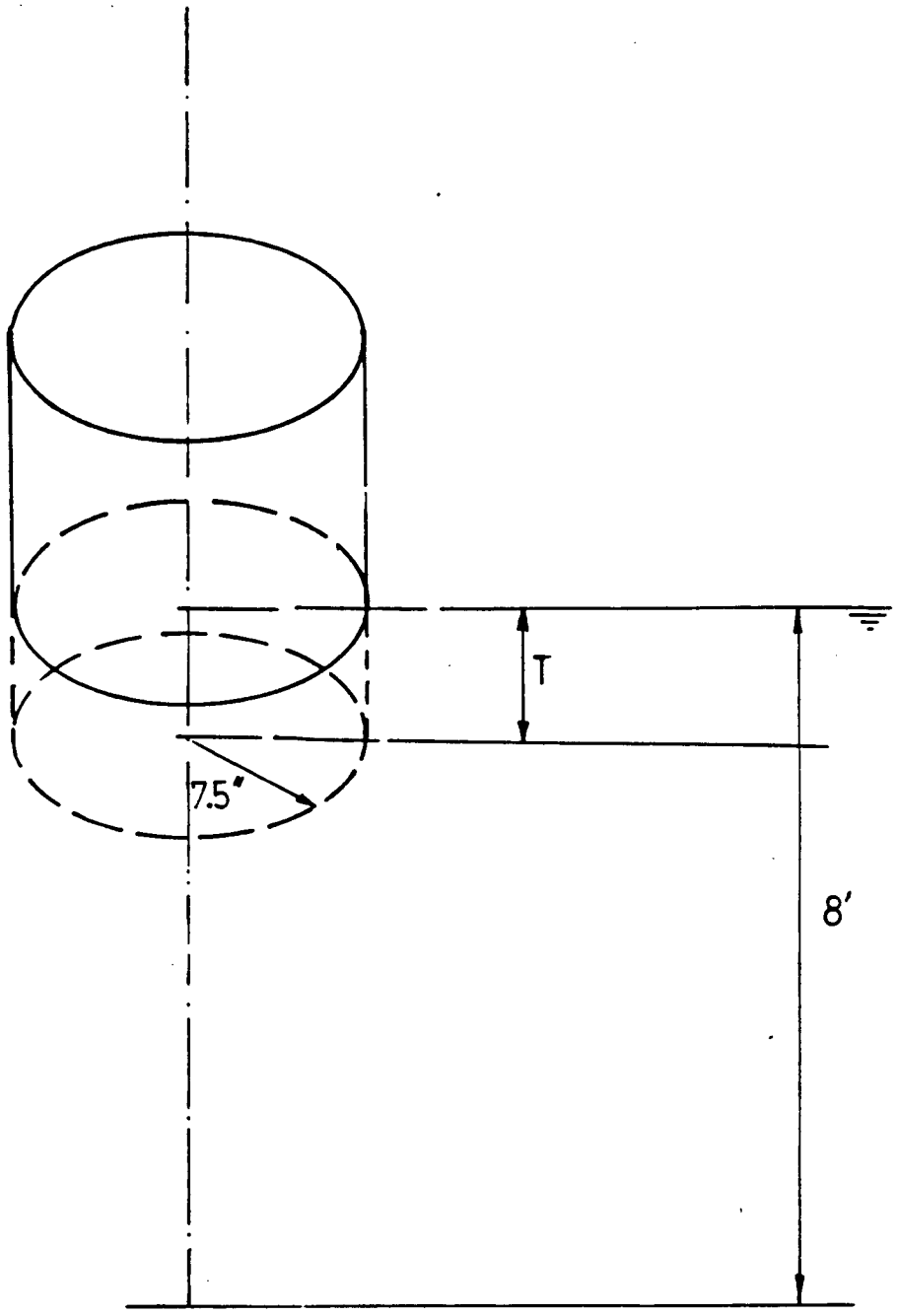

Fig.6 Single cylinder model

Fig.7 Towing tank at B.C. Research

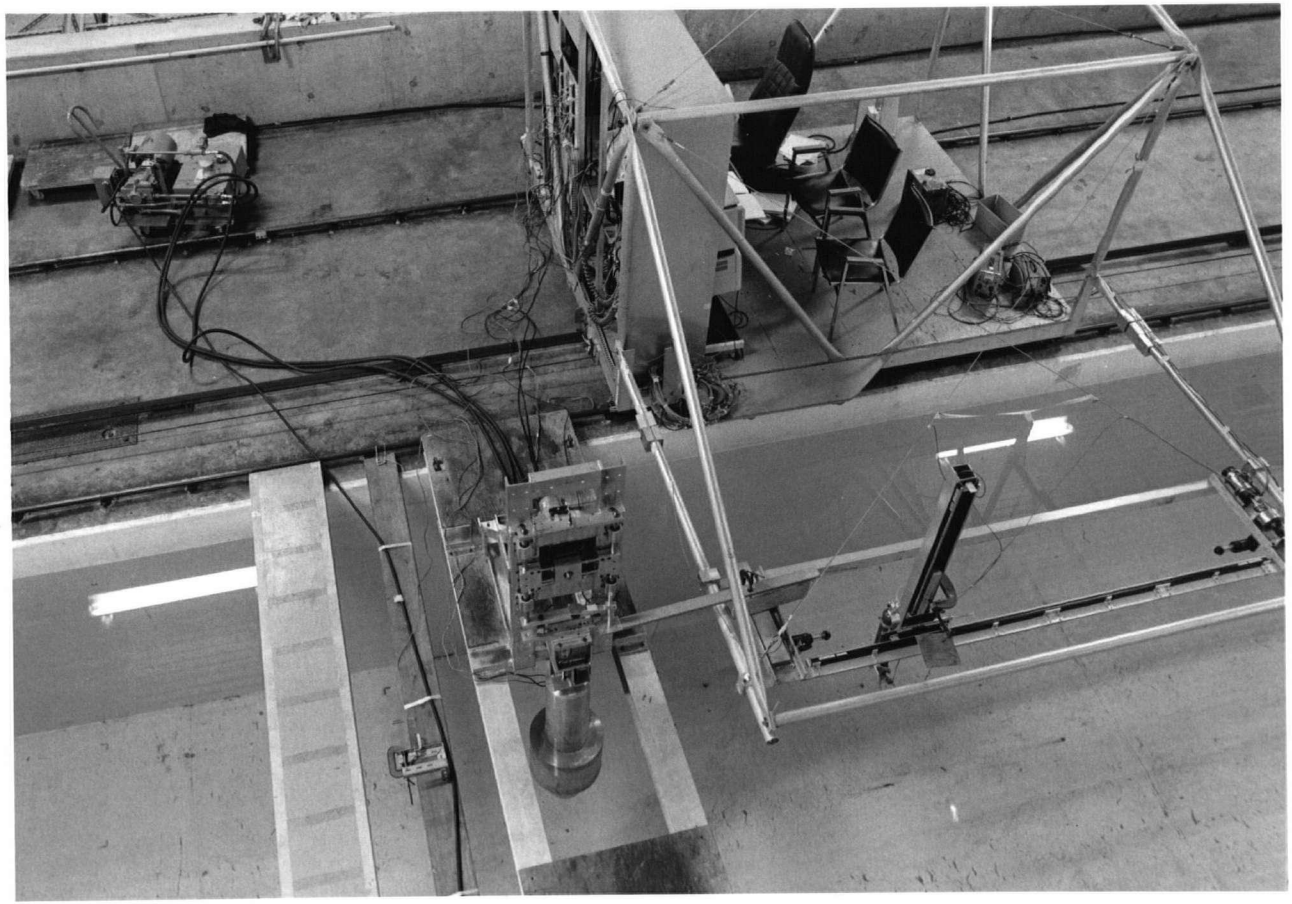

Fig.8 Motion generator

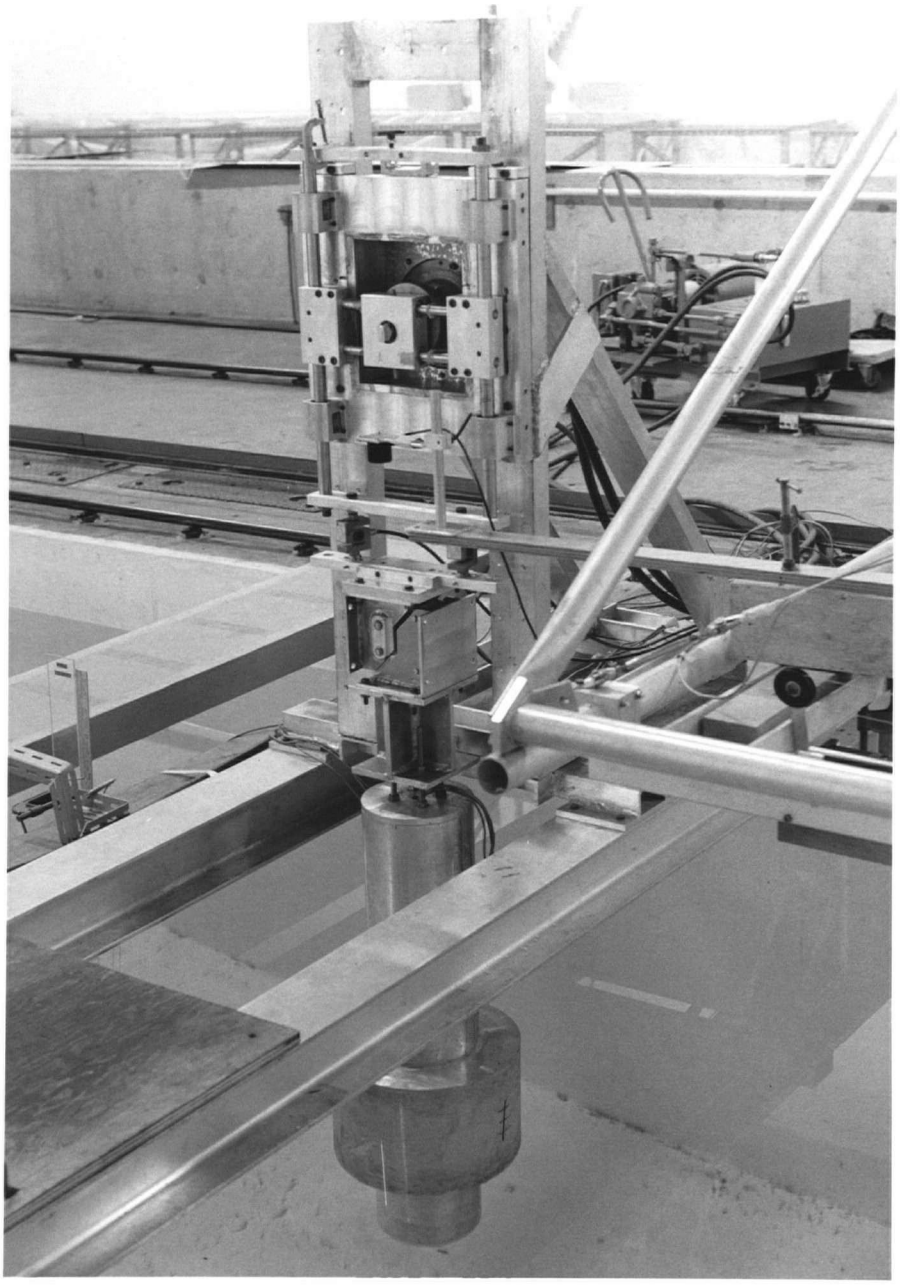

Fig.8a Positioning of load cells

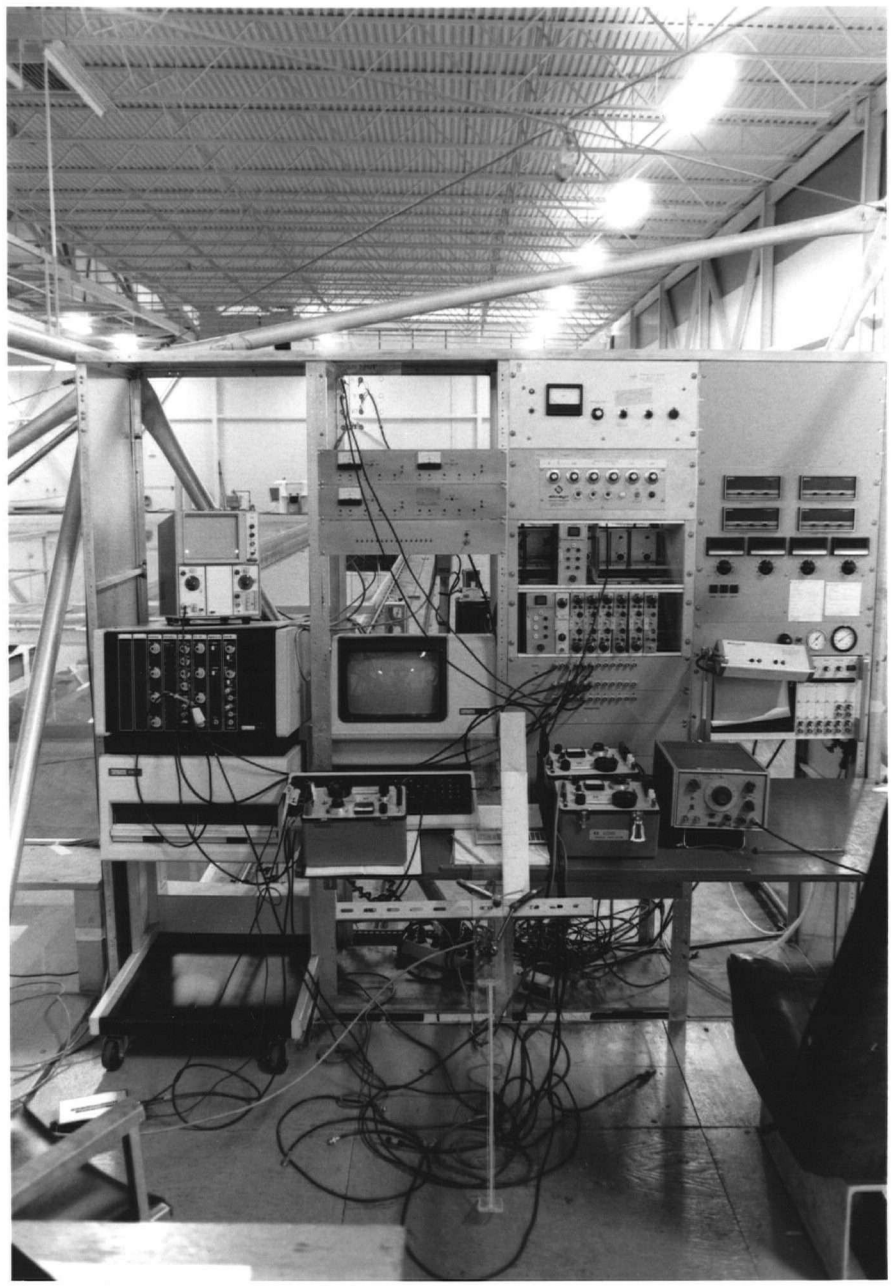

Fig.9 Data collection equipment

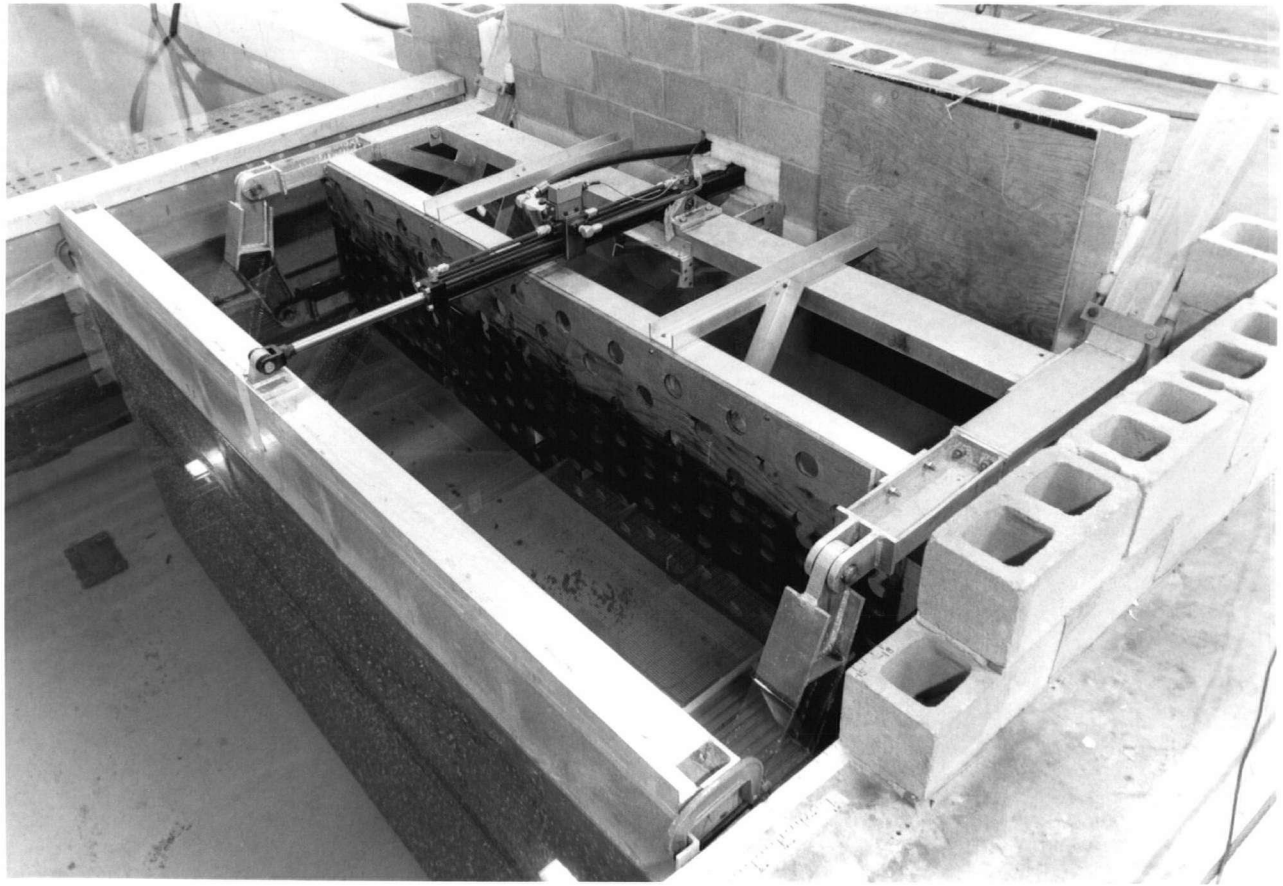

Fig.10 Wave paddle

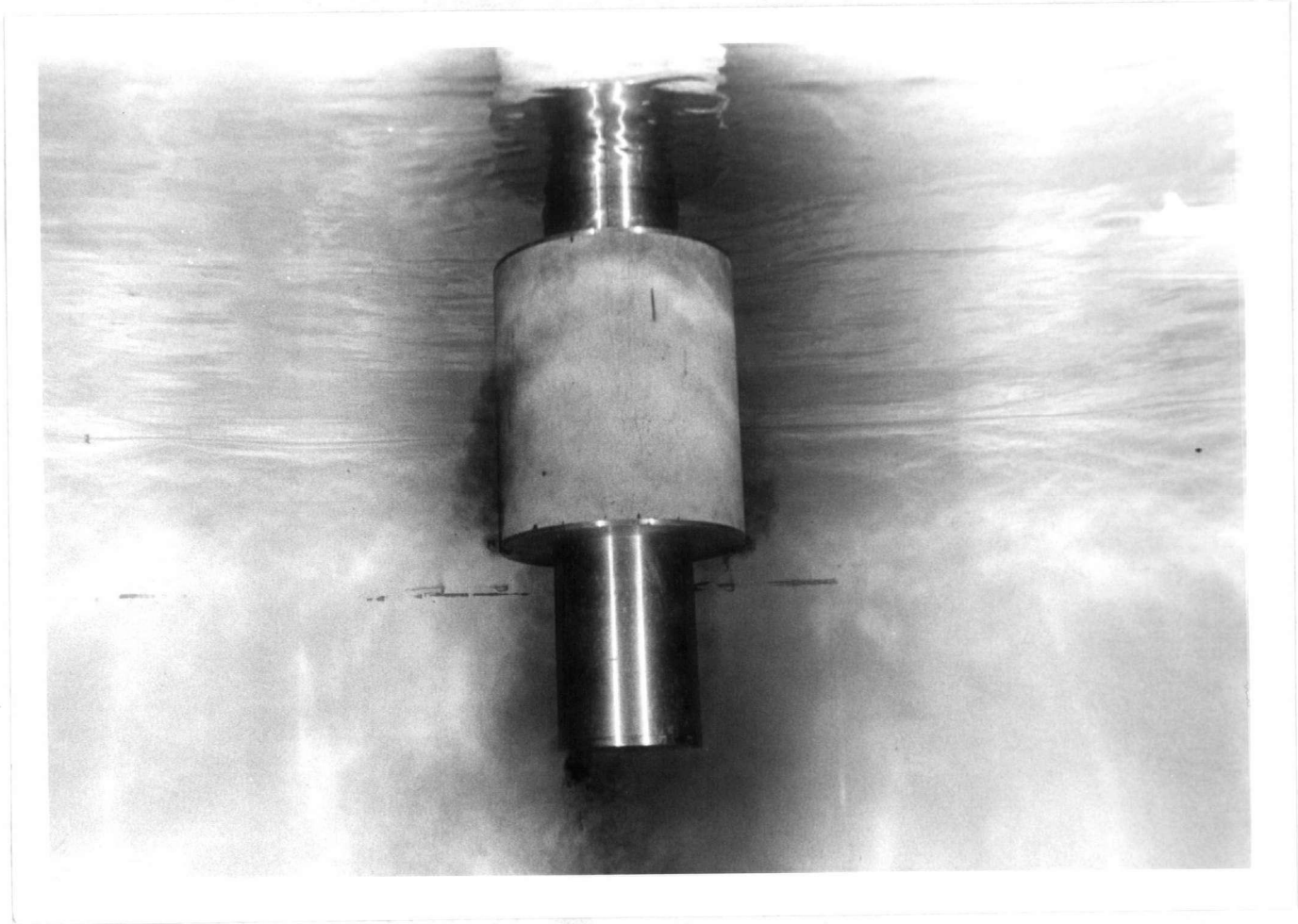

Fig.11 Flow visualization

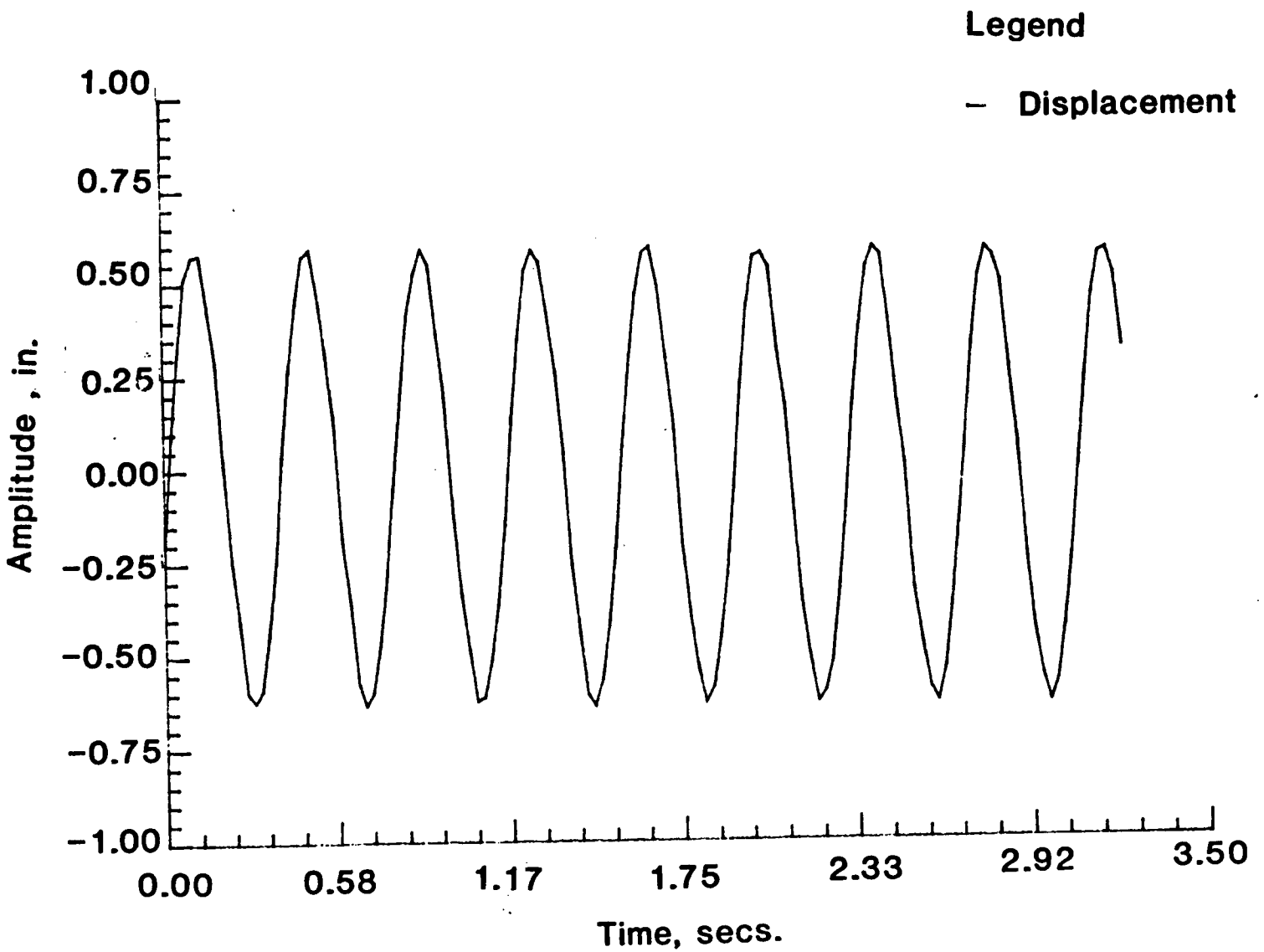

Fig.12 Displacement record . Compound cylinder T=35.5" f=2.5Hz

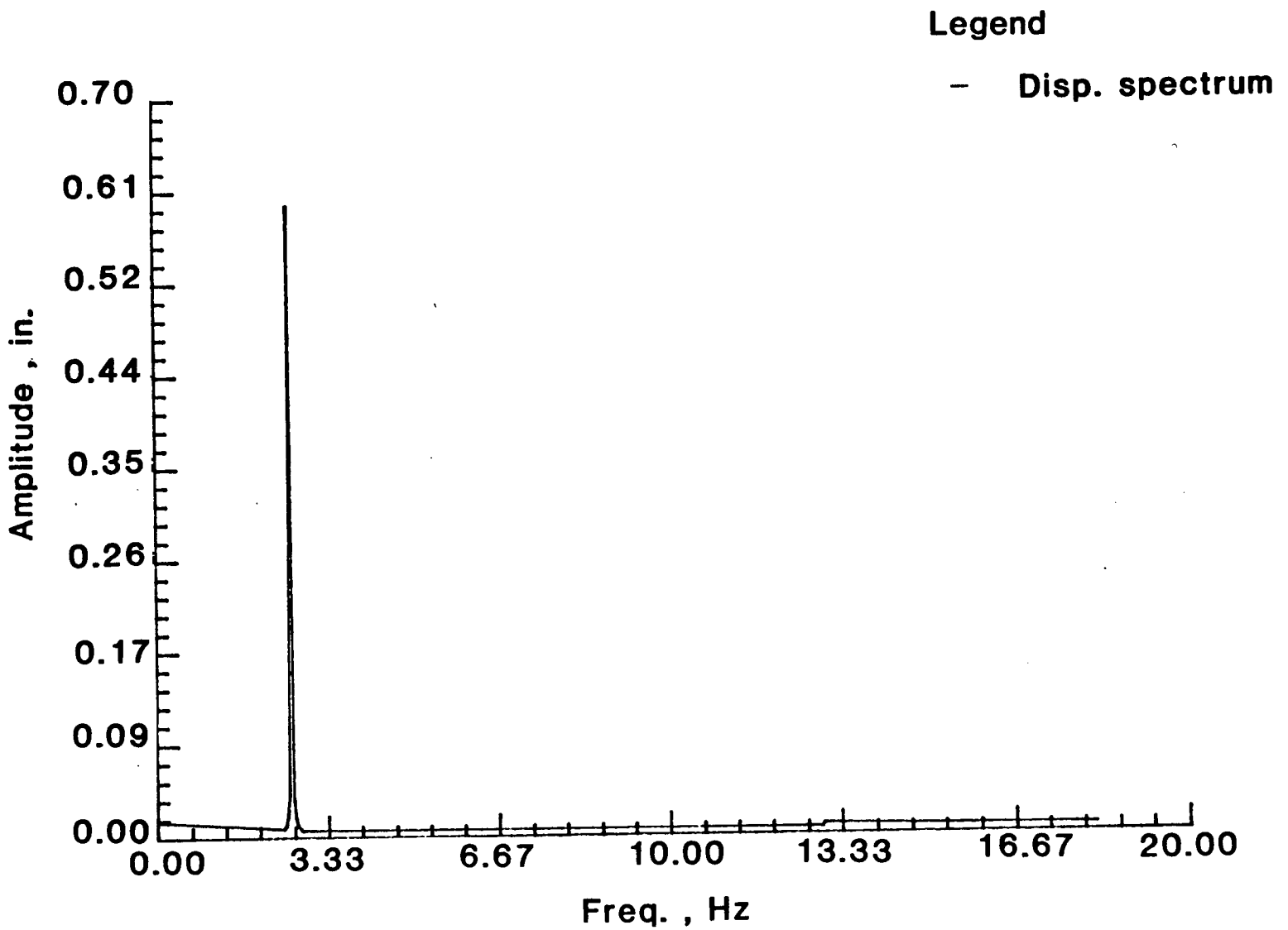

Fig.12a Disp. amplitude spectrum. Compound cylinder T=35.5" f=2.5Hz

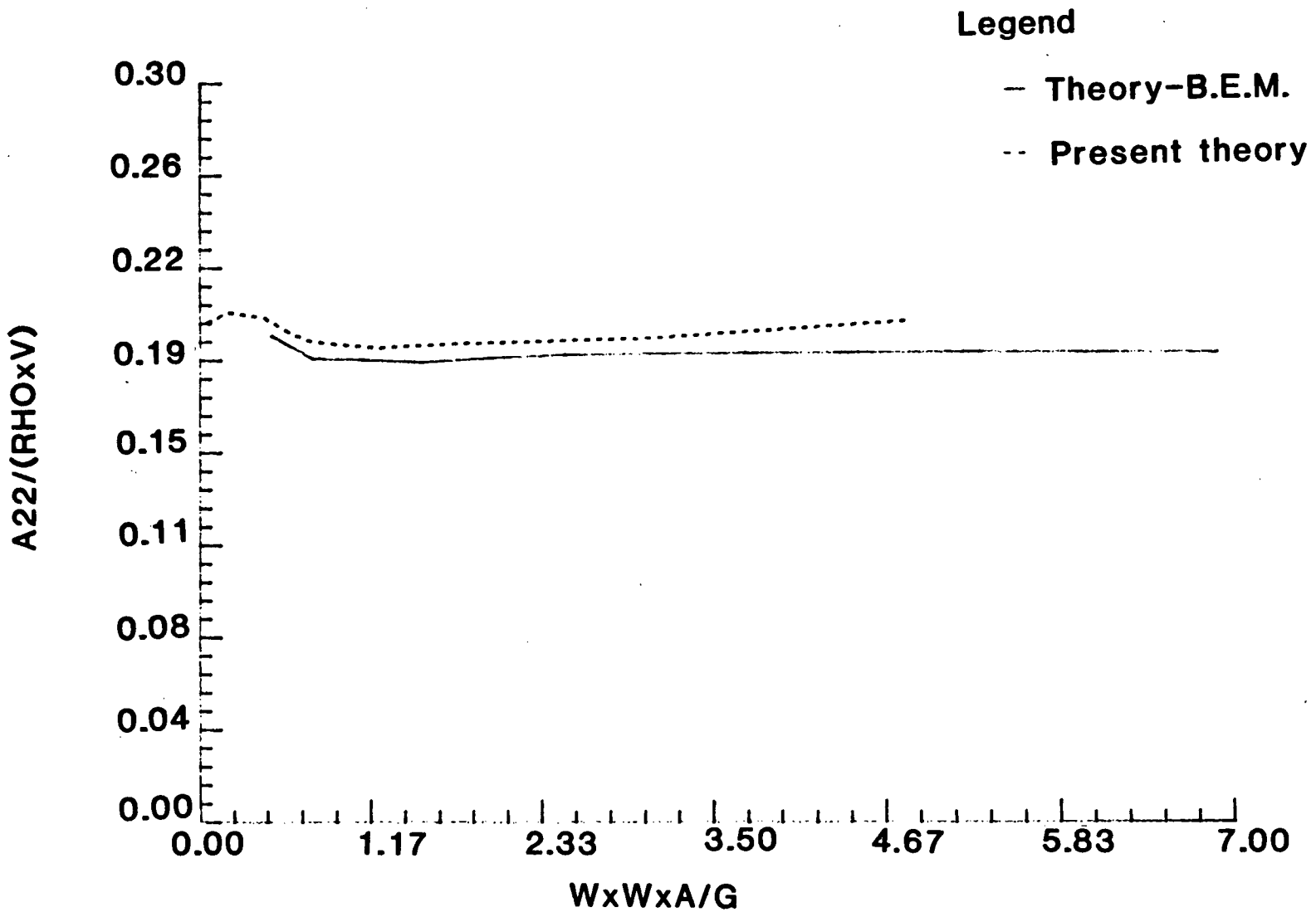

Fig.13 Heave added mass. Compound cylinder T=42.625" D'=13.125"

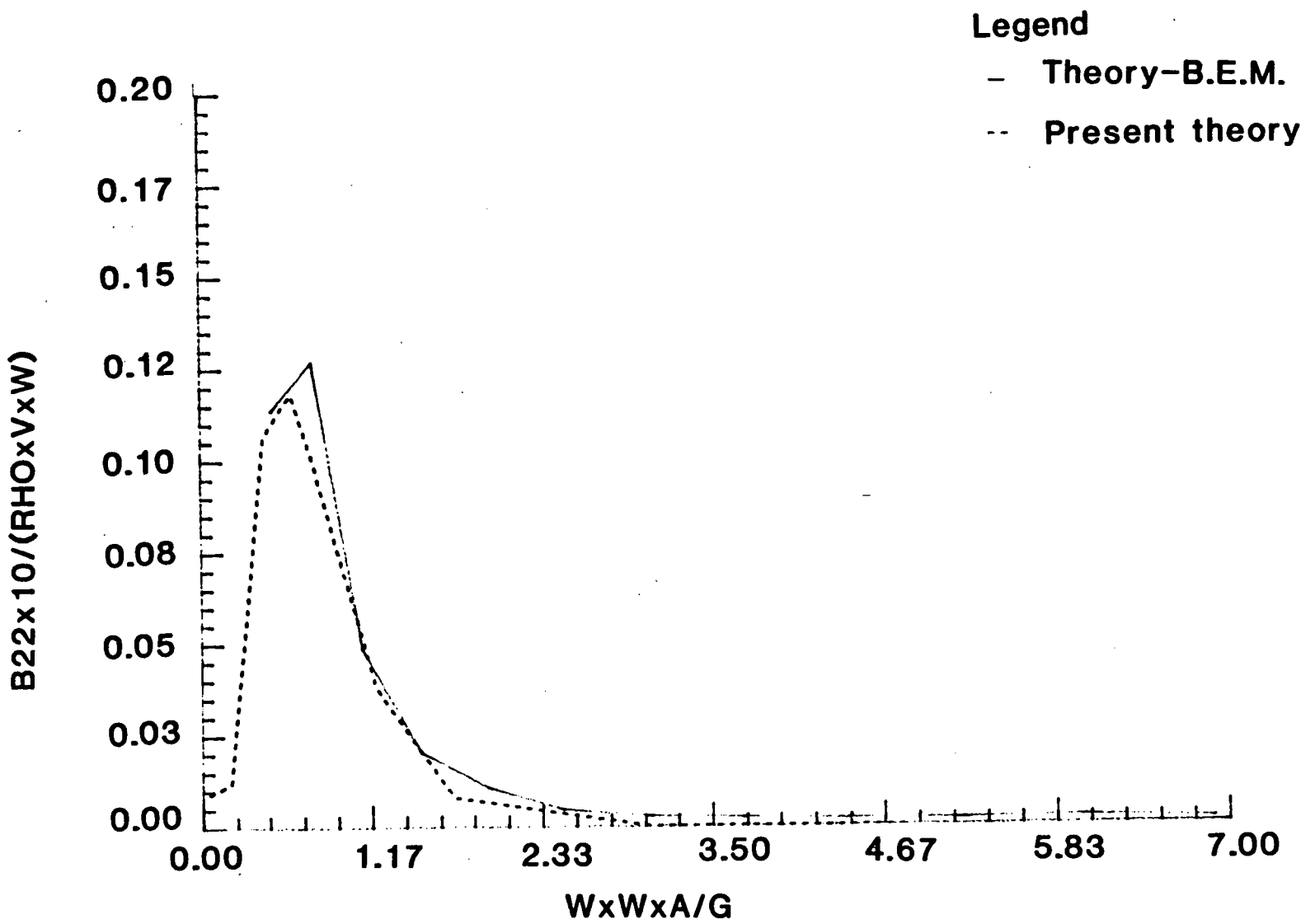

Fig.14 Damping coefficient. Compound cylinder T=42.625" D'=13.125"

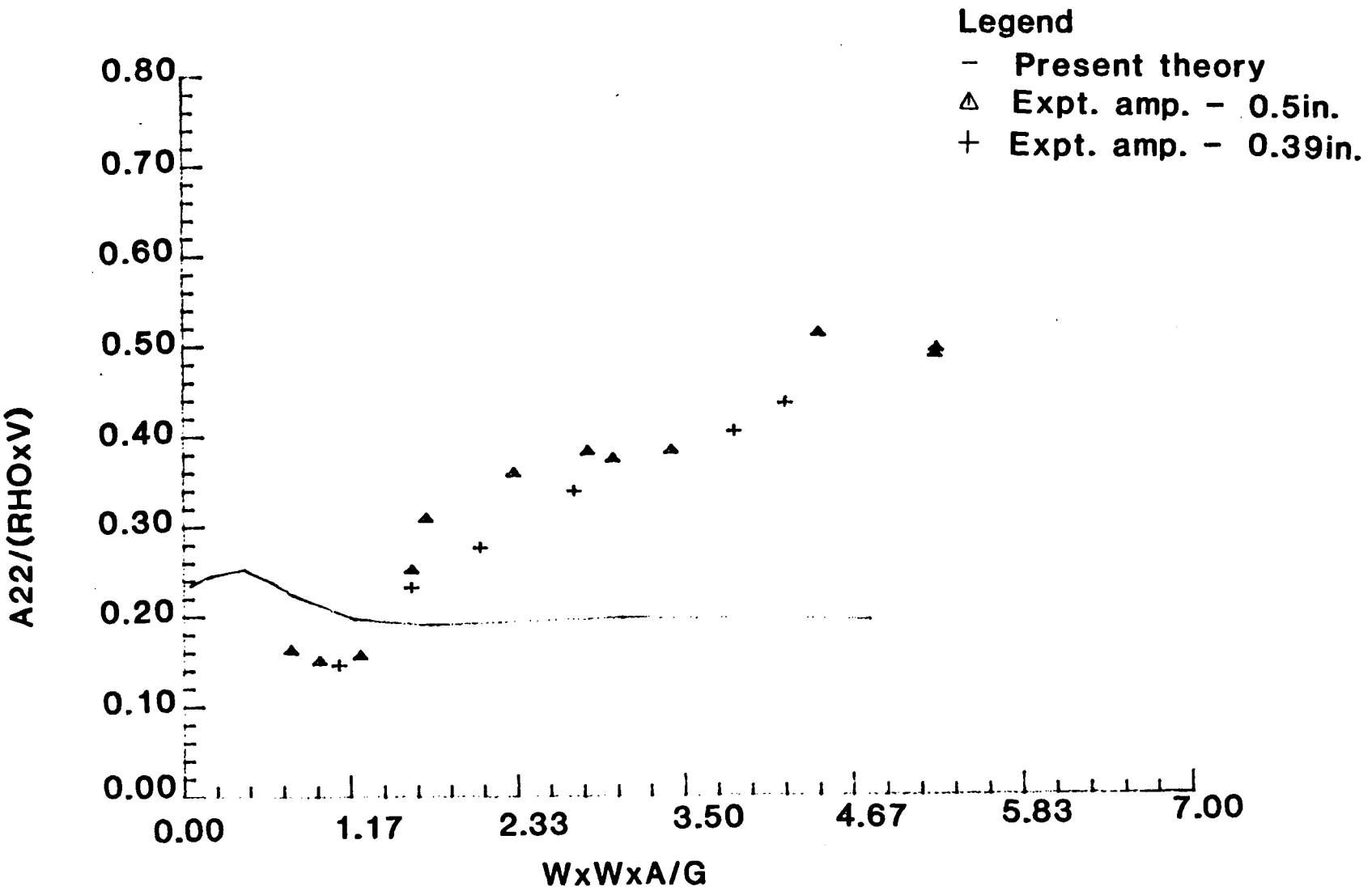

Fig.15 Heave added mass. Compound cylinder T=35.5" D'=6"

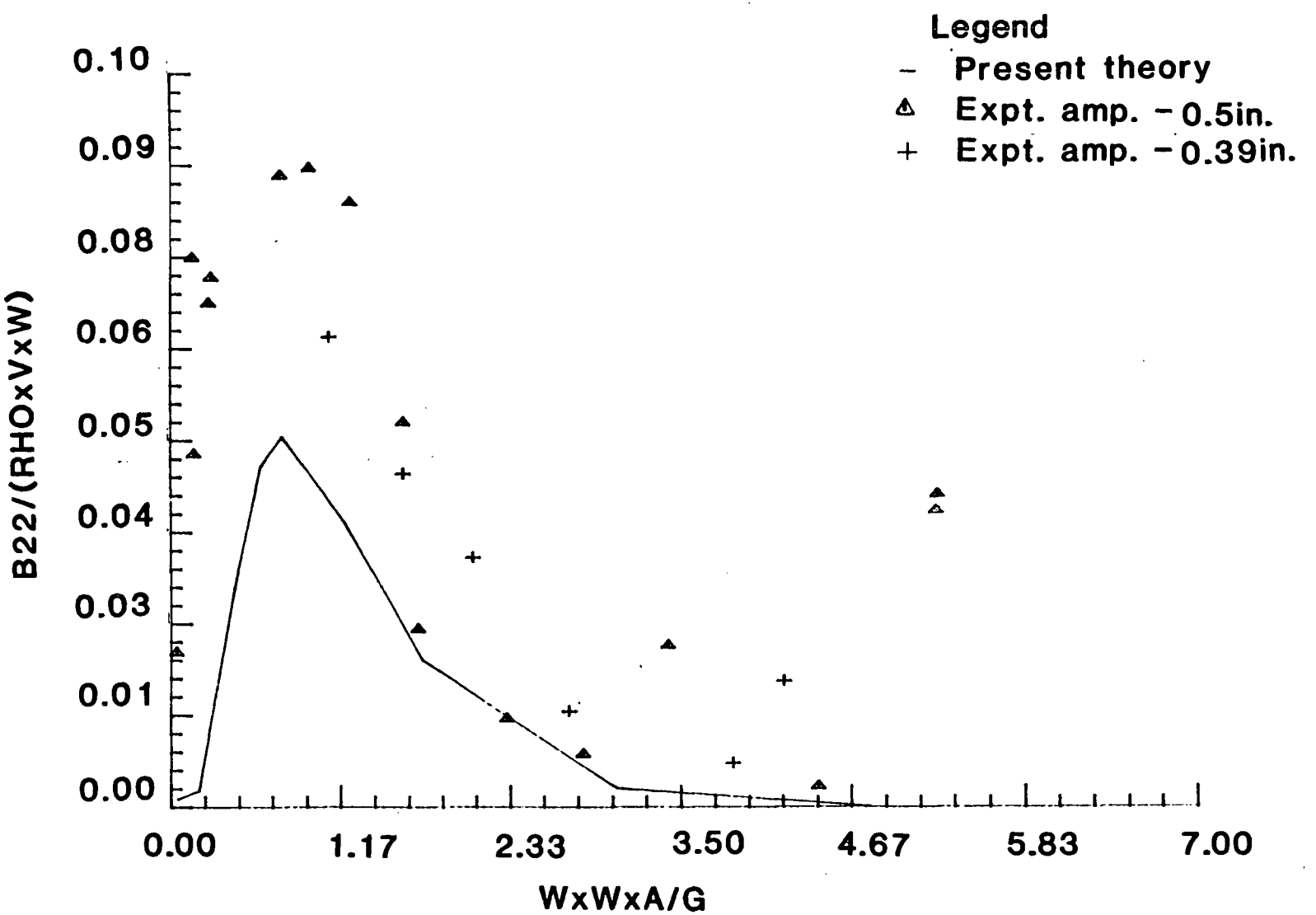

Fig.16 Damping coefficient. Compound cylinder T=35.5" D'=6"

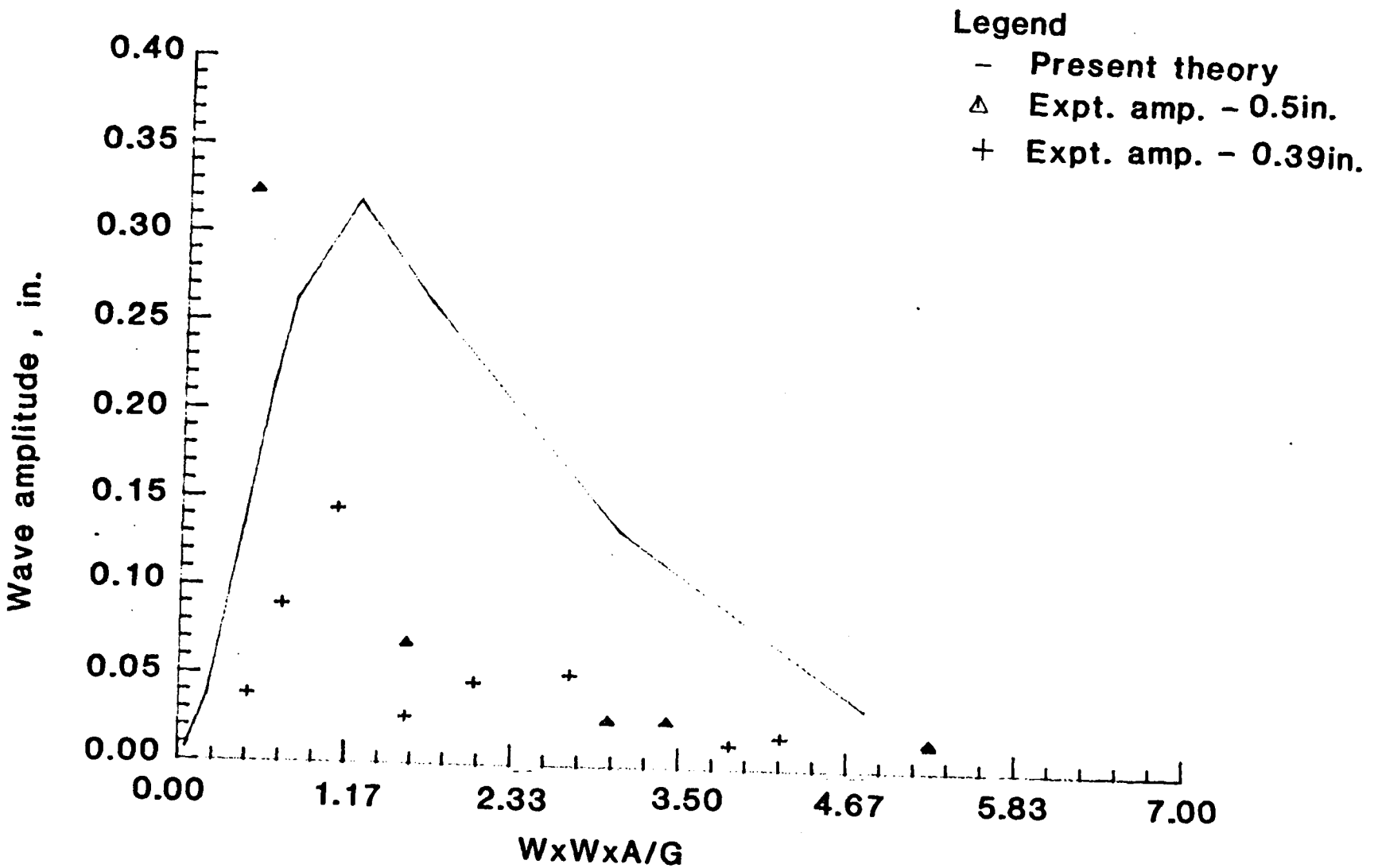

Fig.17 Wave amplitude. Compound cylinder T=35.5" D'=6"

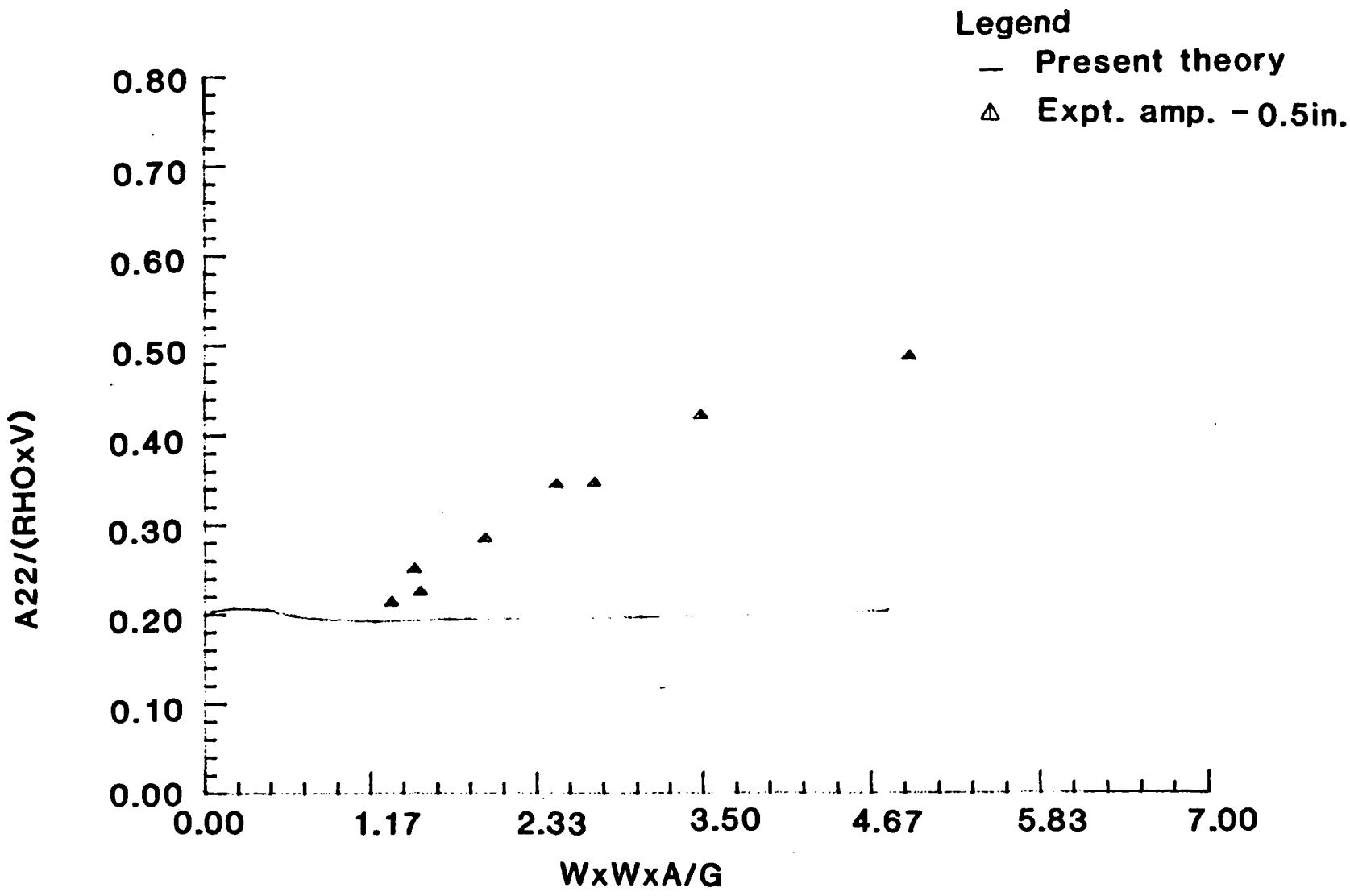

Fig.18 Heave added mass. Compound cylinder T=39.5" D'=10"

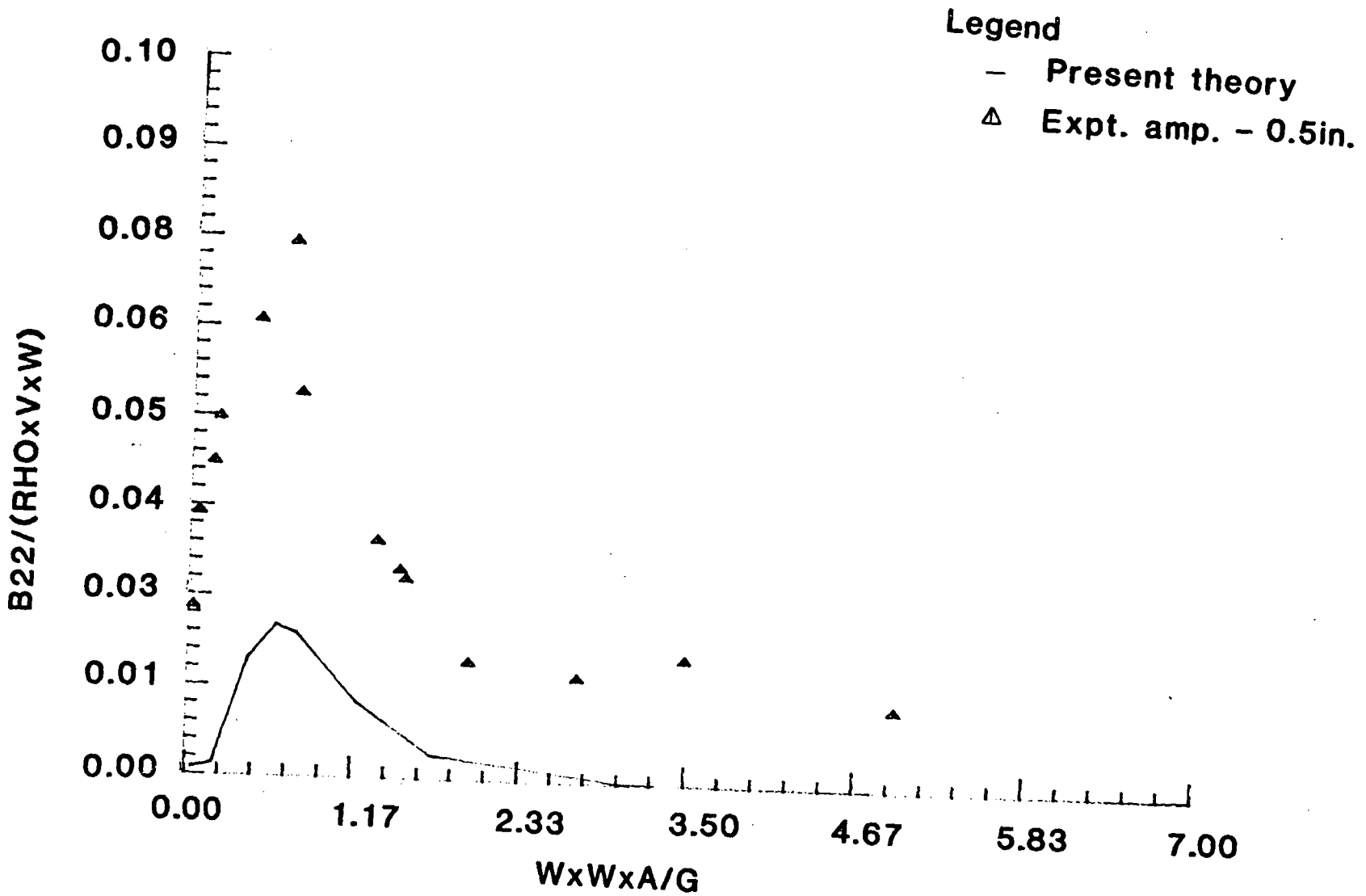

Fig.19 Damping coefficient. Compound cylinder T=39.5" D'=10"

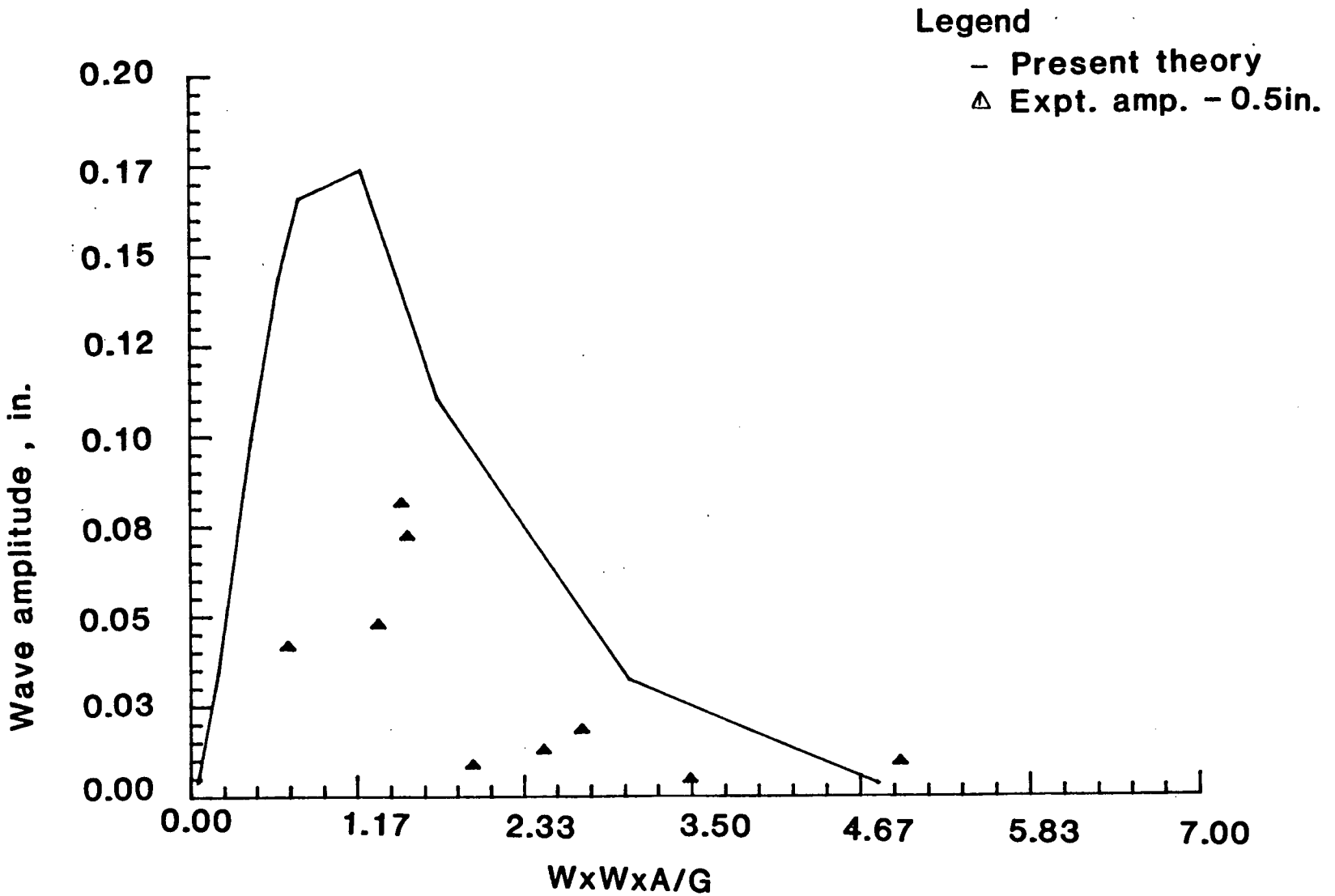

Fig.20 Wave amplitude. Compound cylinder T=39.5" D'=10"

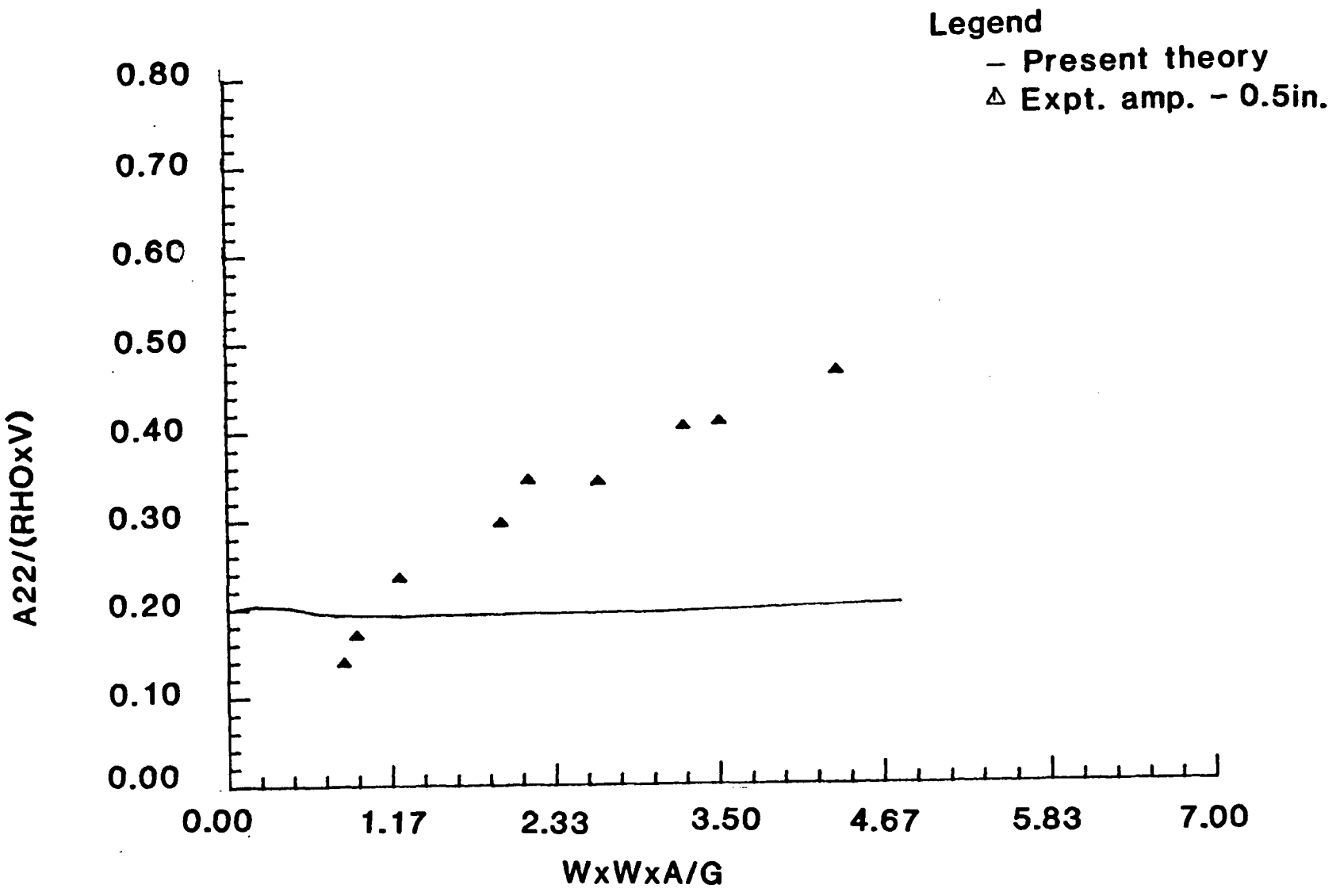

Fig.21 Heave added mass. Compound cylinder T=43.5" D'=14"

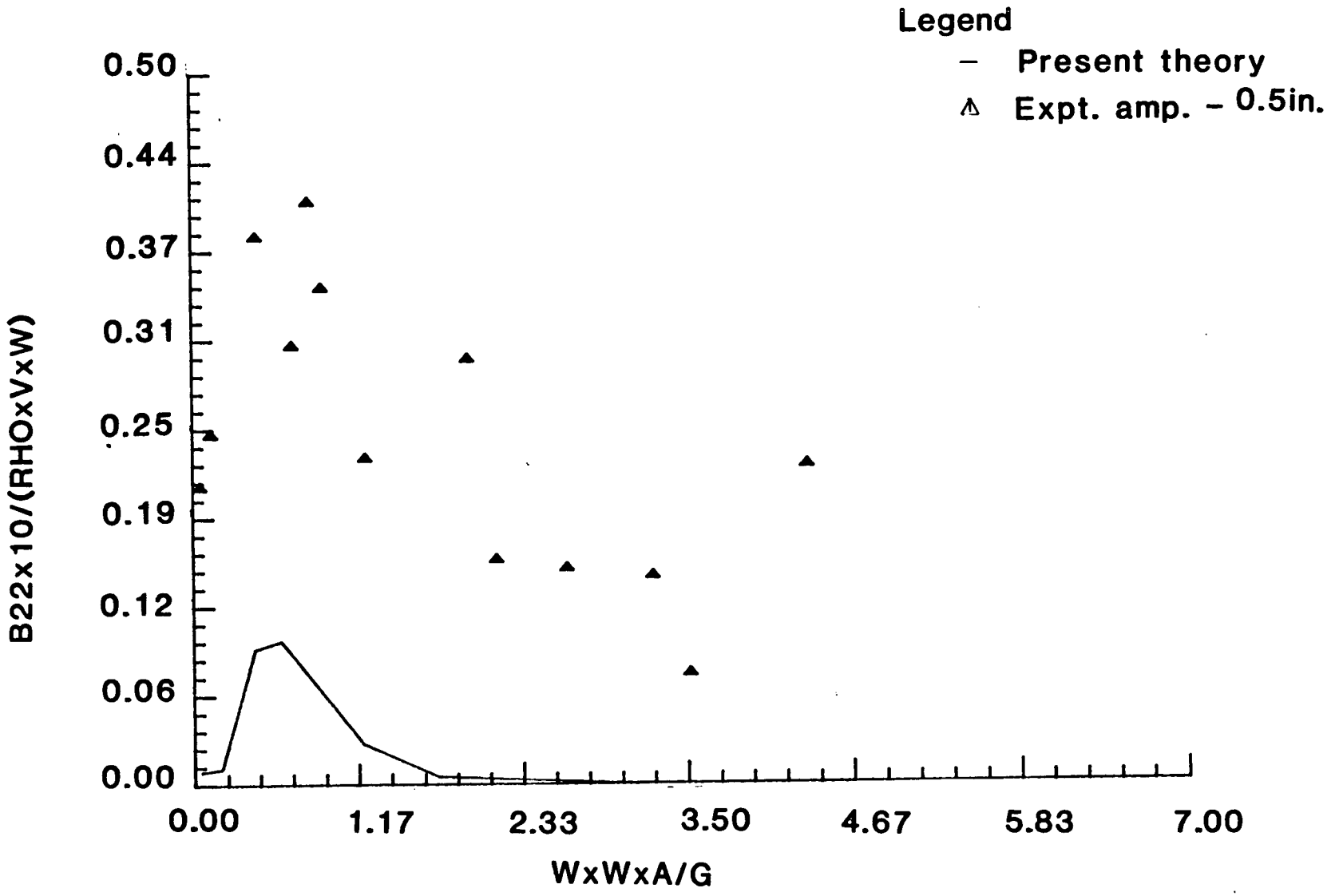

Fig.22 Damping coefficient. Compound cylinder T=43.5" D'=14"

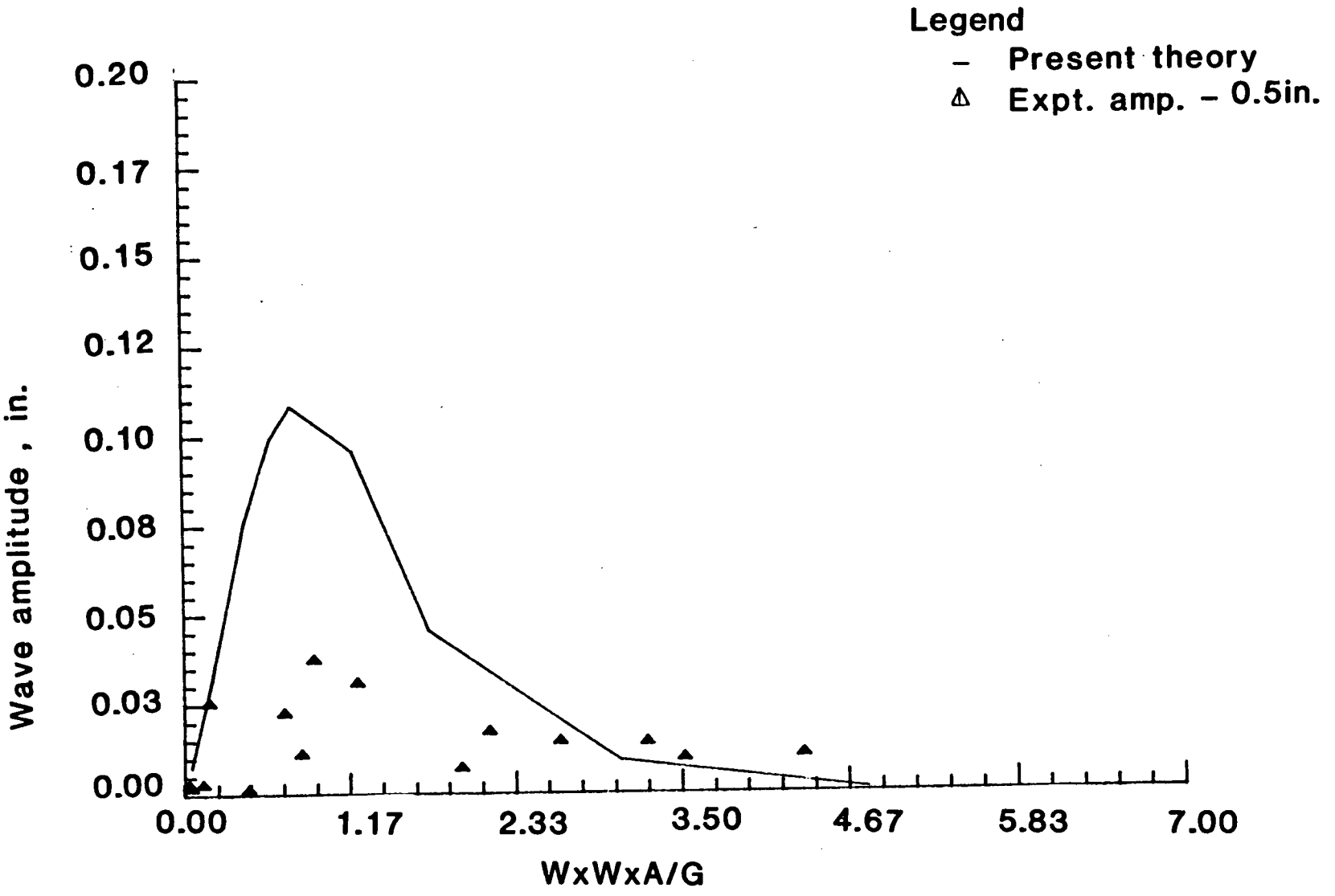

Fig.23 Wave amplitude. Compound cylinder T=43.5" D'=14"

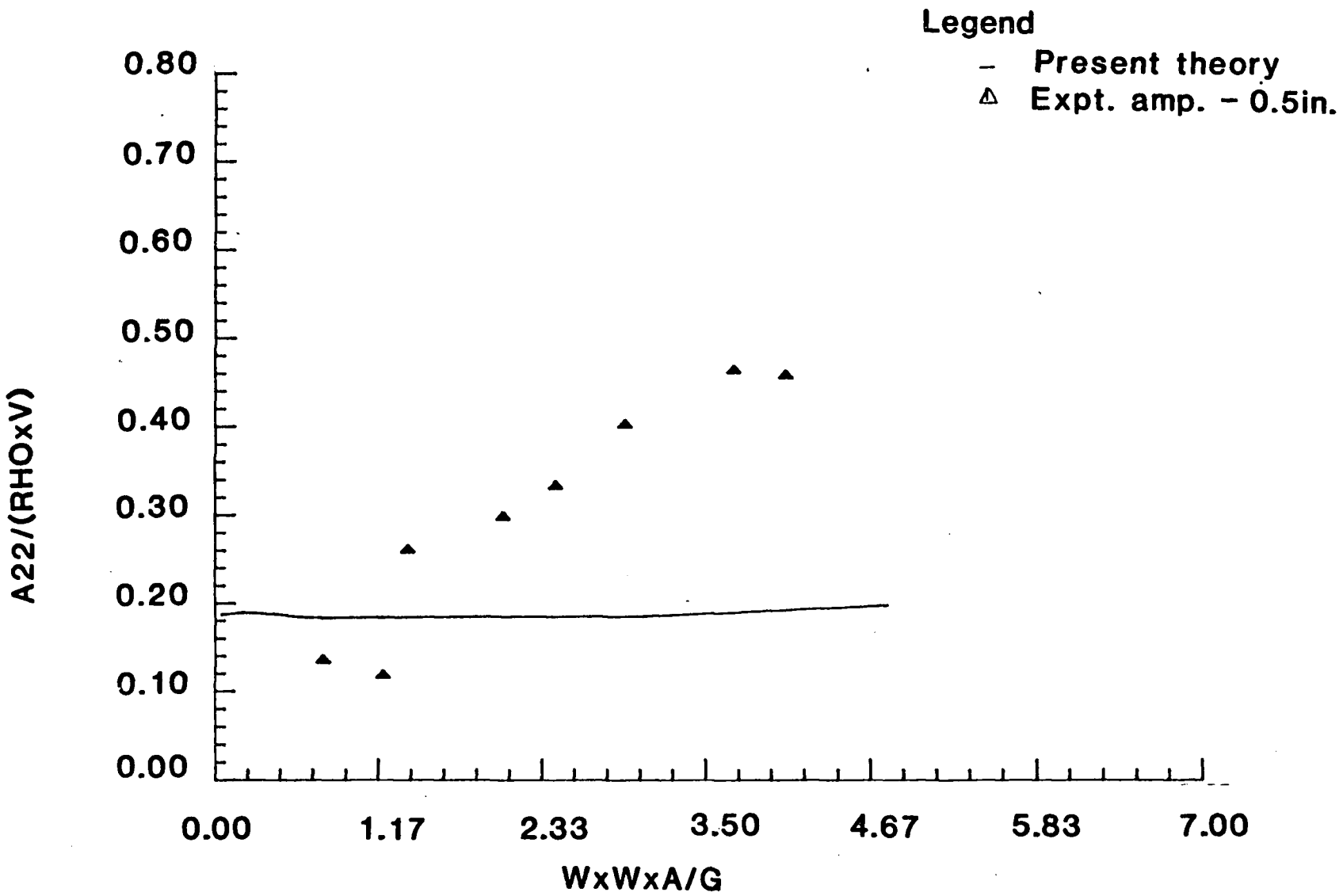

Fig.24 Heave added mass. Compound cylinder T=47.5" D'=18"

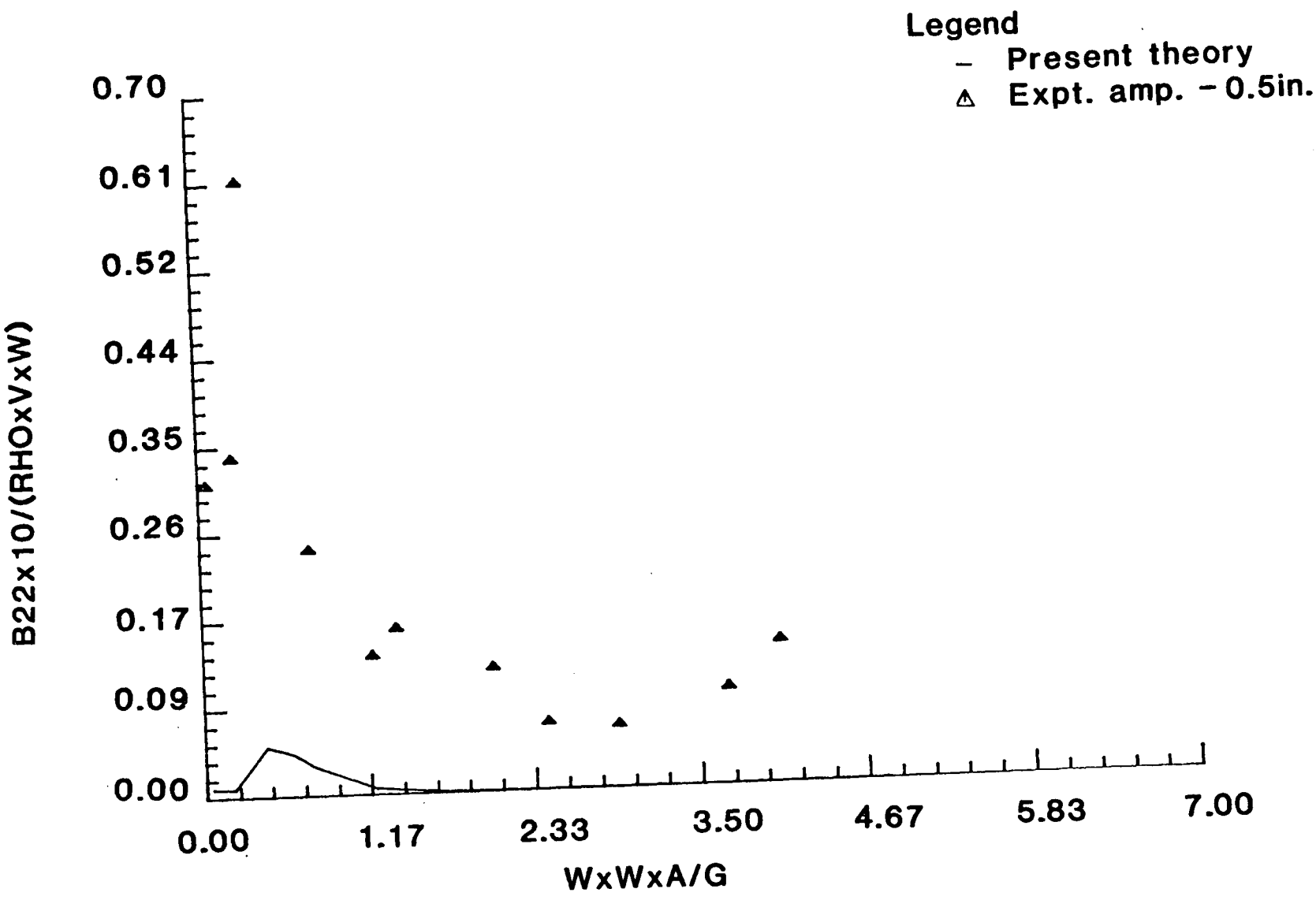

Fig.25 Damping coefficient. Compound cylinder T=47.5" D'=18"

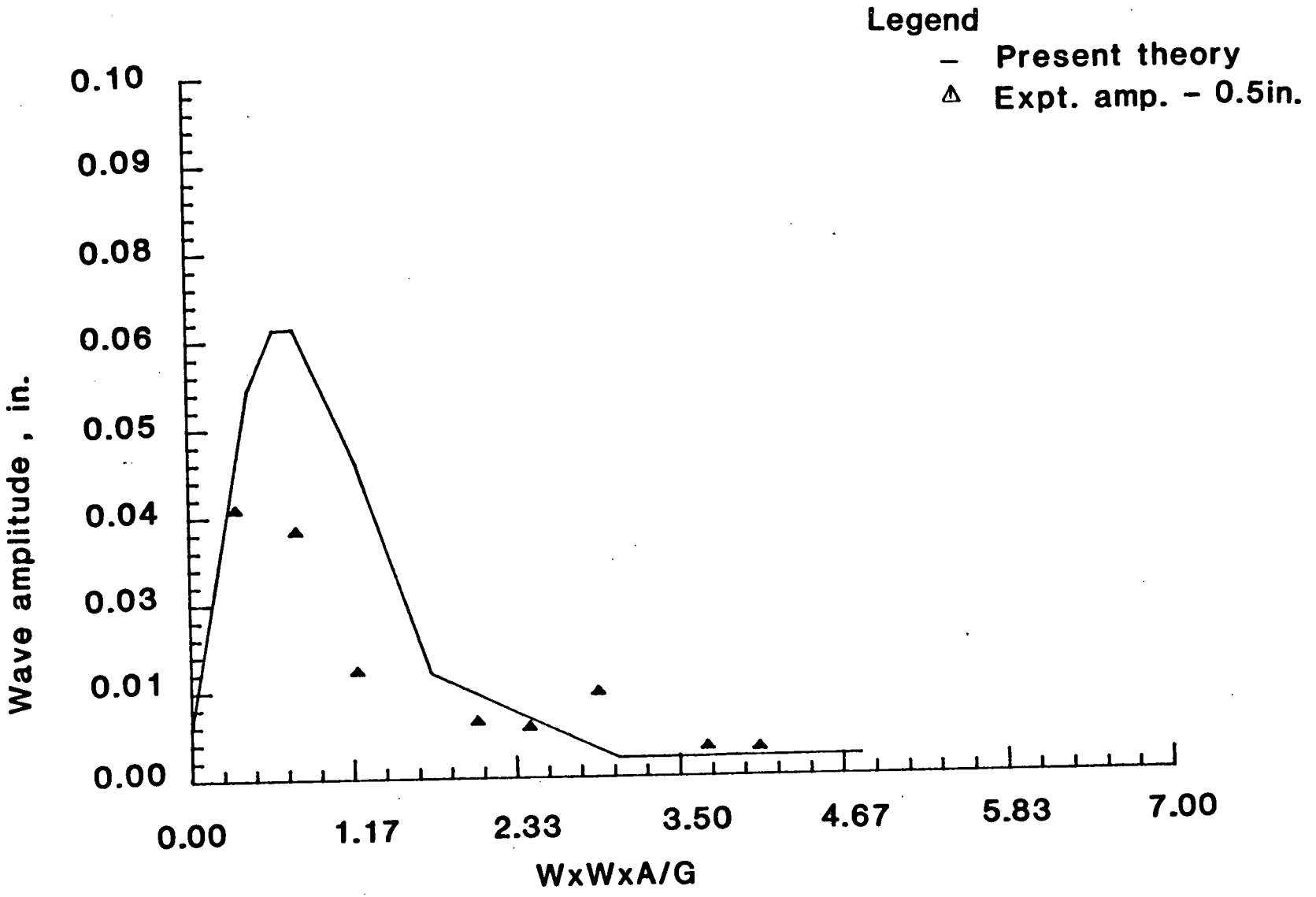

Fig.26 Wave amplitude. Compound cylinder T=47.5" D'=18"

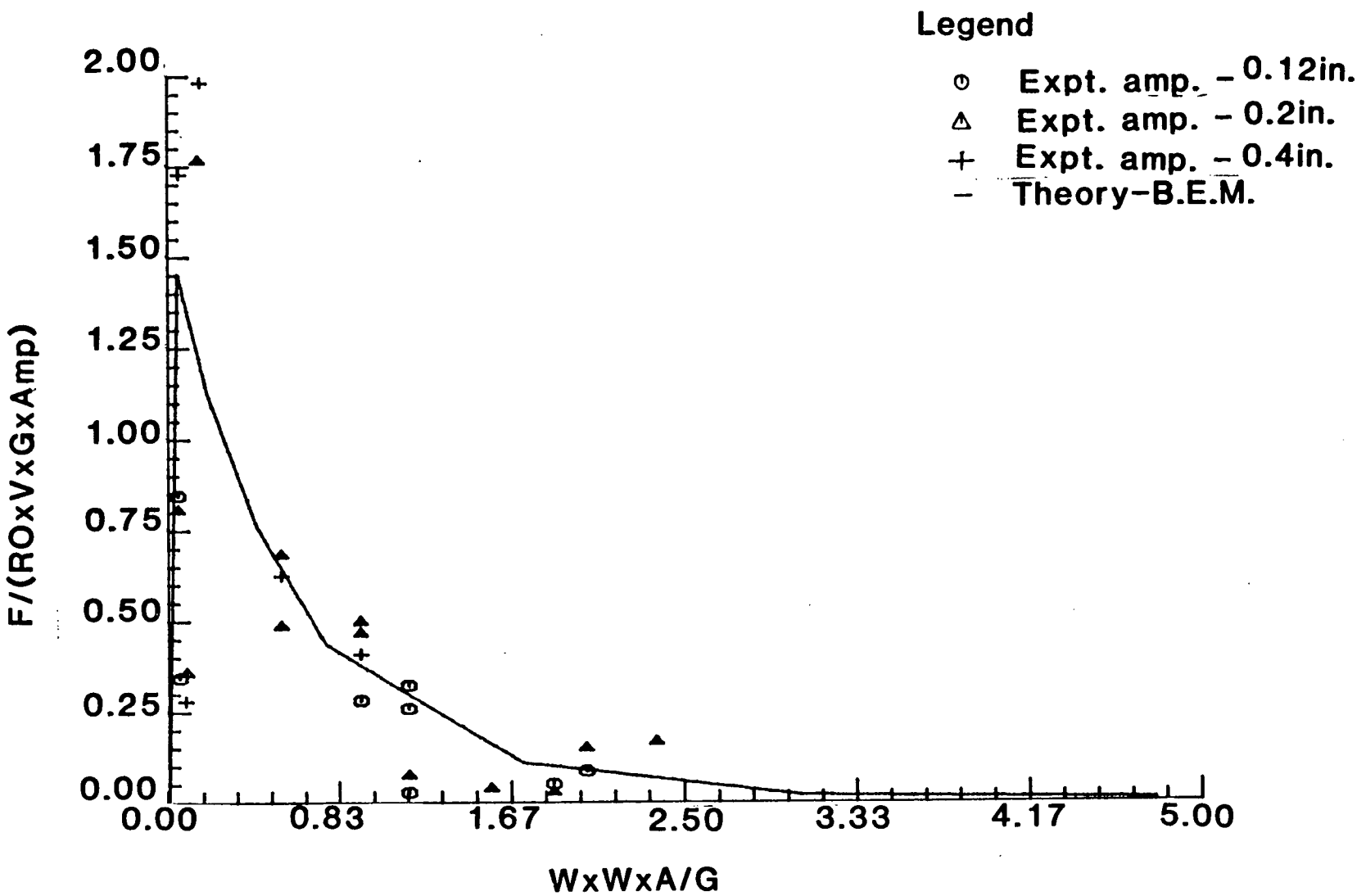

Fig.27 Heave exciting force on single cylinder. T=7"

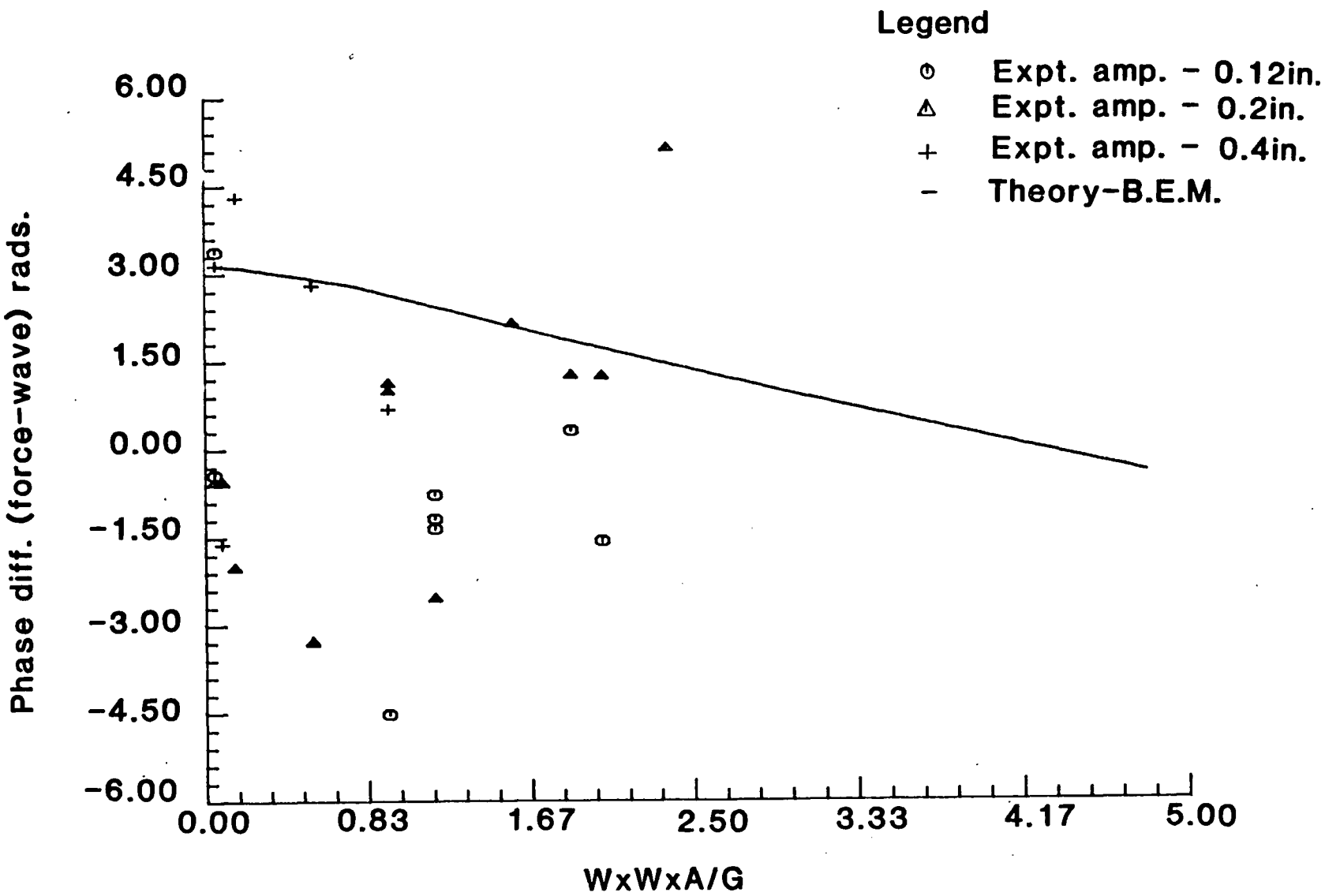

Fig.28 Heave exciting force phase. Single cylinder T=7"

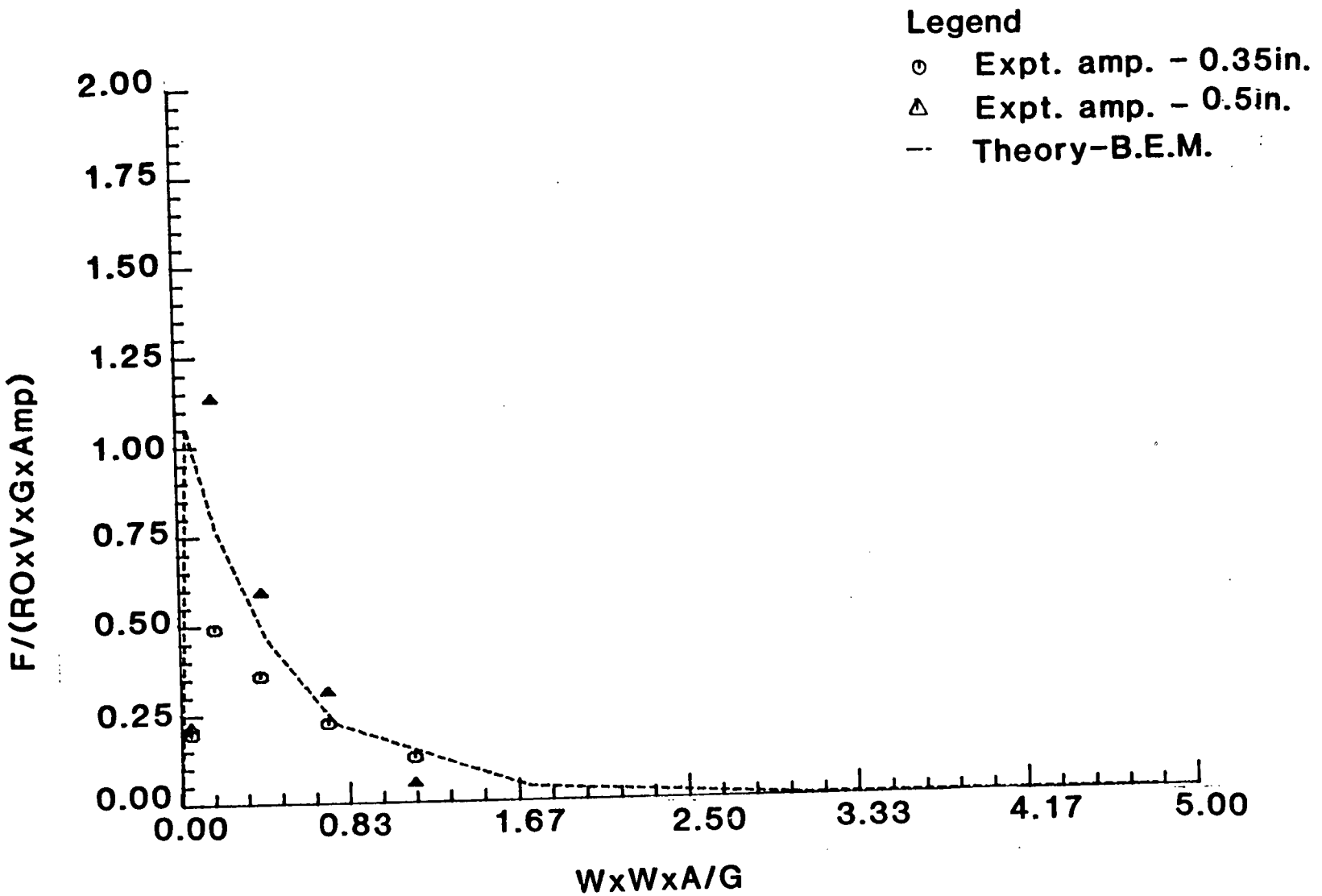

Fig.29 Heave exciting force on single cylinder. T=10.5"

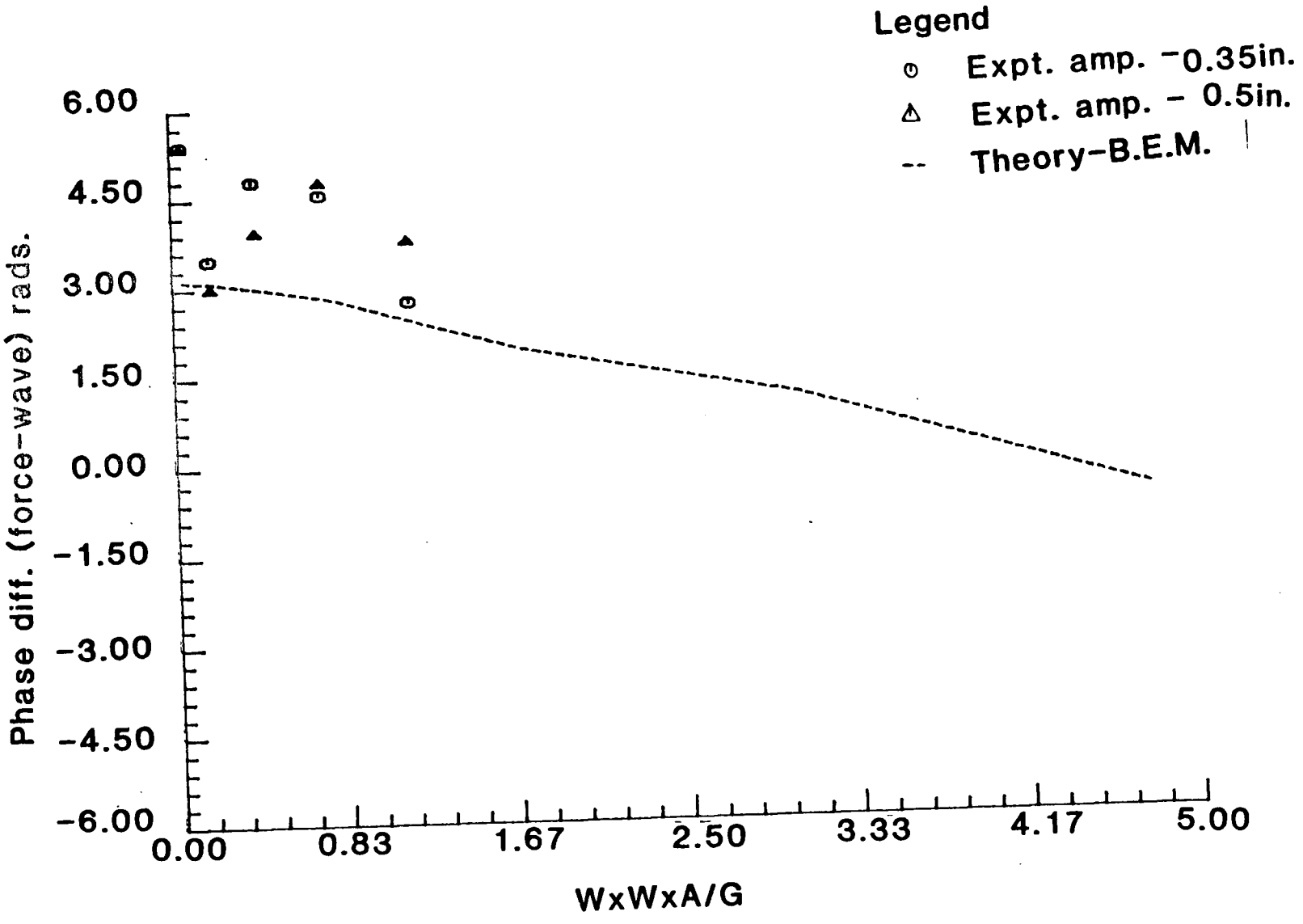

Fig.30 Heave exciting force phase. Single cylinder T=10.5"

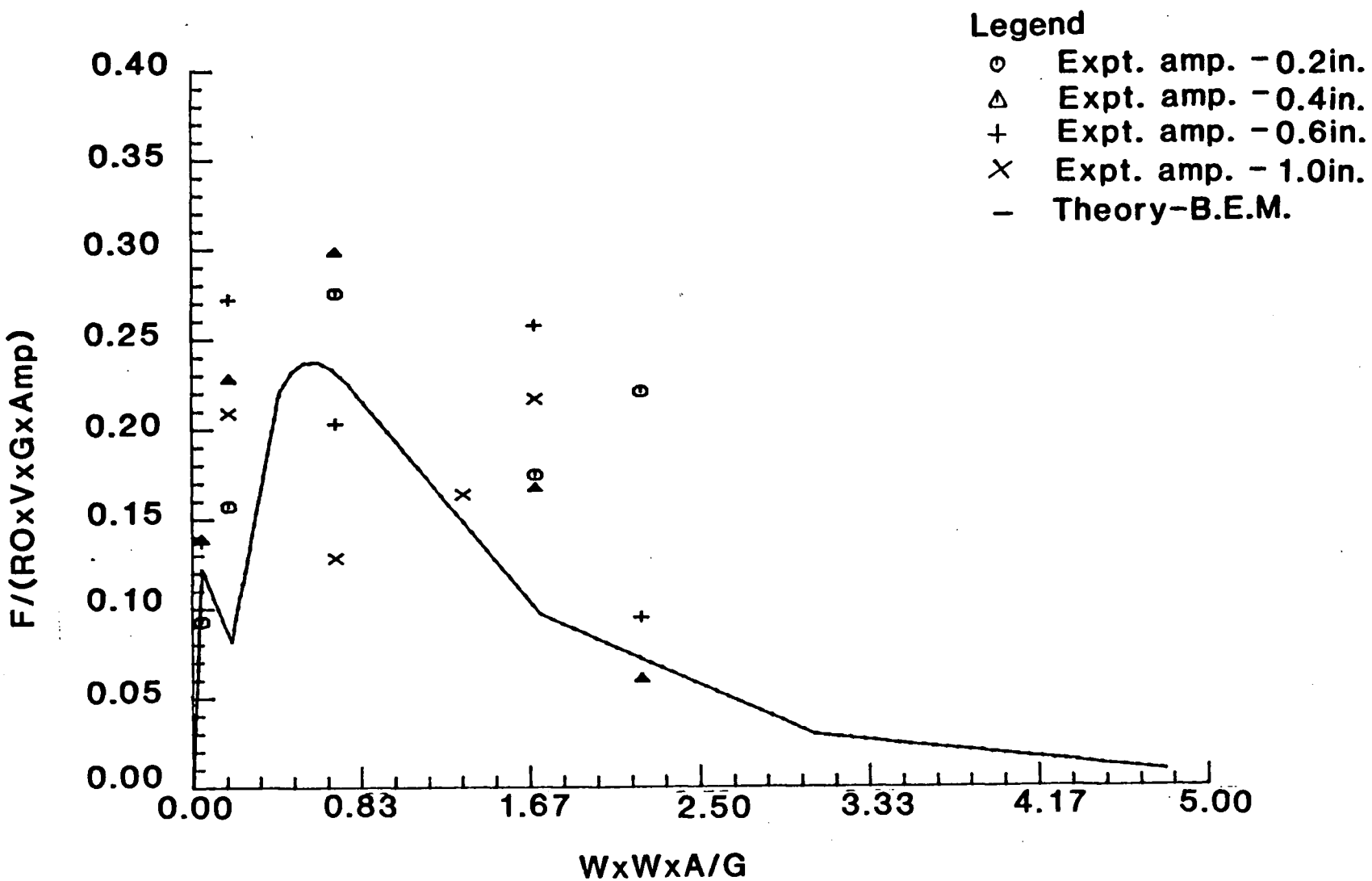

Fig.31 Heave exciting force on double cylinder. T=23.5"

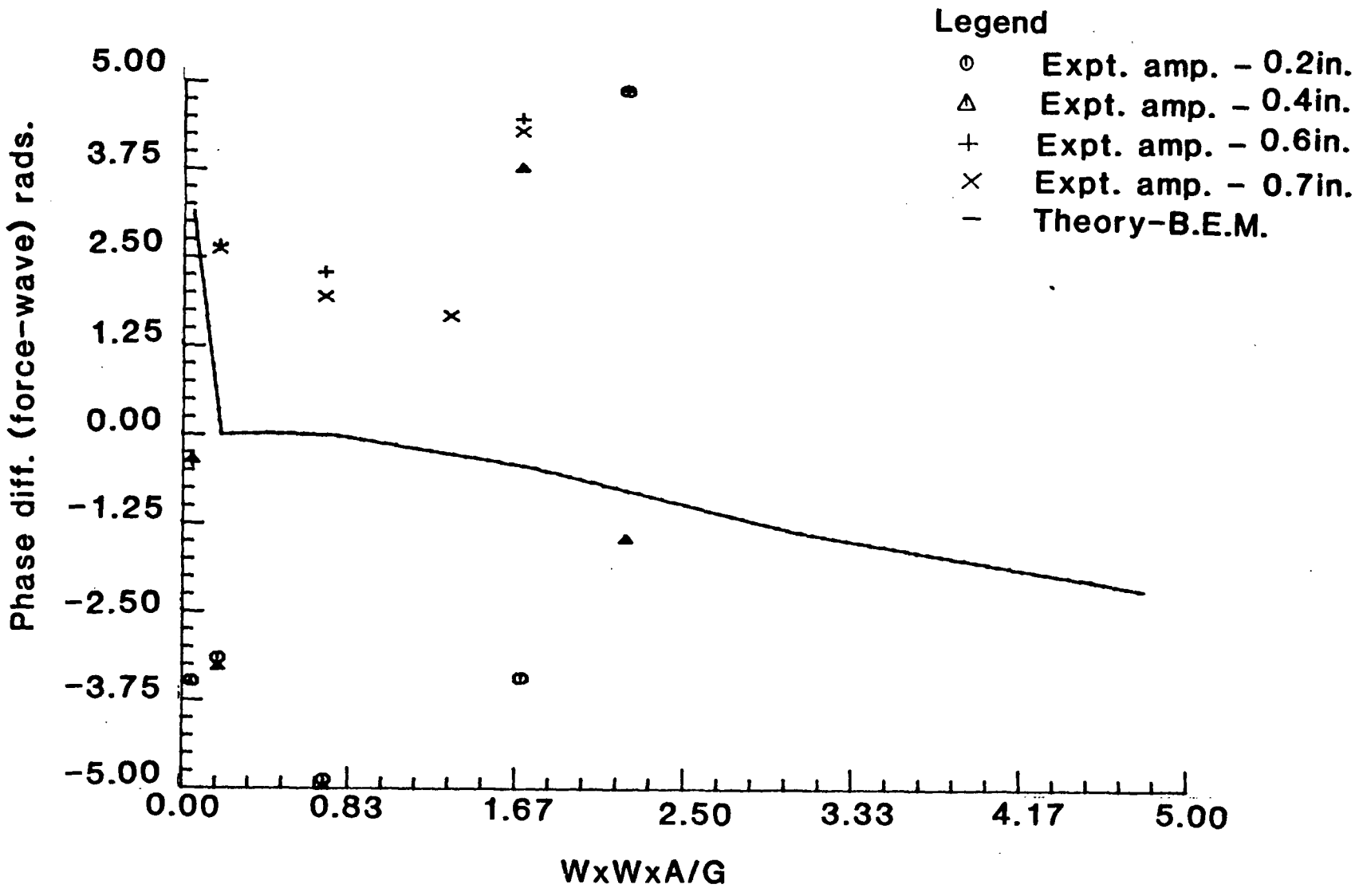

Fig.32 Heave exciting force phase. Double cylinder. T=23.5"

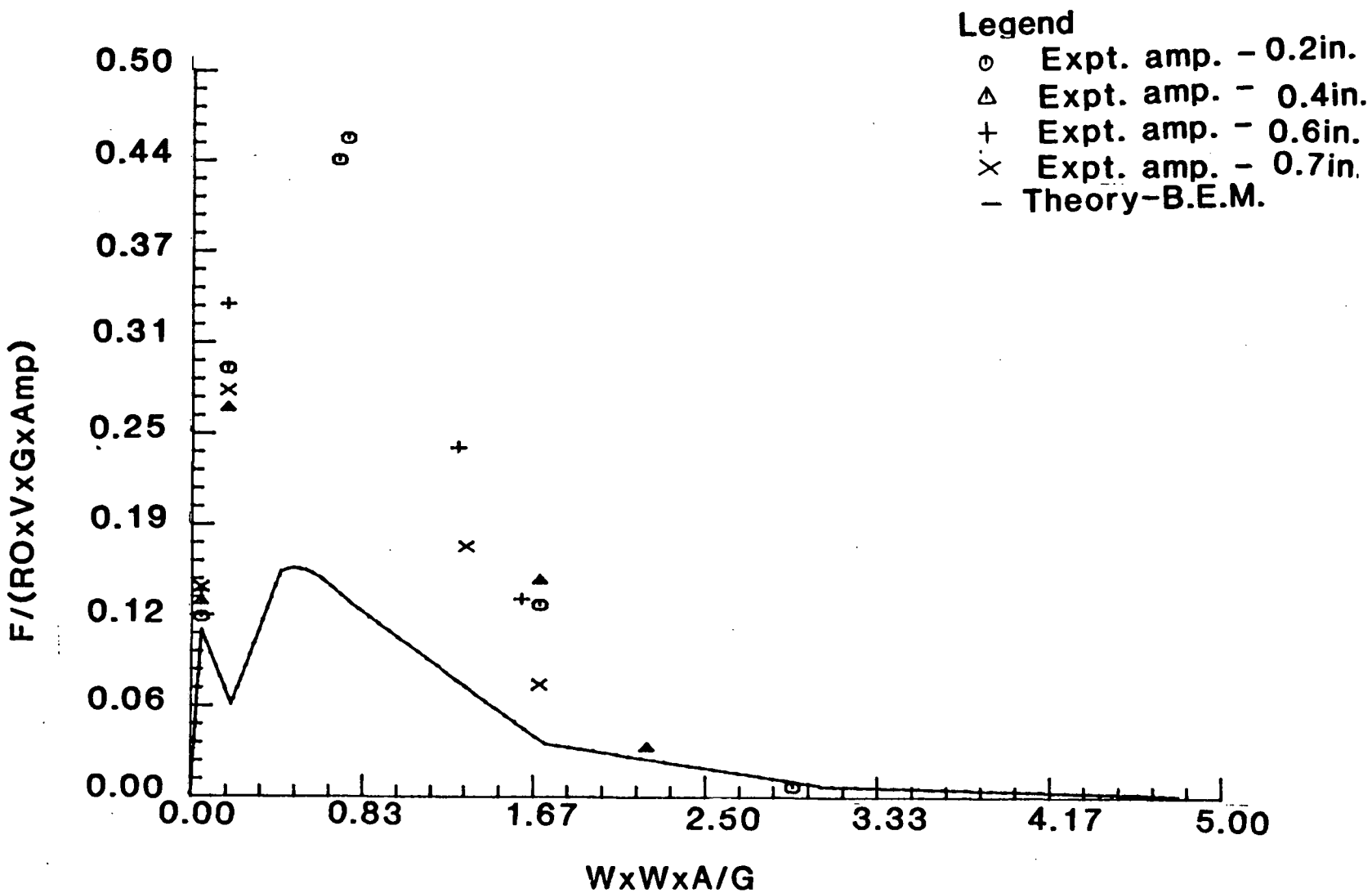

Fig.33 Heave exciting force on double cylinder. T=27.5"

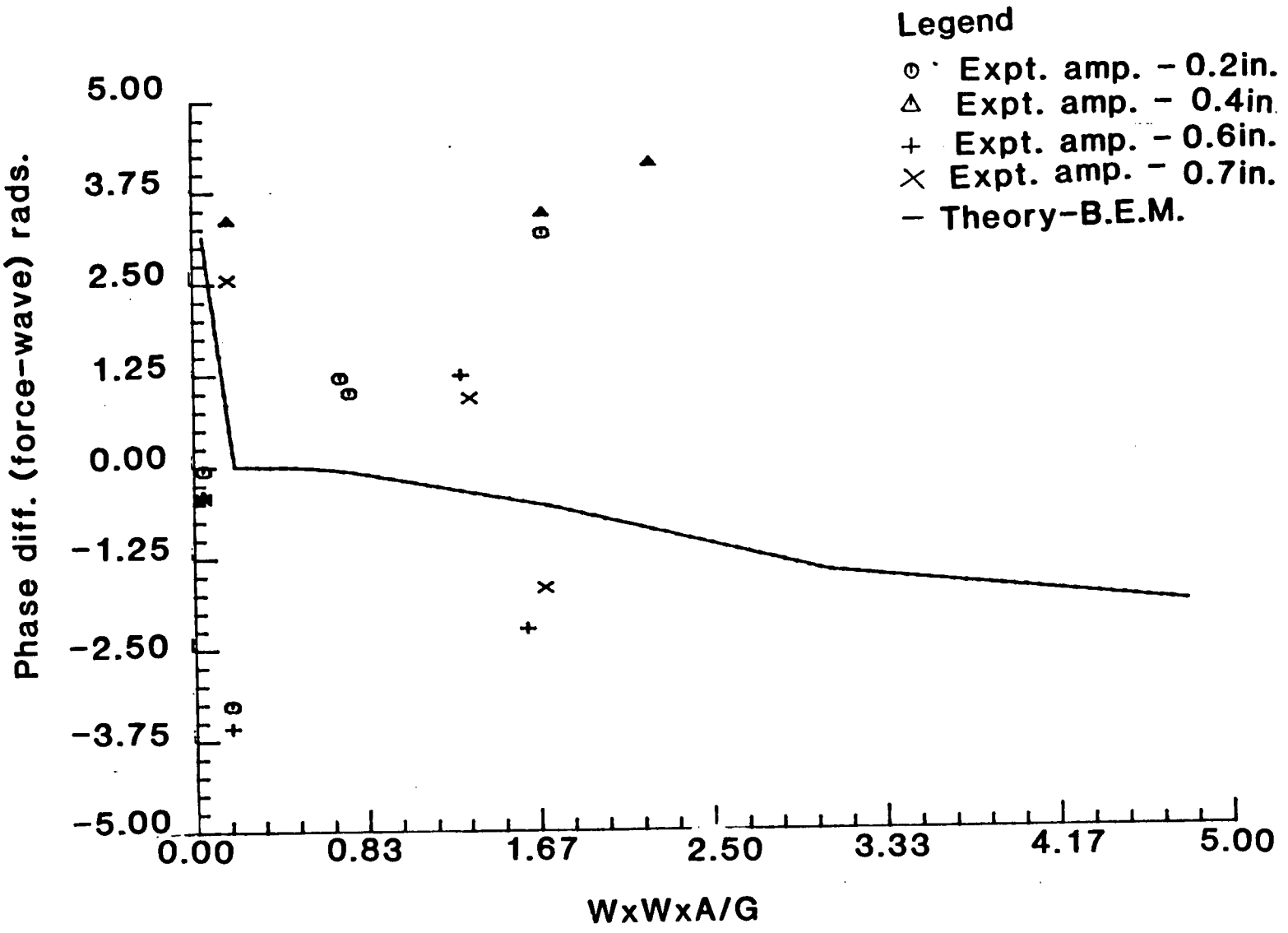

Fig.34 Heave exciting force phase. Double cylinder. T=27.5"

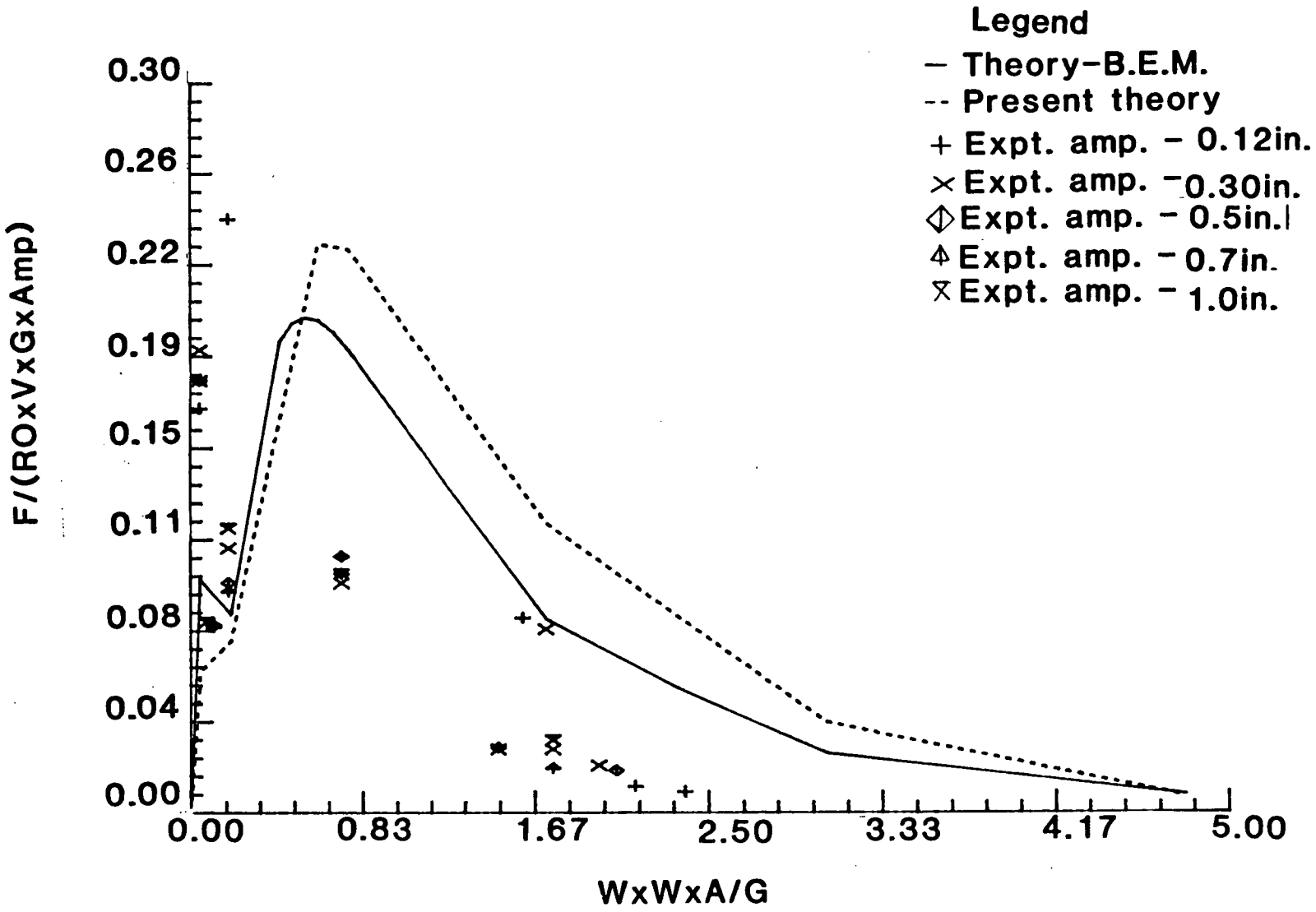

Fig.35 Heave exciting force on compound cylinder. T=35.5"

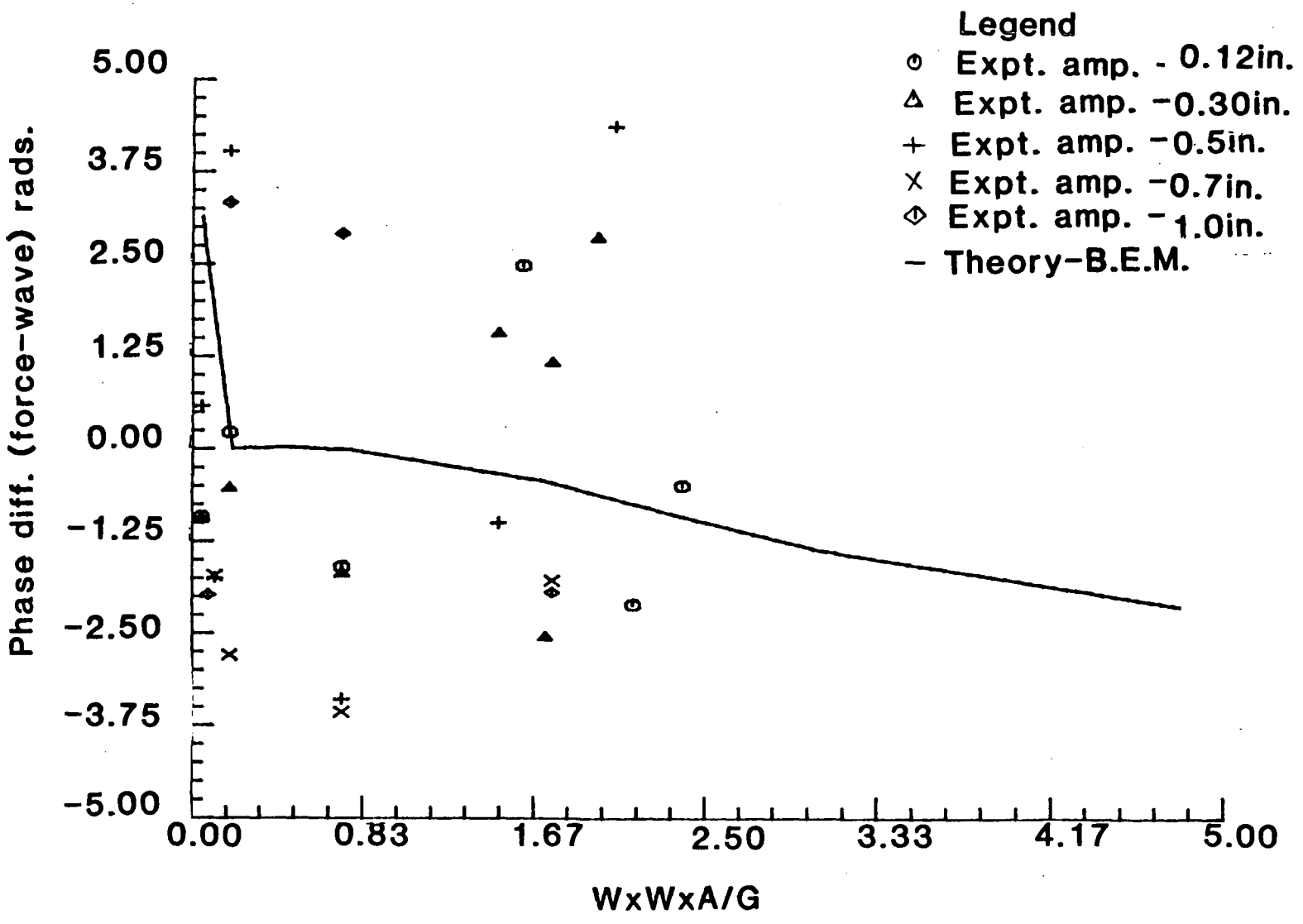

Fig.36 Heave exciting force phase. Compound cylinder. T=35.5"

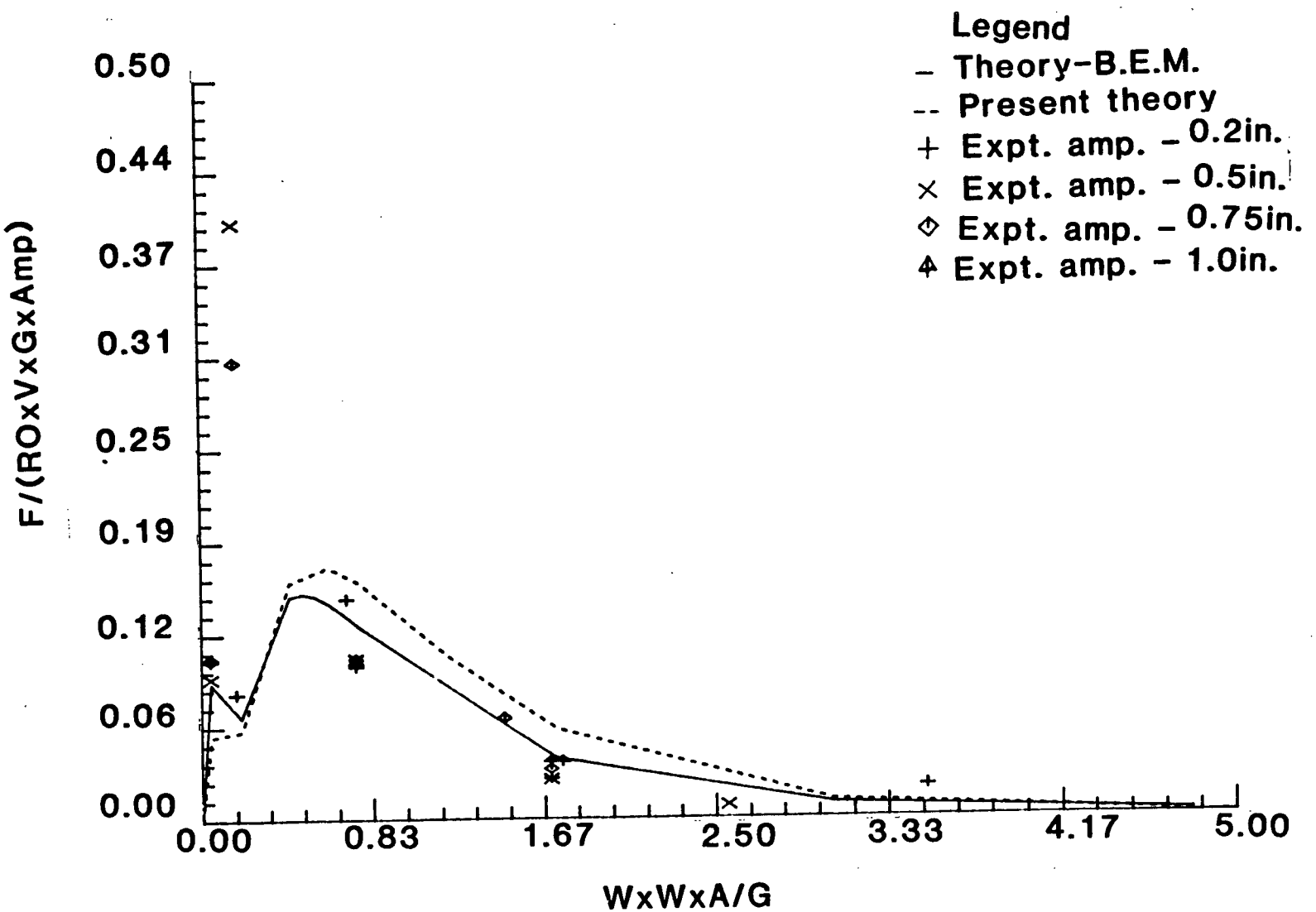

Fig.37 Heave exciting force on compound cylinder. T=38.375"

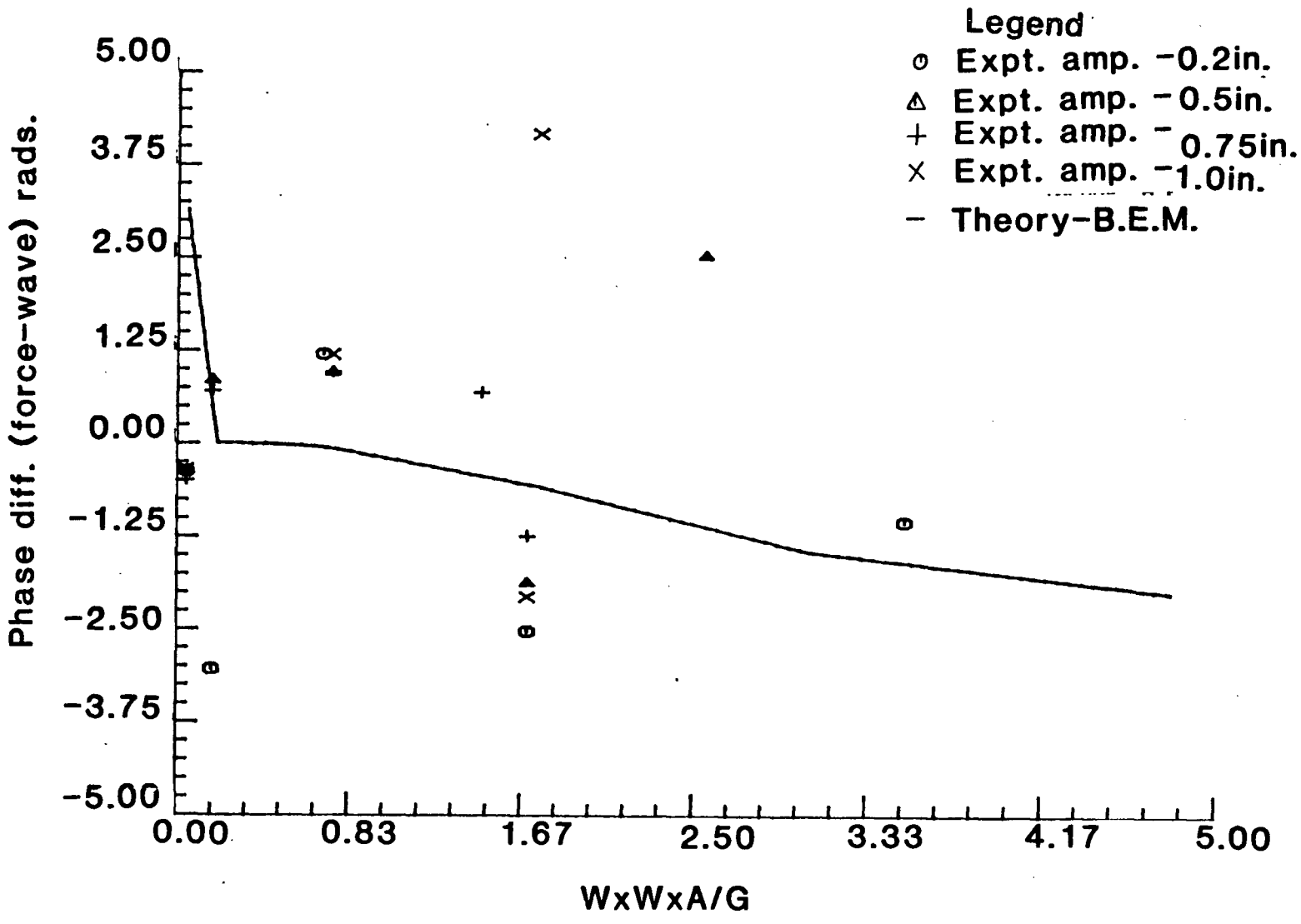

Fig.38 Heave exciting force phase. Compound cylinder. T=38.375"

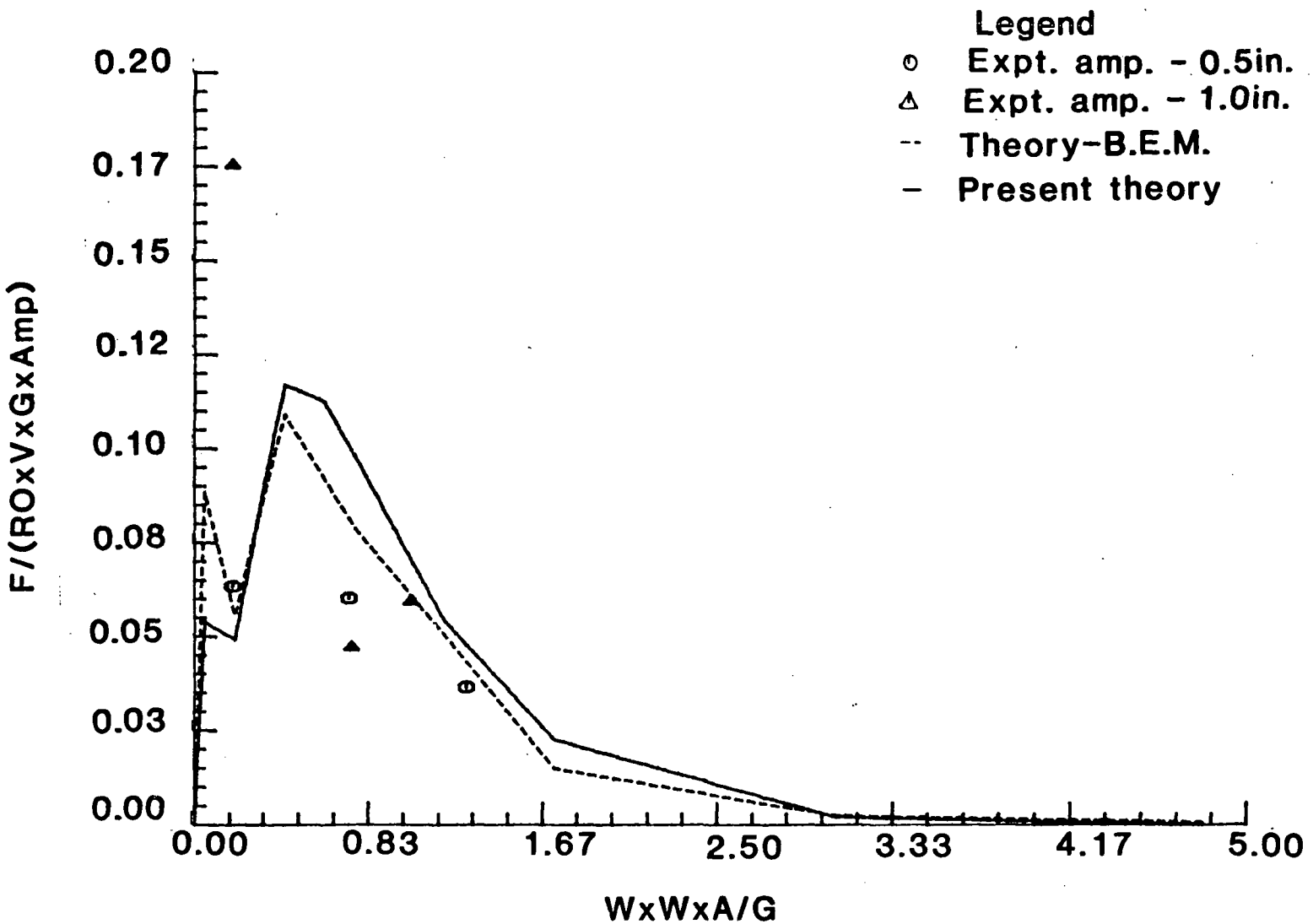

Fig.39 Heave exciting force on compound cylinder T=42.625"

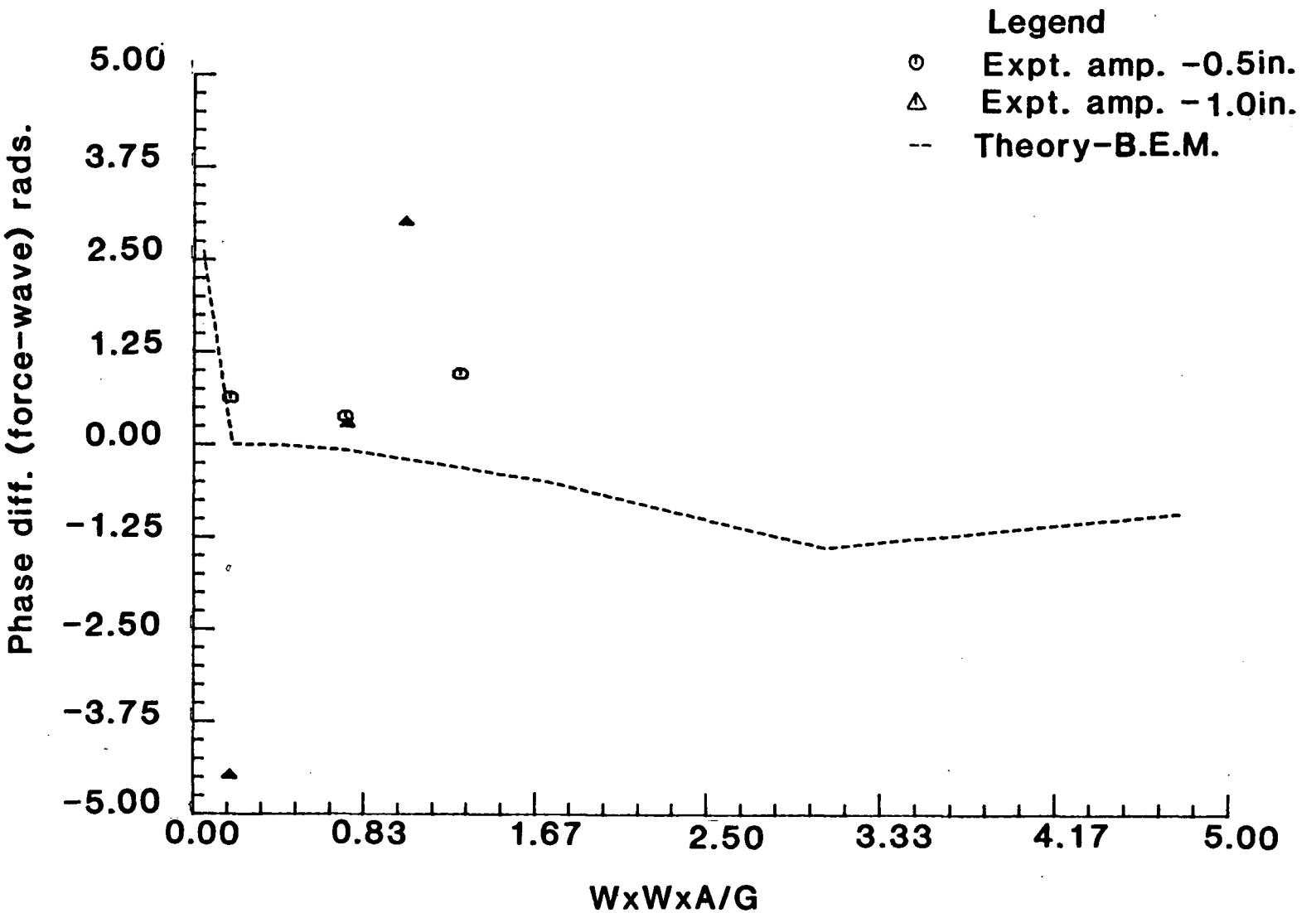

Fig.40 Heave exciting force phase. Compound cylinder T=42.625"

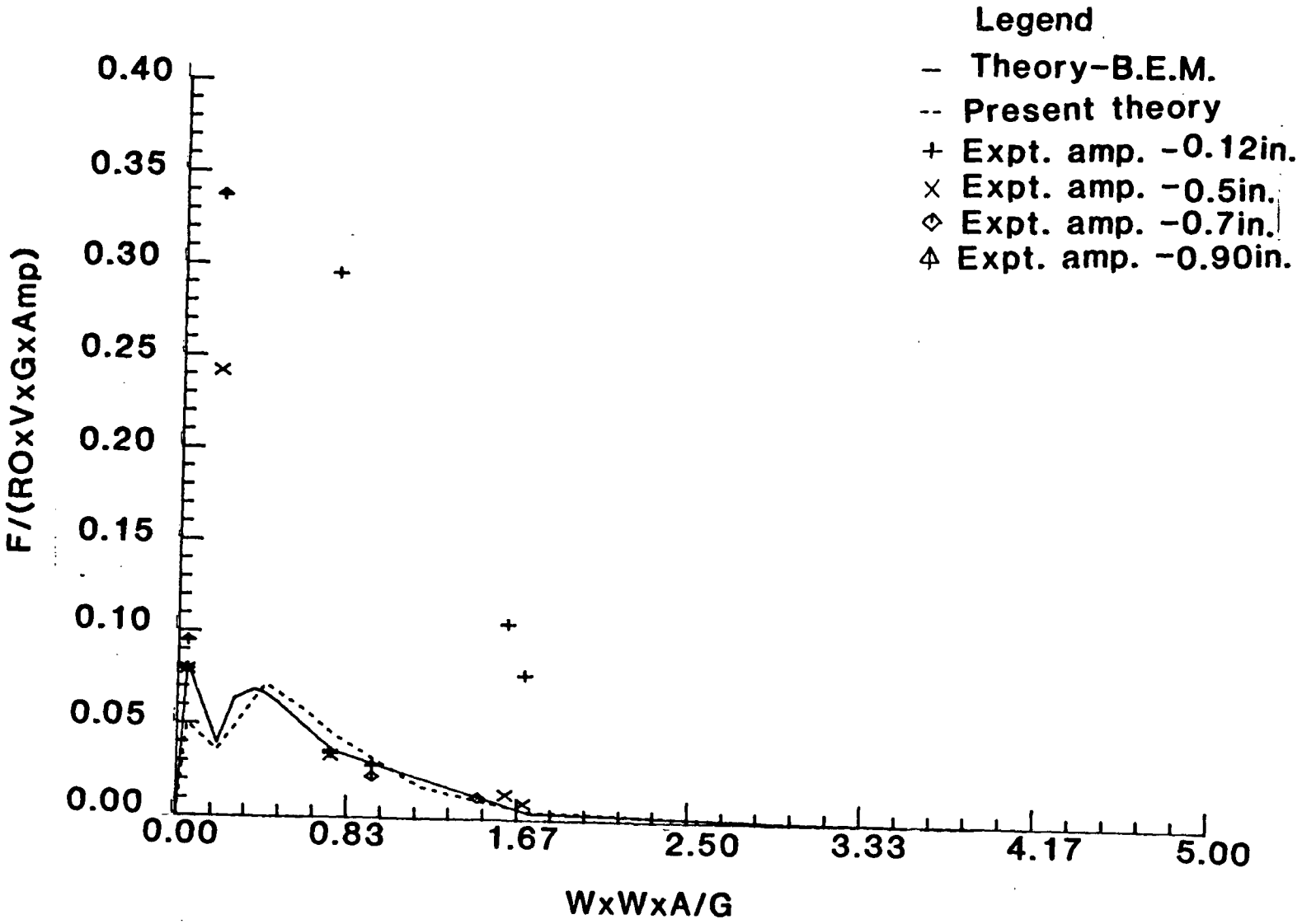

Fig.41 Heave exciting force on compound cylinder. T=49.5"

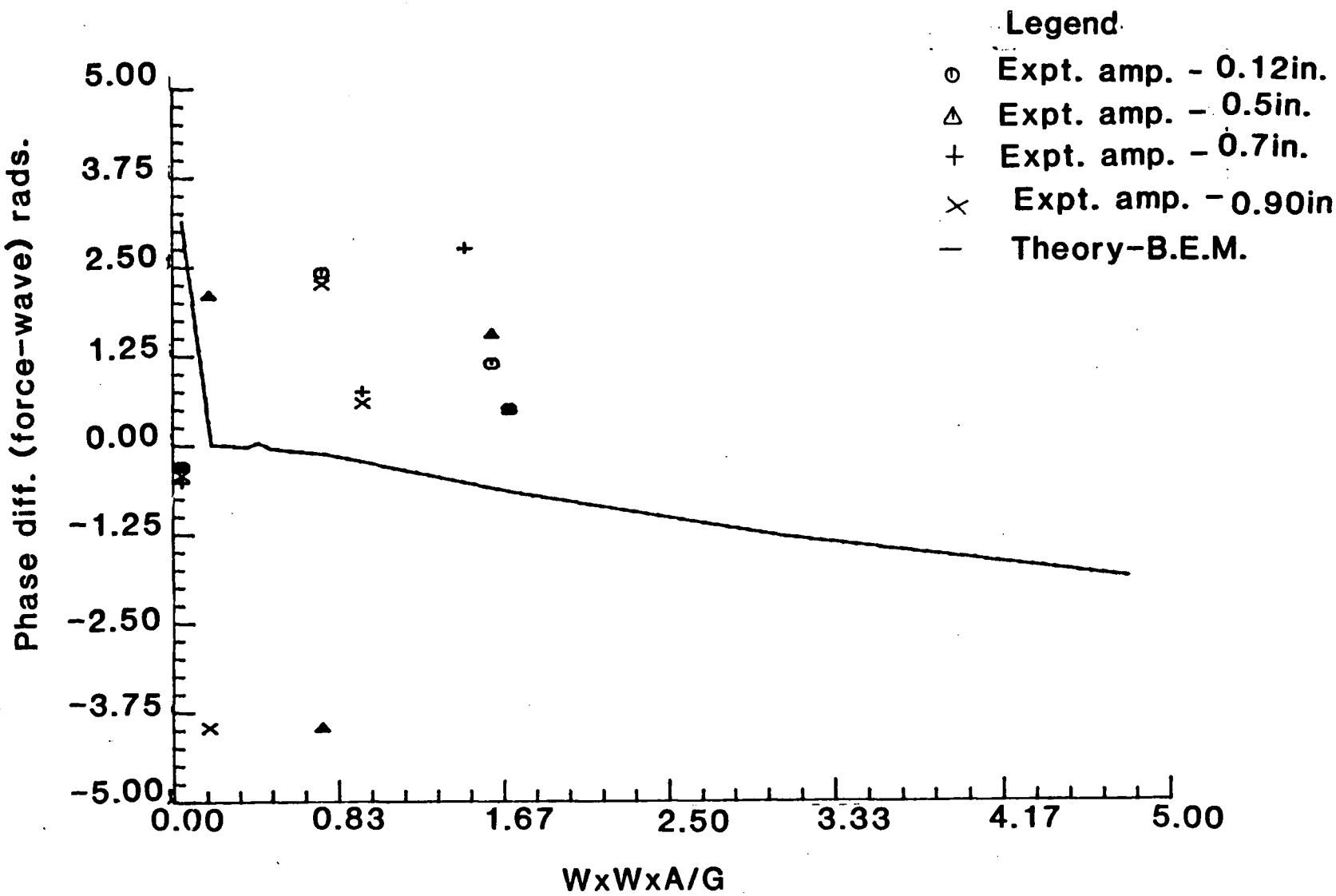

Fig.42 Heave exciting force phase. Compound cylinder. T=49.5"

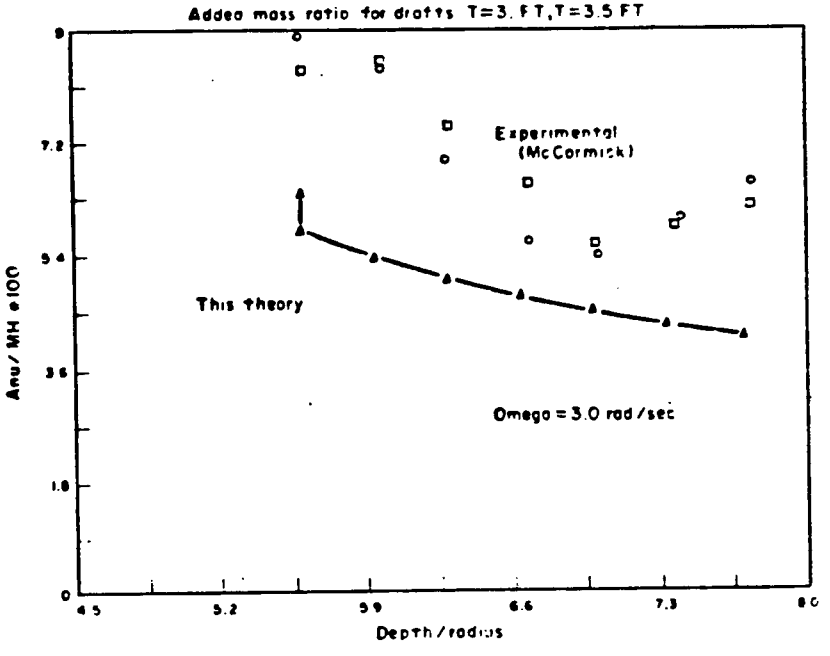

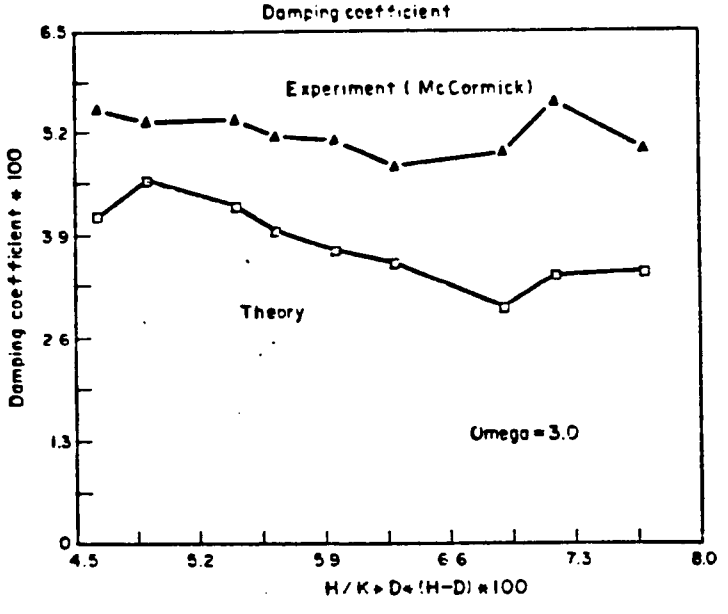

Fig.43 Hydrodynamic coefficients for single cylinder.